IOWA STATE UNIVERSITY
Digital Repository

Graduate Theses and Dissertations

Iowa State University Capstones, Theses and Dissertations

2012

Electrospun micro/nanodevices for controlled biomolecule release

HF Yang
Iowa State University

Follow this and additional works at: https://lib.dr.iastate.edu/etd

 Part of the Biomedical Commons, and the Electrical and Electronics Commons

Recommended Citation
Yang, HF, "Electrospun micro/nanodevices for controlled biomolecule release" (2012). *Graduate Theses and Dissertations*. 12724.
https://lib.dr.iastate.edu/etd/12724

This Dissertation is brought to you for free and open access by the Iowa State University Capstones, Theses and Dissertations at Iowa State University Digital Repository. It has been accepted for inclusion in Graduate Theses and Dissertations by an authorized administrator of Iowa State University Digital Repository. For more information, please contact digirep@iastate.edu.

www.manaraa.com

Electrospun micro/nanodevices for controlled biomolecule release

by

Haifeng Yang

A thesis submitted to the graduate faculty

In partial fulfillment of the requirements for the degree of

DOCTOR OF PHILOSOPHY

Major: Electrical Engineering

Program of Study Committee:

Liang Dong, Major Professor

Jiming Song

Santosh Pandey

Timothy Bigelow

Wei Hong

Iowa State University

Ames, Iowa

2012

Copyright © Haifeng Yang, 2012. All rights reserved.

www.manaraa.com

TABLE OF CONTENTS

www.manaraa.com

www.manaraa.com

LIST OF FIGURES

www.manaraa.com

www.manaraa.com

ABSTACT

Controlled biomolecule release technology represents one of the fastest advancing areas of science and engineering. For instance, in drug delivery area, such release system offers numerous advantages compared to conventional dosage drug forms including improved efficiency, reduced toxicity and controlled release profile. Current challenges in this area include biocompatiblity and biodegrability of the materials used in the system, controllablity and effectivity of the control mechanism, easiness of device fabraiction and drug loading loss as well as total cost. In this work, a simple and effective method is adopted to design and fabricate controlled release devices employing smart conmtrol mechanism. Such a technology could be further applied in pharmaceutics, biomeidical science and biotechnologies.

Controlled molecule release devices in this work employ the advantage of core-shell structures. In the first design, core-shell microcapsules are developed capable of regulating the release profile of encapsulated molecules. These microcapsules uniquely contain embedded miniature actuators inside their liquid core. The internal actuators are made of stimuli-responsive smart hydrogel beads. The embedded hydrogel beads swell in response to external electric fields, regulating the internal pressure of the liquid core, and thus the diffusion rate, of the encapsulated molecules from the microcapsules. The incorporation of the actuators into the interior of the microcapsules provides an internal control variable to a conventional diffusion-based release process. The microcapsules, which behave much like micro-electro-mechanical systems (MEMS), are fabricated by a simple co-electrospray

www.manaraa.com

process. This fabrication technique allows integrating the hydrogel beads, forming the polymer shell, and loading the releasable molecules simultaneously in one step.

The other controlled release device is developed by embedding nanofluidic biomolecule reservoirs into a polymer network of a stimuli-responsive hydrogel. The reservoirs are made of liquid core-polymer shell nanofibers using co-electrospinning technique. The mechanism of controlled release is based on buckling instability of the polymer shell under combined axial and radial compression, caused by volume changes of hydrogel responding to a specific external stimulus. The device decouples releasable biomolecules from a hydrogel polymer matrix, avoiding chemical interactions between biomolecules and hydrogel polymer chains, and thus, alleviating nontrivial chemical and biological engineering design of hydrogel formulations. Temperature-sensitive hydrogel is used as a model hydrogel.

www.manaraa.com

CHAPTER 1. INTRIDUCTION TO CONTROLLED DRUG RELEASE

1.1 Introduction to Controlled Drug Release

Controlled drug release technology represents one of the fastest advancing areas of science and engineering in which scientist and engineers are contributing to human health care [1]. Such release systems offer numerous advantages compared to conventional dosage drug forms including improved efficiency, reduced toxicity and controlled release profile. Conventional oral drug administration does not usually provide rate-controlled release or target specificity. In many cases, conventional drug delivery provides sharp increase of drug concentration at potentially toxic levels. Following a relatively short period at the therapeutic level, drug concentration eventually drops off until re-administration. The goal of developing novel drug release system is to revolutionize the traditional drug release format, improving the effectiveness of drug therapy. This improvement can take the form of increasing therapeutic activity compared to the intensity of side effects, reducing the number of drug administrations required during treatment, or eliminating the need for specialized drug administration.

The idea of controlled release from polymers dates back to 1960s through the employment of silicone rubber and polyethylene. The lack of degradability in these systems implies the requirement of eventual surgical removal and therefore limits their further application. In the 1970s, biodegradable polymers were suggested as appropriate drug delivery candidate materials circumventing the requirement of post-removal. The idea of

www.manaraa.com

polymer microcapsules as delivery systems was reported as early as the 1960s and degradation was incorporated by Mason *et al.* through the employment of a degradable polymer coating [2].

Two classes of control over drug release can be realized: temporal control and distribution control [1]. In temporal control, drug delivery systems aim to delivery the drug over an extended duration or at a pre-defined specific time during treatment or administration. Controlled release over an extended duration is highly desired for drugs that are rapidly metabolized and eliminated from the body after administration. There are two major situations in which distribution control can be beneficial. The first is when the natural distribution causes drug molecules to encounter tissues and cause major side effects that prohibit further treatment. This situation is often the cause of chemotherapy failure when bone marrow cell death prevents the patient from undergoing a complete drug treatment. The second situation is when the natural distribution of the drug does not allow drug molecules to reach their molecular site of action. For instance, a drug molecule that acts on a receptor in the brain will not be active if it is distributed by the patient's blood system but cannot across the blood-brain barrier. The advantage of sustained release is shown in Figure 1-1 in which the drug concentration at the site of activity within the body is compared after immediately release from four injections administered at six hourly intervals and after extended release from a controlled release system.

A variety range of mechanisms have been employed to achieve both temporal and distribution controlled release of drugs using polymers. This diversity is a necessary consequence of different drugs imposing various restrictions on the type of delivery system

www.manaraa.com

employed. Polymers have been employed extensively in drug release applications. One of the significant concerns in designing polymers for any controlled release system is the fate of the polymer after drug release. Therefore, polymers that are naturally excreted from the body are the most desirable one for many controlled release applications. Non-degradable polymers could be used in applications where such polymers could be recovered after drug release.

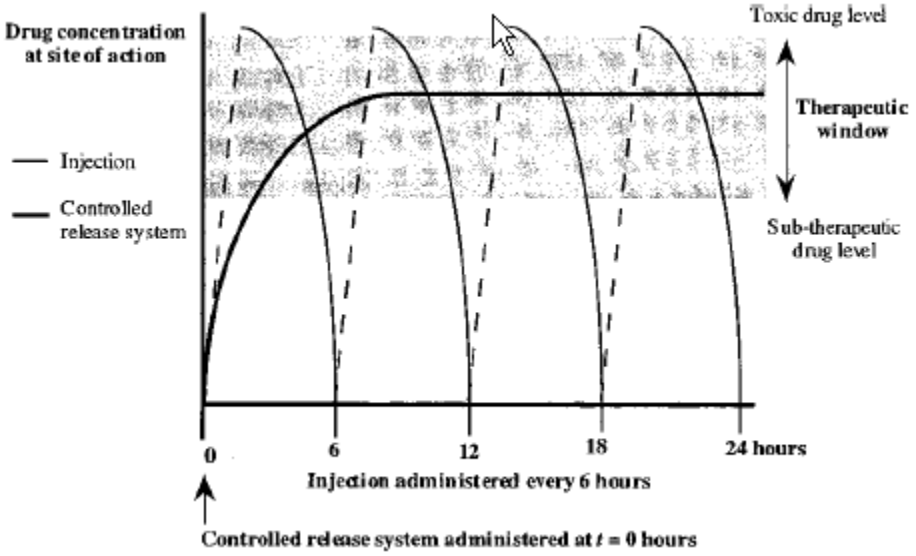

Figure 1-1 Drug concentrations at site of therapeutic action after delivery as a conventional injection (thin line) and as a temporal controlled release system (bold line).

1.2 Controlled Release Mechanism

Most drug molecules need to be dissolved in the aqueous environment of the patient and freely diffuse within that media before they can be functional on their target acceptors or locations. Temporal controlled release protects drug molecules from this aqueous living environment for preprogrammed periods of time. This protection can involve delaying the

www.manaraa.com

dissolution of drug molecules, inhibiting the diffusion of the drug out of the device, or controlling the flow of drug solutions.

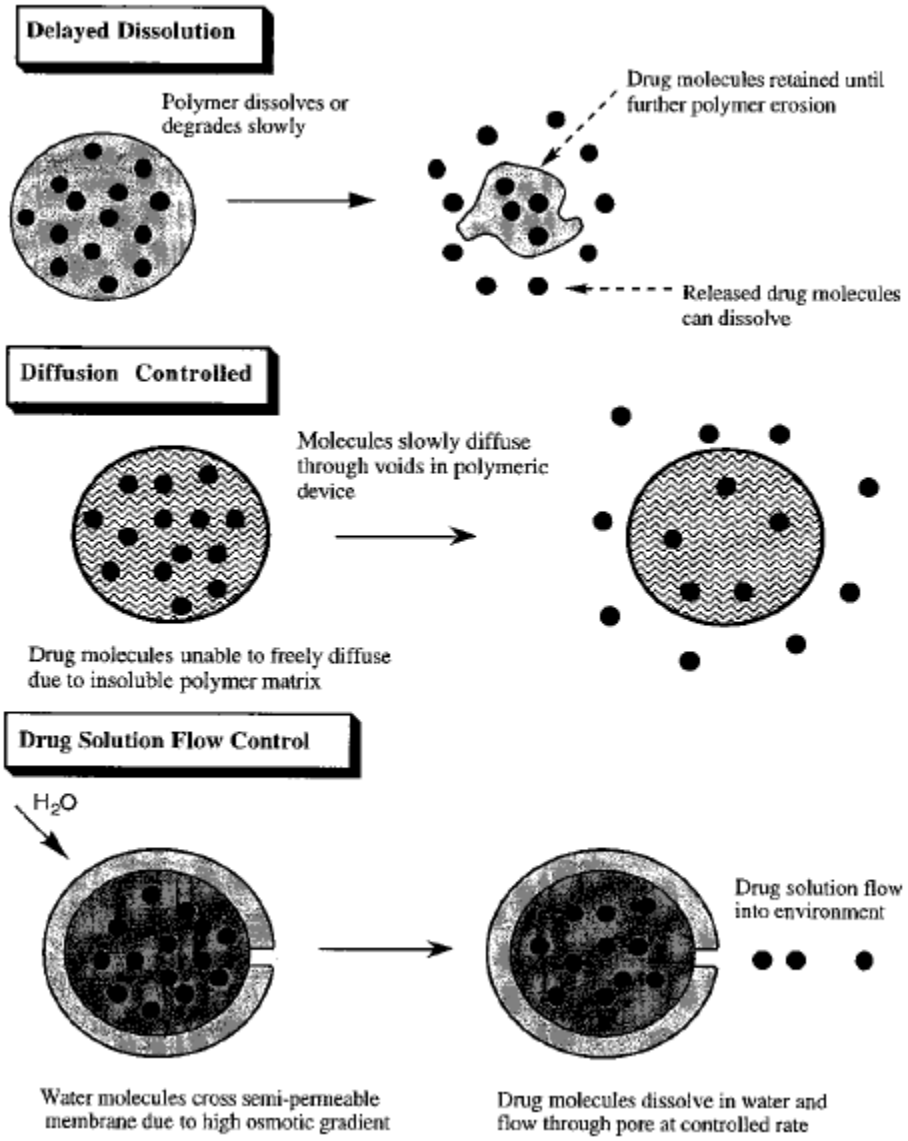

Figure 1-2 Examples of temporal release mechanisms

Polymers employed to delay drug dissolution aim to slow the rate at which drug molecules are exposed to water from the aqueous environment surrounding the drug delivery system. This might be achieved by a polymer coating or matrix that dissolves at a slower rate than the drug. In diffusion controlled release mode, drug molecule diffusion within an

www.manaraa.com

aqueous solution is inhibited by the insoluble polymer matrix in which drug molecules must travel through pathways to exit the device. The barrier to diffusion can be decreased by swelling of the hydrogel which creates voids in the gel structure. Such hydrogels may also benefit from bio-adhesive properties which allow them to reside for extended time periods. Polymers used for diffusion controlled release can be fabricated as either matrices in which drug is uniformly distributed or as a rate reservoir from the living environment as shown in Figure 1-2. Devices that regulate the flow of drug solution sometimes use osmotic potential gradients across semipermeable polymer barriers to generate pressurized chambers containing aqueous solutions of the drug. This pressure is relieved by the flow of the solution out of the delivery device. The rate of flow is controlled through a micrometer scale to a larger diameter pores. Many of the temporal controlled release devices utilize the diffusion controlled mechanisms.

Another form of temporal control release is responsive drug delivery in which drug is released in a pulsatile manner only when required by the body [3]. An example for this application is the delivery of insulin to diabetics. Responsive drug delivery is proposed to revolutionize such therapy with the design of systems that release drugs in response to increased blood glucose levels. Generally, responsive drug delivery system contains two components: a sensor that detects the environmental parameter of interests that stimulates the drug release and a delivery device that releases drugs. The concept of responsive drug delivery can be used for any drug therapy in which a sensor and delivery device can be coupled.

www.manaraa.com

The other controlled mechanism is distribution controlled drug release. The simplest method of achieving distribution control is to implant the drug delivery system directly at the site where drug is necessary. For most of diseases that require distribution controlled release of drug, a targeting mechanism should be employed that allows the delivery system to search the desired target. Polymers are used in two types of delivery systems for these applications, colloidal carriers and polymer-drug conjugates. In colloidal formulations, the polymer encapsulates drug within nano and microparticles. In polymer-drug conjugates, the drug is covalently coupled to the polymer. In these forms of distribution controlled release, the polymer acts as a carrier but is not responsible for targeting the delivery device. Biological molecules such as immuniglobulins and carbohydrates are frequently utilized as targeting moieties.

1.3 Polymers Used for Controlled Drug Release

Polymers are very widely used in drug delivery science. Classifications of polymer in controlled release applications can be difficult due to the inherent diversity of structures. However, it is beneficial to attempt this classification because it can highlight common properties within groups of polymers. In broad terms, polymers can be classified as either biodegradable or non-biodegradable. Biodegradable systems have attracted much of the recent interest and development in drug delivery systems because non-biodegradable systems need retrieval or further manipulation after introduction into the body.

In degradable polymers, there is another level of classification based upon the mechanism of erosion. The term ‘degradation’ specifically refers to bond cleavage, whereas ‘erosion’ refers to the depletion of material. Degradation is a chemical process whereas

www.manaraa.com

erosion is a physical phenomenon reliant on dissolution and diffusion process. Two mechanisms of polymer erosion can be identified, surface and bulk erosion. In practical terms, these two mechanisms represent extremes. For most biodegradable polymers both mechanisms will occur, but the relative extent of surface or bulk erosion varies radically with the chemical structure of the polymer backbone.

Surface erosion occurs when the rate of erosion exceeds the rate of water permeation into the bulk of the polymer. This is often considered to be a desirable mechanism of erosion in drug delivery because the kinetics of erosion as well as the rate of drug release is highly reproducible. The magnitude of the erosion may be changed by simply changing the surface area of the drug delivery device. The slow rate of water permeation into surface eroding devices has a further beneficial effect of protecting water labile drugs up to the time of drug release. Water permeation is retarded by designing the polymers with hydrophobic monomer units. Besides, hydrophobic components could be added to stabilize the polymer bulk. In ideal surface erosion, the erosion rate is directly proportional to external surface area. Surface erosion can lead to zero order drug release provided that diffusional release is limited and the overall shape remains constant. Bulk erosion occurs when water molecules are able to permeate into the bulk of the polymer matrix at a quicker rate than erosion. As a consequence, polymer molecules in the bulk may be hydrolyzed and the kinetics of the polymer degradation or erosion is more complex than for surface eroding systems. The majority of the biodegradable polymers used in controlled drug delivery undergo bulk erosion. While the more limited predictability of erosion and the lack of protection of drug molecules are inherent disadvantages to the bulk eroding systems, these properties do not

www.manaraa.com

inhibit their successful employment as drug delivery devices. Many new applications in controlled release use nano and microparticle formations that posses mass surface areas resulting in bulk and surface eroding materials possessing similar erosion kinetics. Within the scope of biodegradable systems, natural polymers, particularly those in the poly (saccharide) family, are being investigated. They are referred as biopolymers, and synthesis of this class of polymers is limited to the manipulation of bulk material to enhance their viability. Due to the physicochemical limitations of natural materials, there is significant exploration of synthetic polymer which can be readily tailored to offer properties for specific applications. Degradation polymers can be limited to 1 month, depending on the desired range of therapeutic effect. The ability of designing biomaterials with specified release, mechanical and processing properties has opened opportunities for synthetic chemists in the controlled release area.

Among the biodegradable polymers, poly (esters) is the best characterized and the most widely studied biodegradable polymer system. The synthesis of polyesters has attracted much interest as the degrading of these materials. The mechanism of the degradation in polyester materials is classified as bulk degradation with random hydrolytic scission of the polymer backbone. The well known polymer poly (lactic acid) (PLA) is a member of such class. Poly (esters) have been widely employed in drug delivery applications and comprehensively studied. The predominant synthetic pathway for production of poly (esters) is from ring-opening polymerization of the corresponding cyclic lactone monomer.

Poly (esters) based on poly (lactic acid) (PLA), poly (glycolic acid) (PGA), and their copolymers, poly (lactic acid-co-glycolic acid) (PLGA), are some of the best defined

www.manaraa.com

biomaterials with regard to design and performance. Lactic acid contains an asymmetric alpha-carbon which is typically described as D or L form in classical stereochemical terms and sometimes as the R and S form. For homopolymers, the enantiomeric forms are poly (D-lactic acid) (PDLA) and poly (L lactic acid) (PLLA). The physicochemical properties of optically active PDLA and PLLA are nearly the same, whereas the PLA has very different characteristics. Because the naturally occurring lactic acid is L, PLLA is considered more biocompatible. The polymers are derived from monomers that are natural metabolites of the body; therefore the degradation of these materials yields the corresponding hydroxyl acid, making them safer for in vivo use. Biocompatibility of the monomer is the foundation for biocompatibility of degradable polymer systems. To this end, the degradation products often define the biocompatibility of a polymer-not necessarily the polymer itself. Even though PLGA is extensively used and represents the gold standard of degradable polymers, increased local acidity due to the degradation can lead to irritation at the site of the polymer employment. Introduction of the basic salts has been investigated as a technique to control PH in local environment of PLGA implants.

From a physical level of understanding, poly (esters) undergoes bulk degradation. PLA homopolymers degrade slower than PGA homopolymers on the basis of crystallinity as well as steric inhibition by the pendent methyl group of PLA to hydrolytic attack. Other class of polymers often used in drug release applications includes poly (ethylene glycol) block polymers, poly (ortho esters), poly (anhydrides) and etc.

www.manaraa.com

1.4 Hydrogel in Controlled Release Applications

Traditional delivery systems suffer from the limitations and disadvantages of minimal synchronization between the required time for therapeutically effective drug concentrations and the actual drug release profile exhibited by the dosage form. Controlled delivery systems through targeted drug delivery of a predetermined dose over a sustained period have been used to overcome the shortcomings of conventional dosage forms. This is mainly because the reason that controlled drug release system can offer sustained therapeutic level of drug concentration without introducing toxicity. Responsive drug release system would respond to physiopathological signals from an underlying disease. The appropriate amount of drug would be released based on the stimulation of such a physiopathological signal.

Hydrogels are one of the upcoming classes of polymer-based controlled-release drug delivery system. The existence of hydrogels dates back to 1960, when Wichterle and Lim first proposed the use of hydrophilic networks of poly (2-hydroxyethyl methacrylate) (PHEMA) in contact lenses [4]. Since then, the applications of hydrogels have extended to various biomedical and pharmaceutical applications. In comparison to other synthetic biomaterials, hydrogels resemble living tissues closely related to their physical properties because of their relatively high water content and soft and rubbery consistency. Hydrogels show minimal tendency to absorb proteins from body fluids because of their low interfacial tension. Further, the ability of molecules of different sizes to diffuse into and out of hydrogels allows the possible use of dry or swollen polymeric networks as drug delivery systems for oral, nasal, ocular administration. Several terms have been named for hydrogels, such as smart gels and intelligent gels. The smartness of a material is critical to its ability to

www.manaraa.com

receive, transmit or process a stimulus, and respond by producing a useful effect. Once activated, stimuli can result in changes in phases, shapes, optics, mechanics, electrical fields and etc. Hydrogels are smart or intelligent in the sense that they can perceive the stimuli and respond by exhibiting changes in their physical or chemical behavior, resulting in the release of entrapped drug in a controlled manner.

A common misunderstanding in polymer science is the use of the terms ‘gel’ and ‘hydrogel’ synonymously. As polymeric networks, both gels and hydrogels might be similar chemically, but they are physically different. Technically, gels are semi-solid systems comprising small amounts of solid, dispersed in relatively large amounts of liquid, yet possessing more solid-like than liquid like character. Hydrogels are also described as aqueous gels because of the prefix ‘hydro’. Although the term hydrogel implies a material already swollen in water, in a true sense hydrogels are a cross-linked network of hydrophilic polymers. They possess the ability to absorb large amounts of water and swell, while maintain their three dimensional structure. The definition differentiates hydrogel from gels, which are polymeric networks already swollen to equilibrium, and the further addition of fluids results only in dilution of polymeric network. Although some of the gels are rigid enough to keep their structure under a tiny stress, after exceeding the yield-value, gel fluidity is observed with loss of polymer structure. A hydrogel exhibits swelling in aqueous media for the same reasons that an analogous linear polymer dissolves in water to form an ordinary polymer solution. Thus, the feature central to the functioning of a hydrogel is its inherent cross-linking. Because the basic framework of both gels and hydrogels is the polymer

www.manaraa.com

network, these polymers produce systems that span a range of rigidities, beginning with a sol and increasing to mucilage, jelly, gel and hydrogel.

Hydrogels are considered to be a polymeric material that has the ability to absorb >20% of its weight of water and still maintain a distinct 3D structure. The hydrophilicity of the polymer imparts water attracting properties to the system. Their characteristic water-insoluble behavior is attributed to the presence of chemical or physical cross-links, which provide a network structure and physical integrity to the system. Hydrogels are elastic in nature because of the presence of a memorized reference configuration to which they return even after being deformed for a long period. Hydrogels consist of polymers combined with water to create a solid with certain water like properties, such as permeability for many water-soluble substances. Hydrogels are available in various structural and chemical forms, on which basis they have been broadly classified.

Traditionally, controlled release polymeric systems have been classified into matrix and reservoir types. Matrix systems are most commonly employed because of their ease in development, cost-effectiveness and better performance. However, these systems tend to follow Higuchi's model, wherein drug release is proportional to the square root of time. This leads to non-uniform release rates, continuously decreasing in the beginning and more rapidly thereafter. They key benefit of hydrogels for controlled drug delivery lies in the near constant release rates.

Preparation of hydrogel based drug product involves either cross-linking of linear polymers or simultaneous polymerization of monofunctional monomers or cross-linking with poly-functional monomers. Further, the mechanical strength of poorly cross-linked hydrogels

www.manaraa.com

can be adequately enhanced by various methods. Polymers form natural synthetic or semi-synthetic sources can be used fro synthesizing hydrogels. Usually, polymers containing hydroxyl, amine, amide, ether, carboxylane and suffocate as functional groups in their side chains are used.

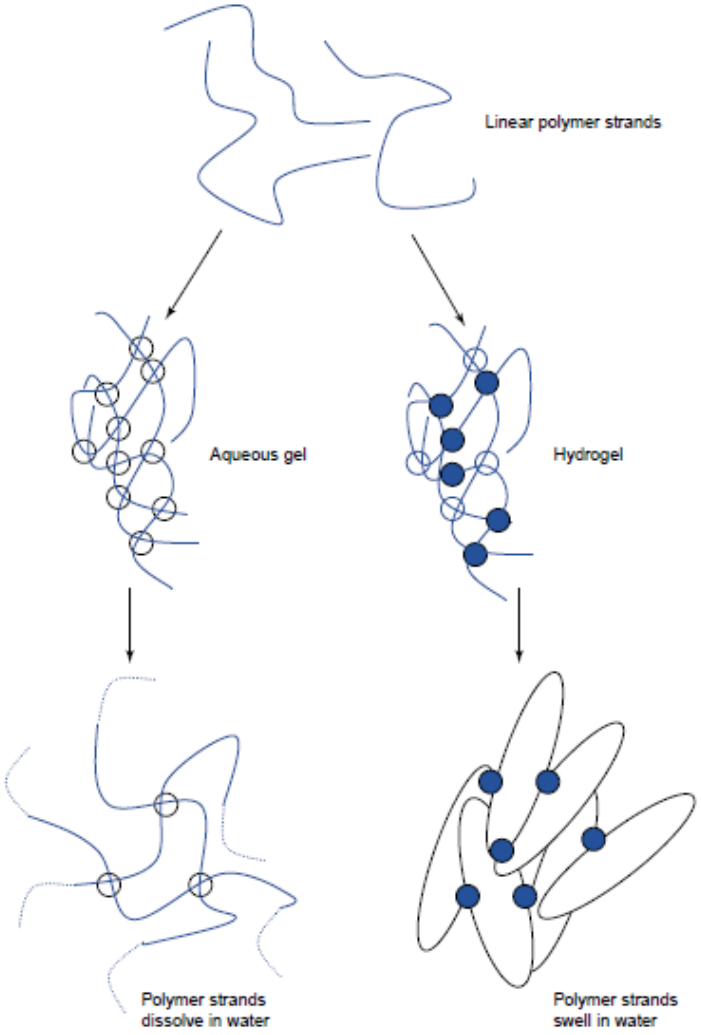

Figure 1-3 Polymer stands forming a gel and a hydrogel, showing different behavior in an aqueous environment. Solid circles represent covalent cross-links and hollow circles represent virtual cross-links formed by entanglements.

www.manaraa.com

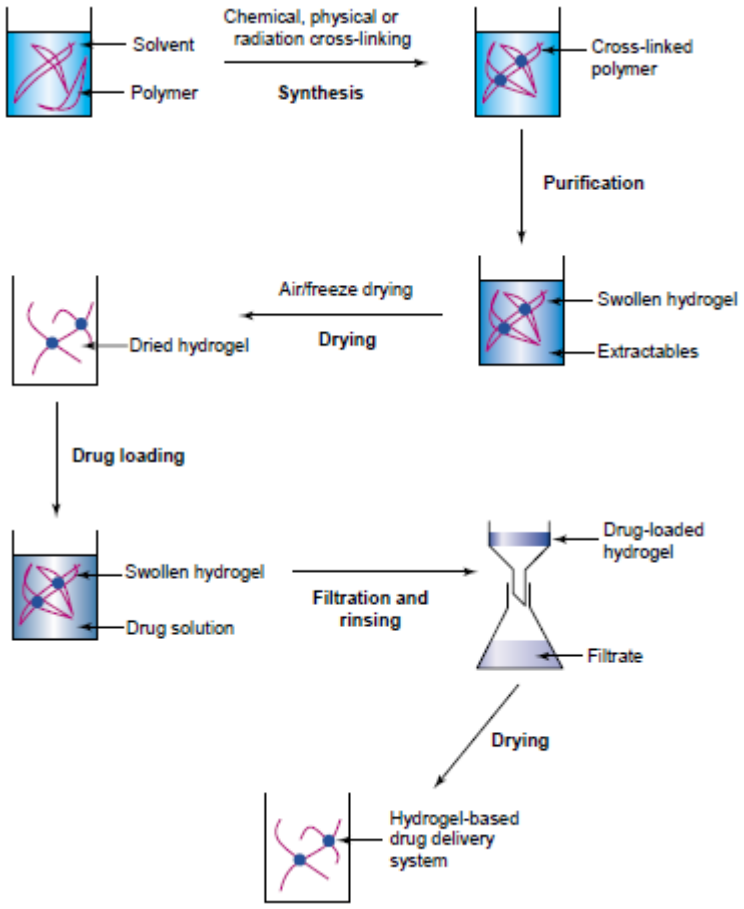

Figure 1-4 Schematic representation of the steps involved in preparation of a hydrogel-based drug delivery system.

Most of the hydrogels are glassy in their dehydrated state, and drug release generally involves simultaneous absorption of water and desorption of drug via a swelling controlled mechanism. The rate-controlling factor mediating drug delivery is the resistance of the polymer to an increase in volume and change in shape. A glassy hydrogel, on coming into contact with water or any other thermodynamically compatible medium, allows solvent penetration into free spaces on the surface between the macromolecular chains. When enough water has entered the matrix, the glass transition temperature of the polymer drops to the experimental temperature. The presence of solvent in a glassy polymer causes the

www.manaraa.com

development of stresses that are accommodated by an increase in the radius of gyration and end-to-end distance of polymer molecules, which is seen macroscopically as swelling. The movement of solvent into the dry polymer matrix takes place with a well defined velocity front and a simultaneous increase in the thickness of the swollen region with time in the opposite direction. Such swelling and diffusion do not generally follow a Fickian diffusion mechanism. The existence of a slow macromolecular relaxational process in the swollen region is believed to be responsible for the observed non-Fickian behavior.

The past few years have witnessed great advances in polymer-based controlled release drug deliver system .Several products displaying constant or decreasing releasing rate have progressed from the lab to the clinic in the short period of time. Most of these systems are therapeutically advantageous over conventional systems, but are insensitive to changing metabolic states in the body. To synchronize the drug release profile with physiological conditions, mechanism are responding to physiological variations must be provided. An ideal drug delivery system should respond to physiological requirements, sensing the changes and accordingly change the drug-release profile as desired. Thus, drug delivery patterns need to be optimized for pulsed or self-regulated mechanisms.

Hydrogels can exhibit dramatic changes in their swelling behavior, network structure, permeability or mechanical strength in response to different stimuli, both internal and external to the body. Various stimuli that have been explored for modulating drug delivery are presented in Figure 1-5. The mechanisms of action of these stimuli on structural changes in the polymer network and corresponding modulation in drug release have been well studied. External stimuli have been produced with the help of different stimuli generating

www.manaraa.com

devices, whereas internal stimuli are produced within the body to control the structural changes in the polymer network and to exhibit the desired drug release. Much research has been directed towards single-stimulus responsive hydrogel for drug delivery. This might not be advantageous in pathological conditions with more than one physiological stimulus present, where drug release is required in the presence of both stimuli rather than a single one.

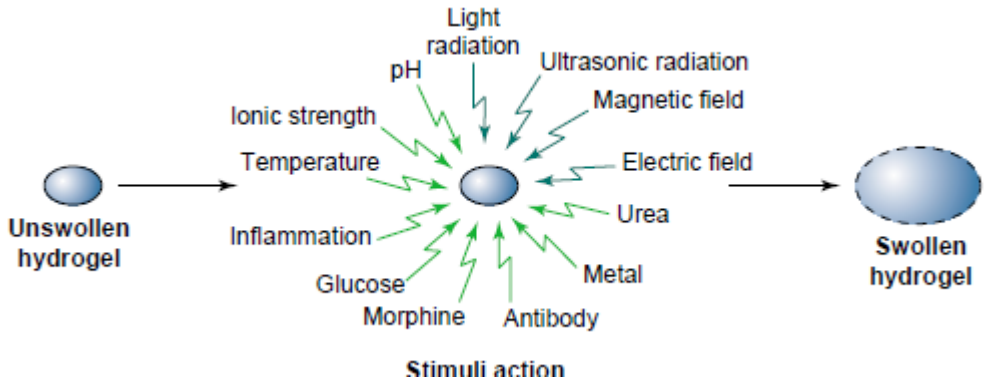

Figure 1-5 Stimuli responsive of swelling of hydrogels

Variations in pH are well known to occur at several body sites, such as the gastro-intestinal sites and blood vessels. The pH variations of these locations can provide a suitable base for pH sensitive drug release. Besides, local pH changes in response to specific substances can be generated and used for modulating drug release. The pH-responsive drug delivery system has been targeted for controlled drug release. pH responsive hydrogels are composed of polymeric back-bones with ionic pendant groups. Most commonly studied ionic polymers for pH sensitive behavior include poly (acrylamide) (PAAm), poly (acrylic acid) (PAA), poly (methacrylic acid) (PMAA) and poly (dimethylaminoethylmethacrylate) (PDEAEMA) and poly (dimethylaminoethylmethacrylate) (PDMAEMA). In aqueous medium of appropriate pH and ionic strength, the pendant groups ionize and develop fixed

www.manaraa.com

charges on the polymer network, generating electrostatic repulsive forces responsible for pH responsive swelling or deswelling of the hydrogel, thereby controlling the drug release. Small changes in pH can result in significant change in the mesh size of the polymeric networks. Pedant groups of anionic hydrogels are un-ionized below and ionized above the pKa of the polymeric network, leading to swelling of the hydrogel at a pH above the polymer pKa because of a large osmotic swelling force by the presence of ions. The reverse is the same for cationic hydrogels, which swells at lower pH. Differential swelling of ionic hydrogels in acidic and alkaline buffers is present in Figure 1-6.

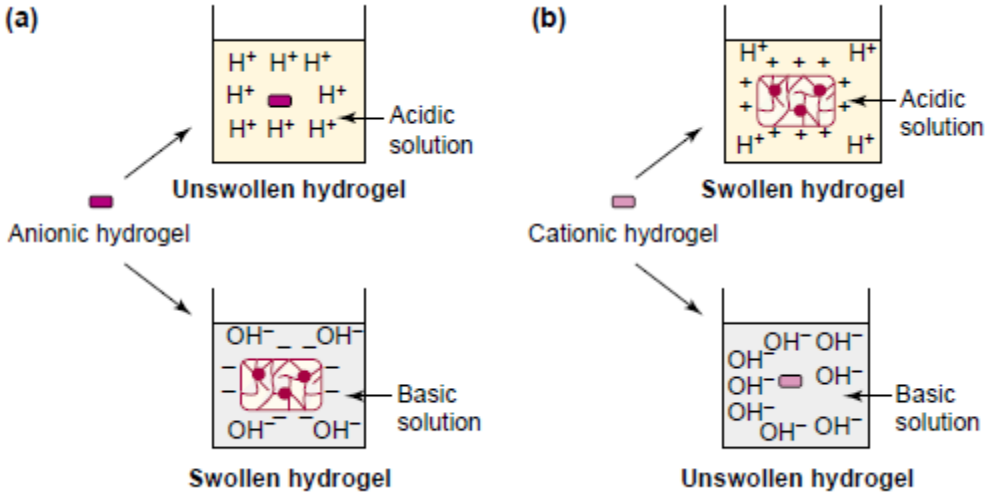

Figure 1-6 The pH responsive swelling of (a) anionic and (b) cationic hydrogels.

Apart from the use of synthetic polymers, various natural polymers, such as albumin and gelatin have also shown pH responsive swelling behavior. Under appropriate conditions of pH and temperature, the linear polymers form helices in regions stabilized by extensive hydrogel bonding. These helices function as cross links holding the amorphous regions together. These proteins with minimal surface charge at their isoelectric point show extensive

www.manaraa.com

swelling at a pH away from their isoelectric point because of the development of high surface net-charge and increased electrostatic repulsive force.

Among the polymers that can respond to external stimuli, poly (N-isopropylacrylamide) (PNIPAAm) hydrogel has been widely examined as a smart drug delivery material due to its unique phase separation behavior upon external temperature changes. PNIPAAm hydrogels are well known for their discontinuous phase separation near their phase transition temperature or lower critical solution temperature (LCST) and exhibit a sudden shrinking in volume at a temperature right above LCST. This transition is mainly controlled by the rapid alternation in hydrophilicity and hydrophobicity among the hydrogel sub-groups, and thus structural collapse takes place upon heating.

Various studies have proposed a novel class of hydrogels that exhibit pH and temperature sensitive swelling property. These materials could rove extremely useful in enzymatic applications and protein drug delivery. Hydrogels made of poly (N-isopropylacrylamide) PNIPAAm and PAA exhibited dual sensitivities. PNIPAAm is well known for its temperature sensitivity, and PAA and PMAA show pH sensitivity. These kind of hydrogels were able to respond rapidly to both temperature and pH changes. The application of this type of hydrogel has been used for the delivery of insulin and calcitonin. This type of polymers has also been engineered to gain faster respond time. Major factors that affect the degree of swelling of ionic polymers include the properties of the polymer, such as charge, concentration, and pKa of the ionizable group, degree of ionization, cross-link density and hydrophilicity or hydrophobicity, as well as the properties of the swelling medium.

www.manaraa.com

1.5 State of the Art Controlled Release Systems

Increasing efforts have been put into developing controlled release systems. Most of the recent controlled release systems employ smart materials as one of the most important component. As introduced in the previous sessions, these systems are usually environmentally sensitive. Several state of the art controlled release systems which are published recently are introduced in this session.

Abidian M. R. *et al*. reported a controlled release system employing conducting nanotubes, which are fabricated through conducting polymers [5]. Conducting polymers are of considerable interest for a variety of biomedical applications. Their responds to electrochemical oxidation or reduction can produce a change in conductivity, color and volume. A change in the electronic charge is accompanied by an equivalent change in the ionic charge, which requires mass transport between the polymer and electrolyte. Electrochemical actuators using conducting polymers based on the principle have been developed by several groups. They can also be used to dope with bioactive drugs, and can be used in actuators such as microfluidic pumps. The researchers reported that their method can be used to precisely control drug release. The fabrication process involves electrospinning of a biodegradable polymer, into which a drug has been incorporated, followed by electrochemical deposition of a conducting polymer around the drug loaded, electrospun biodegradable polymers. This will lead to a decrease of the impedance and increase of the charge capacity of the recording electrode. The controlled release is realized through responding to electrical stimulation applied on nanotubes.

www.manaraa.com

Conducting nanotubes are prepared using poly pyrrole (PPy) and poly (3,4-ethylenedioxythiophene) (PEDOT) in templated nanostructures for neural prosthesis applications. It is significant to minimize the electrode impedance for obtain high quality signals and PPy and PEDOT show potential in improving signal quality. PEDOT tubes have a well-defined internal and external surface texture further decrease the electrode impedance by increasing the effective surface area for ionic to electrode charge transfer to occur at the interface between brain tissue and the recording site. The release of dexamethasone can be precisely controlled by external electrical signals. Nanofibers were prepared firstly by electrospinning biodegradable PLLA or PLGA on the surface of a neural probe, and then deposit conducting polymers electrochemically.

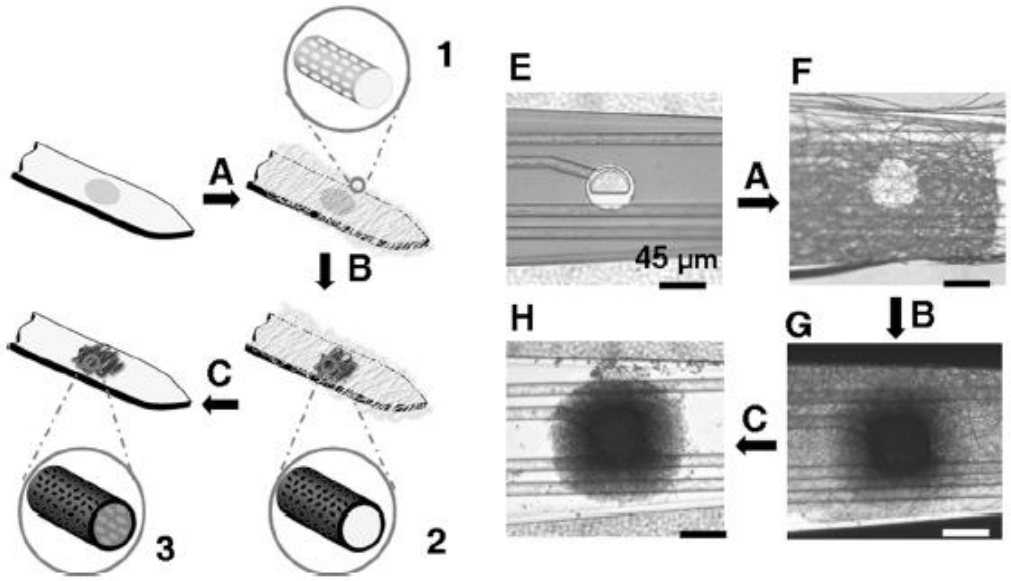

Figure 1-7 Schematic diagrams illustrating the surface modification of neural microelectrodes to create nanotubular PEDOT. A) Electrospinning of PLGA fivers. B) Electrochemically polymerization of conducting polymers. C) Dissolving the electrospun fibers to create nanotubular conducting polymers. E) Gold electrode surface F) The electrode surface after electrospinning of nanofibers. G) Electrode after electrochemical deposition of PEDOT polymers. H) Electrode after removal of core nanoscale fiber templates.

www.manaraa.com

In their work, the decrease of impedance of the neural microelectrodes can be significantly decreased by about two orders of magnitude and the charge transfer capacity also increased dramatically by creating conducting polymer nanotubes on a gold electrode surface. Individual drugs and bioactive molecules are controllably released at desired points in time by using electrical stimulation of the nanotubes.

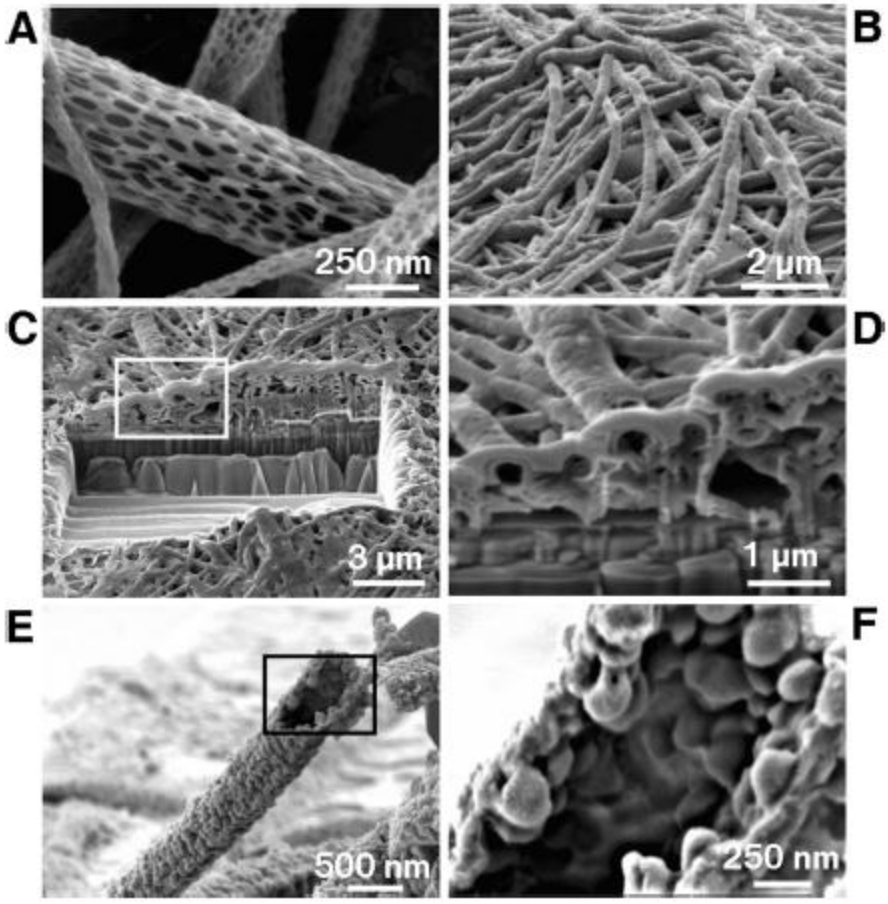

Figure 1-8 SEM micrographs of PLGA nanoscale fibers and PEDOT nanotubes. A) PLGA electrospinning fibers. B) Silicon substrate layer and PEDOT coating. C) PEDOT nanotubes crossing each other. D) Higher magnitude of C. E) Single PEDOT nanotube polymerized around a PLGA fiber. F) High magnitude E.

Slowing I.I. *et al.* reported a new structure called "Mesoporous silica nanoparticles" (MSN) as controlled release drug delivery and gene transfer carriers [5]. Mesoporous silicas,

www.manaraa.com

which are composed of a honeycomb-like porous structure with hundreds of empty channels (mesopores) that are able to absorb and encapsulate relatively large amounts of bioactive molecules. The unique properties, such as large pore volume and high surface area, and good chemical and thermal stability make them potentially suitable for various controlled release applications. While the meoporous silica nanospere are potentially useful for many significant applications in biotechnological and biomedical areas, these materials cannot be used as efficient agents for gene transfection or carriers for intracellular drug delivery because the mammalian cells cannot efficiently engulf large particles via endocytosis.

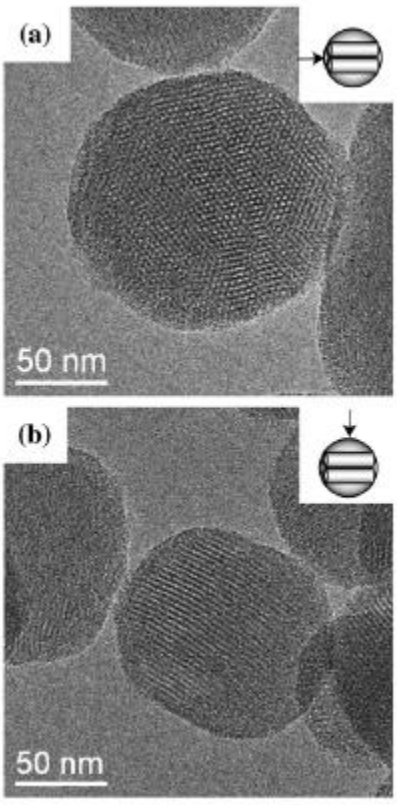

Figure 1-9 TEM images of MSN.

Besides, MSNs are within the size window of bacteria and could potentially trigger acute immune response in vivo. To circumvent these problems and concerns, they developed

www.manaraa.com

a synthetic approach for preparing a series of mesoporous siclica nanoparticles materials. The MSNs has several advantages over conventional counterparts, such as tunable particle size, stable and rigid framework, uniform and tunable pore size and etc. TEM of MSN particles are reprinted in Figure1-9. MSN based controlled release systems have demonstrated to be able to delivery different kinds of guest molecules. The loading is usually in the order of hundred milligrams per gram of MSN. The molecules that have been used the most are imaging agents, such as fluorescein, texas red, and rhodamine B, with the main goal of testing the working principle of the stumulus controlled release drug and gene delivery system.

Radt *et al*. developed controlled release system using NIR laser [21]. Such a system is reacted to heat as a source stimulus. The microcapsule was intact before several nano seconds of NIR laser activation; however, after the activation of NIR laser nanocomposite capsule shell will rupture due to the presence of the metal nanoparticles as shown in Figure 1-10. Similarly, Shchukin *et al*. developed a ultrasound irritated system for drug release [11] (Figure 1-11). The disadvantage of these methods involves in complicate fabrication process, besides, shell rupture mechanism does not support sustained release, which means break shell also breaks the control mechanism simultaneously.

www.manaraa.com

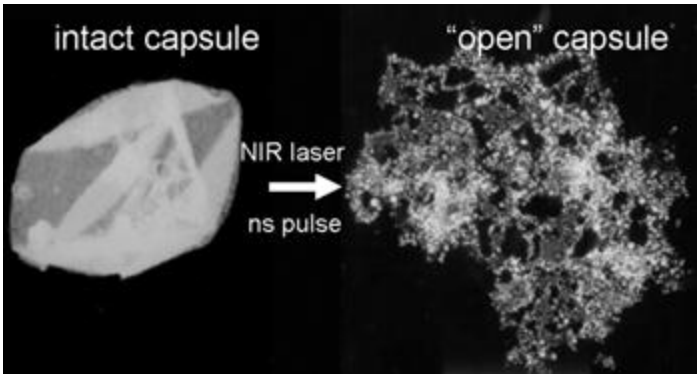

Figure 1-10 Optically addressable nanostructured capsules of polyelectrolyte multilayers containing gold nanoparticles are prepared via layer-by-layer colloid templating. The nanocomposite capsule shell, due to the presence of the metal nanoparticles, can be addressed with laser light in the near-infrared (NIR) to induce morphological changes in the capsules. Enzyme encapsulated within these capsules is released remotely and on demand with nanosecond laser pulses in the NIR, while retaining its activity.

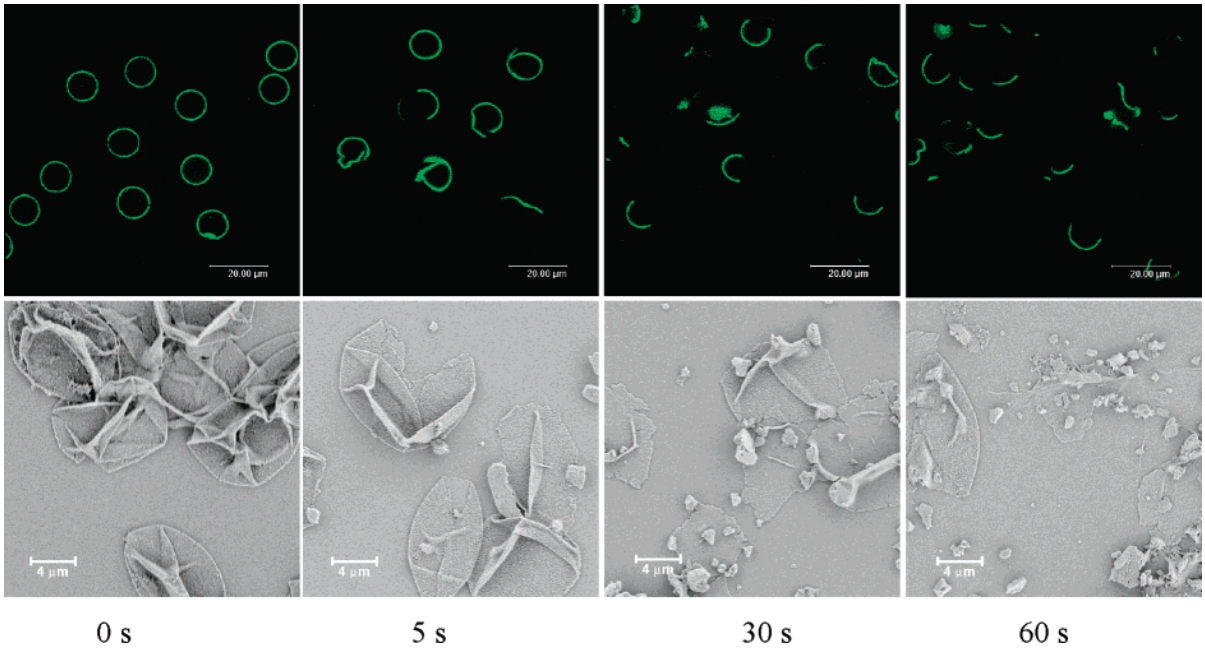

Figure 1-11 SEM (bottom panels) and fluorescence confocal (top panels) images of the Fe3O4/polyelectrolyte capsules, which were incubated at 70 °C for 90 min, treated by ultrasound (500 W) for different time durations.

www.manaraa.com

1.6 Challenges

Although controlled release systems have been extensively investigated in recent years, there still exist challenges in moving toward clinical usage with more efficiency, from both therapeutic effects and cost. Obviously, the success of this method hinges upon the ability to construct a biocompatible carrier that allows high loading of drug molecules without any premature release of the cargo before reaching the destination or a pre-define period of time. There are still many problems and concerns in real applications.

As stated in the previous sections, a variety of materials, polymers and hydrogels are already available due to the fast development of materials science and engineering. Although biocompatibility and biodegradability are the major concerns of using these carrier and actuator materials, other aspects of these materials need to be considered. For example, carrier material is used as a component in the drug delivery system and the compatibility of such material with respect to the drugs should be tested. The addition of carrier materials should not impact or interact with the drug pharmaceutical property. Otherwise, certain isolation mechanism is necessary to isolate the carrier material and drugs which obviously make the system design even complicated. Besides, carrier materials used in the controlled drug release system need also be compatible with fabrication process. Harsh fabrication process will denature material properties; these processes include high temperature, high pressure, chemical reactions and etc. These materials should keep their chemical and physical properties after fabrication process. All the actual concerns and problems make the selection of an appropriate material in a system a very difficult and significant step.

www.manaraa.com

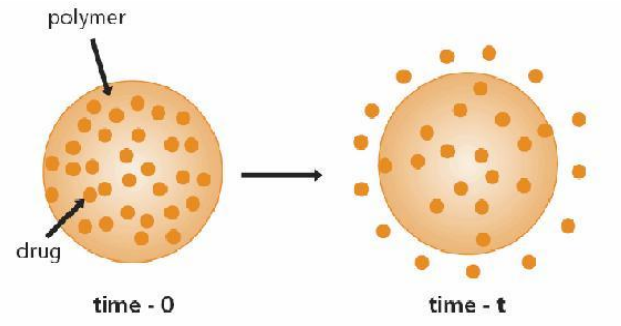

(a) Matrix diffusion system.

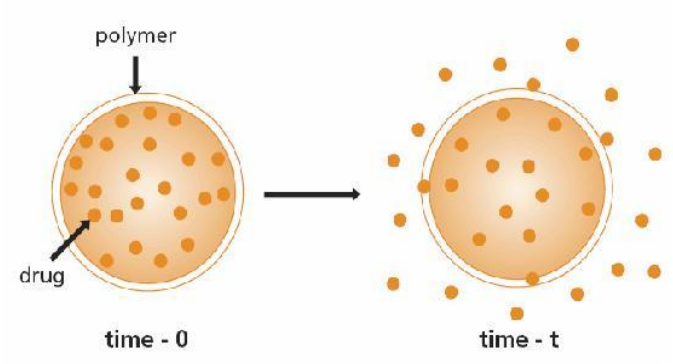

(b) Reservior release system

Figure 1-12 Matrix and reservoir system.

How the carrier and actuator materials will assist the controlled drug release is another difficulty in the design process. There are many different choices of integrating drugs and carrier, such as embedding drugs in the polymer matrix and encapsulating drugs in a hollow carrier material compartment, as shown in Figure 1-12. The employment of integration format depends on the device requirements, such as drug loading capacity and drug regulation profile. Current drug delivery applications favor a high loading capability to reduce the cost of carrier materials as will as the size of the device. The integration of drug and its carriers should add minimum volume compared to the drug itself. In terms of this, encapsulation of drugs method is more effective than embedding drugs in carrier matrix. However, encapsulation usually requires a more complicate and delicate fabrication process.

www.manaraa.com

Leakage is another important concern in real applications. Here, leakage is defined as the amount of drug released during device travelling to desired location, or during the period of time in which the device is waiting for certain receptor or stimulus. All these premature release is highly undesirable, which will impact the prior efforts in improving drug loading and the total effectiveness of the drug release system. Therefore, leakage is a good criterion to check how good the carrier material is to resist body environment during travelling as well as how effective the control mechanism when there is zero stimulus. Therefore, controlled release mechanism with the ability to respond to certain stimulus is highly preferred comparing to conventional diffusion release system where leakage is a major concern.

The easiness of fabrication to achieve a certain drug delivery system decides the cost and time in the developing process. Previous examples shown above employ smart or intelligent control mechanism (electrical, NIR, ultrasound and etc.) to release internal loadings. However, the fabrication process is non-trivial. Complicated multiple steps involves in these processes which will also bring difficulties in materials selection.

Last but not least, the release rate and the response of the controlled drug release system is another critical factor. A proper rate of release is needed to quickly achieve an effective local concentration. These features depends not only on the control mechanism employed, however, also rely on the smart materials employed in the systems.

Highly integrated fabrication process employing elelctrospinning technique incorporated with intelligent hydeogel material in drug release control mechanism is the core of this work. Such sytems could be further applied in pharmaceutics, biomeidical science and biotechnologies.

www.manaraa.com

CHAPTER 2. ELECTROSPINNING TECHNIQUE

2.1 Introduction to Electrospinning

Electrospinning, a technique first patented in 1934 and first known as 'electrostatic spinning' in 1993, is widely used to produce high volume continuous ultrathin fibers and is drawing more research interests since 2000 (Figure 2-1 [12]). Comparing with other techniques producing fibers or other one dimension structures, such as mechanical drawing, chemical synthesis, electrospinning is a 'drawing' method based on electrostatic interactions and is one of the simplest methods with high efficiency in producing fibers with nano and micrometer resolutions. These advantages of electrospinning make it a promising technique in traditional textile engineering. Besides, continuous electrospun fibers with high surface area show application potentials in neural and tissue engineering.

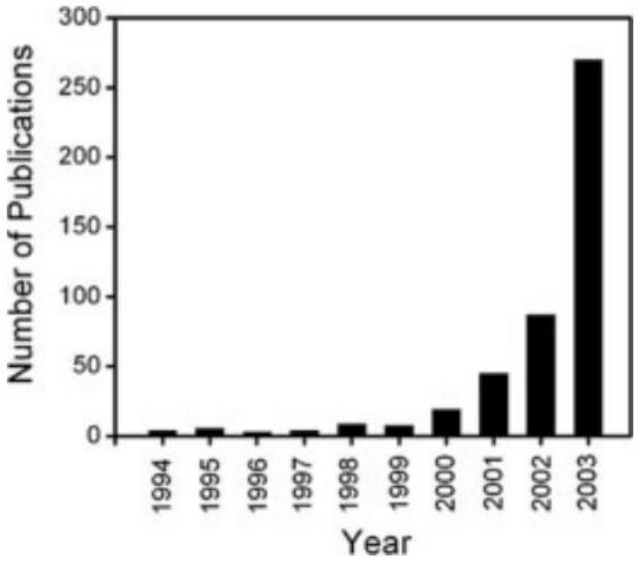

Figure 2-1 Annual Number of Publications on the subject of electrospinning.

www.manaraa.com

Over the last decades, over thirty synthetic and natural polymers were successfully electrospun into fibers with diameters varying from nanometers to micrometers. Polymers which could be used in electrospinning include water soluble polymers such as poly (ethylene oxide) (PEO) and poly (vinvy alcohol) (PVA), and many types of polymers needs organic solvents such as poly lactide (PLA), poly styrene (PS), poly (methylmethacrylate) (PMMA), polyamides, polyimides, polycaprolactone, and polyvinvylidene fluoride. Figure 2-2 shows the product of electrospinning fibers from different polymers.

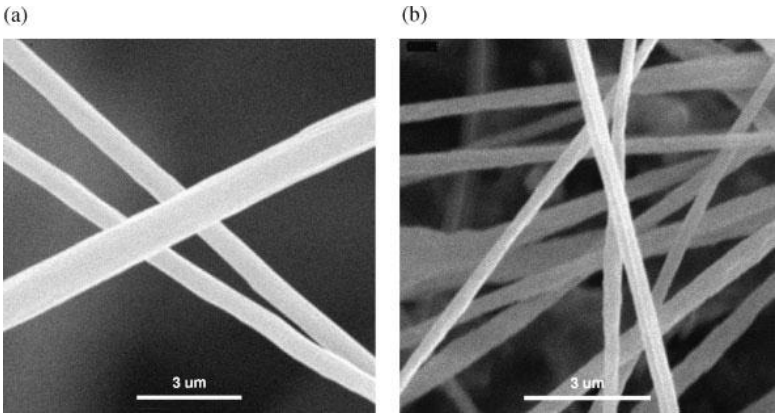

Figure 2-2 Electrospun nanofibers from different polymers. (a) Cellulose acetate from 5% solution in dichloromethane/ethanol, 9:1, (b) Polyvinylidene difluoride from 15% solution in dimethylformamide/tetrohydrofuran, 1:1.

A basic electrospinning setup contains at least three components: A DC voltage power supply (usually can provide up to several kilo-volts voltage), a grounded conductive collector and a spinneret (needle) loaded with electrospinning materials (polymers or other composites). High DC voltage is applied at the end of the spinneret and a high electrical field is formed between the spinneret and the grounded conductive collector. Under such a high electrical field, liquid polymer at the nozzle of the spinneret is electrified and charges are induced on the polymer surface. A 'Taylor cone' structure is formed due to the electrostatic repulsion between surface charges and Coulombic force exerted by the electrical field. When

www.manaraa.com

the electrical force overcome the Taylor cone surface tension, liquid jet will eject from the nozzle towards the conductive grounded collector. With the evaporation of polymer solution, fibers are deposited randomly on the grounded collector surface.

Electrospinning is a multi-factor process involving electrostatics, hydrodynamics, and mechanics. The formation of Taylor cone and the ejection of polymer liquid jet by external electric field is a coupled electro-hydrodynamics problem which attracts considerable research interests. It was initially misunderstood that multiple jets ejected from the Taylor cone simultaneously due to its high speed jet motion, however, recent high speed photograph proves that the conical envelope contains only one very fast moving jet with irregular moving trajectory. Theoretical efforts are trying to interpret this complicate electro-hydrodynamics phenomenon. Reneker D.H. *et al.* developed a general electro-hydrodynamics model of a weakly conductive viscous jet accelerated by an external electrical field [7]. The model takes into account inertial, hydrostatic, viscous, electrical and surface tension factors. Polymer fluid was described by nonlinear rheologic constitutive equation. This mathematics model agrees with experimental electrospinning process. This theoretical analysis will help in understanding the issues and difficulties in designing new experiments.

The versatility of electrospinning also exhibits on its compatibility on different materials. Such a great feature has gained significant attention due to the huge application potential for manifold applications in optics, electronics, biology, medicine, and etc. Many natural and synthetic polymers have been successfully used in electrospinning process. Water soluble poly (ethylene oxide) (PEO) has been widely used with or without the addition of another type of polymer. PEO solutions were used in electrospinning to investigate the

www.manaraa.com

fundamental properties of experimental properties. Synthetic polymers such as water non-soluble poly (lactic acid) (PLA), poly (lactic-co-glycolic acid) (PLGA) are also widely used polymers in electrospinning applications.

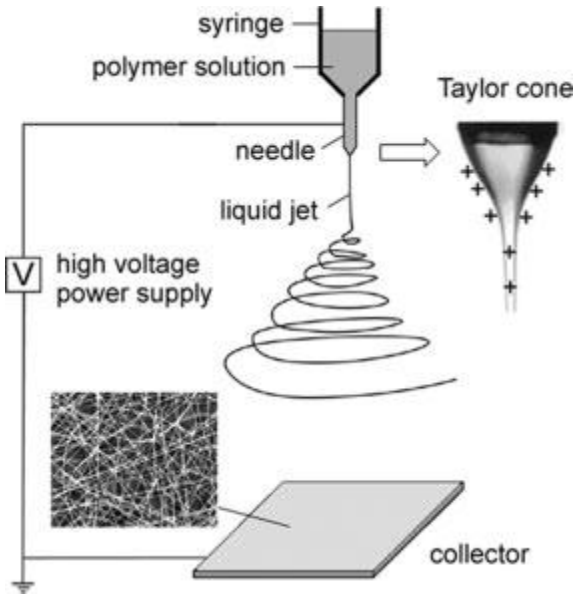

Figure 2-1 Basic Electrospinning Setup [23]

Natural macromolecules are recently found to be compatible with electrospinning; collagen and fibrinogen have been processed into fibrous non-woven scaffolds for biocompatible applications. Although the eligibility of multi types of polymers has enhanced the application of such technique to a great extend, other contributions have focused on the preparation of ultrafine fibers through electrospinning using materials other than polymers. Metal oxide electrospun fibers, such as TiO2 and CuO have been published. Pure copper metal electrospun fibers have recently been reported [13]. Long copper nanofibers were prepared by electrospinning of copper nitrate-polyvinylbutyral (PVB) solutions to composite fibers followed by thermal treatment in air and then followed by thermal treatment in a hydrogen atmosphere. With the join of metal and metal oxide nanofibers, applications of

www.manaraa.com

electrospinning have been greatly enhanced due to better mechanical properties and thermal stabilities.

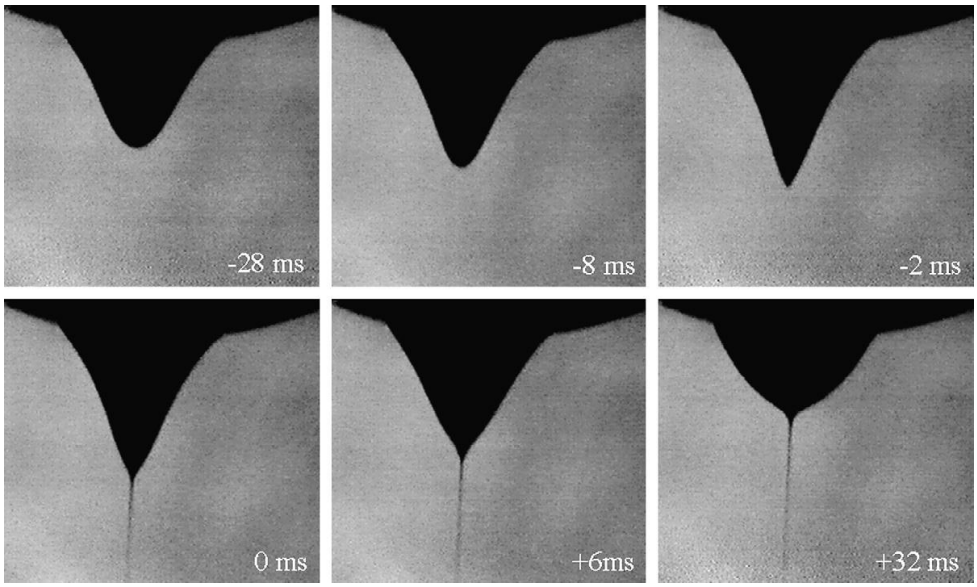

Figure 2-2 The evolution of the shape of a fluid drop in selected images from a video in which a new image was recorded every 2 ms.

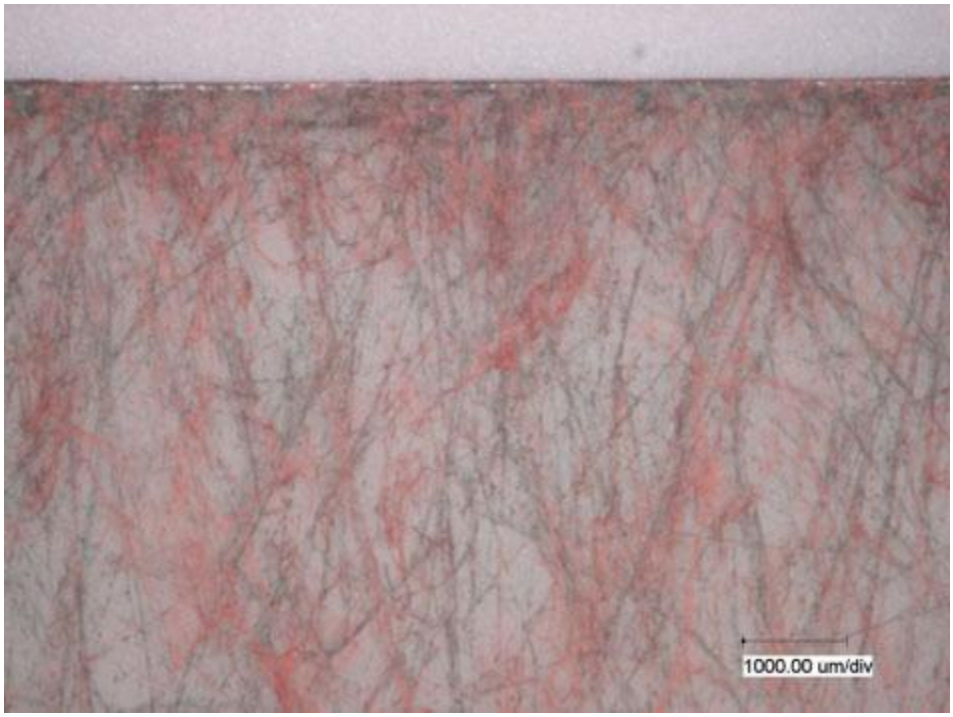

Figure 2-3 Microscopic image of sub-micrometer copper fibers on a thin mica slide [13].

www.manaraa.com

2.2 Applications of Electrospinning

The development of electrospinning technique was driven and accelerated by the multi-disciplinary applications of electrospinning products. Recently, there is an increasing growing trend in the production and deliberate manipulation of nanoscale 3D structure to study cell functions in tissue engineering. The key tasks of tissue engineering are to create a two dimensional or three dimensional scaffolds with suitable degradation rate to meet the requirements of new tissue growth; to supply interconnected pores for cell-cell and cell-matrix communications and to bring cells together to form a tissue. Three methods could be used for the fabrication of nanofibrous scaffolds, which are phase separation, self assembly and electrospinning. As already proved, many synthetic and natural materials, including biocompatible and biodegradable could be applied in electrospinning technique. These materials include but not limited to collagen, poly (e-capralactone) (PCL), ploy (D-lactide) (PDLA) and poly (L-lactide) (PLLA). Electrospinning offers a rapid and effective way to produce scaffolds with nanoscale elements and has been applied across a board range of synthetic and natural polymer systems. The highly porous electrospinning scaffolds offer a wide variety of topographical features to support cellular adhesion and proliferation. It is well known that extracellular environment influences many aspects of cell behavior such as cell morphology, functionalities and cell-cell interactions. Electrospinning fibrous scaffolds could be engineered to change the porosity, mechanical strength, and other parameter to better study the effect of ECM to the growth of cells. Besides, the random nature of the fibers could be changed to get fibers with special pattern and orientation. These oriented fiber scaffold can be used to guide the cell growth and related studies. However, there are still many

www.manaraa.com

unknown factors such as the best fiber diameter and the average distance between internal neighbor fibers to optimize cell function. Another obstacle to mimic the natural ECM using electrospinning scaffolds lies in the bio-mechanical property of fibers. Other materials, such as polymeric-ceramic composite fibers have been investigated to enhance fiber bonding and mechanical properties. Recently, more efforts have been put to develop 3D fibrous structure to further mimic the architecture, functionalization and interfacial properties of natural ECM.

The application of electrospinning products has been extended to highly sensitive detection techniques [8]. Electrospun nanofibrous membrane has been applied in highly sensitive and cost effective optical sensors. The underlying principle of such an application is: the sensitivity of a sensor that detects analytes by interacting with molecules on the surface will increase with increasing surface area per unit mass. Therefore, increasing the sensing surface area is important for detection sensitivity. An inherent nature of electrospinning fibrous structure is its high surface to volume ratio. Electrospun nanofibrous membranes could have approxiamately 1 to 2 orders of magnitude more surface area than conventional thin films. It is therefore believable that the large surface area of electrospun nanofibrous membranes has the potential to provide unusually high sensitivity detection ability in sensing applications. Wang *et al.* reported using electrospun nanofibrous membranes as highly responsive fluorescence quenching-based optical sensors for metal ions. A fluorescent polymer, poly (acrylic acid)-poly (pyrene methanol) (PAA-PM) was used in this application as an sensing material. Their preliminary results show that the sensitivities of electrospun nanofibrous membranes to detect metal ions are 2 to 3 orders of magnitude higher than those obtained from traditional thin film sensors.

www.manaraa.com

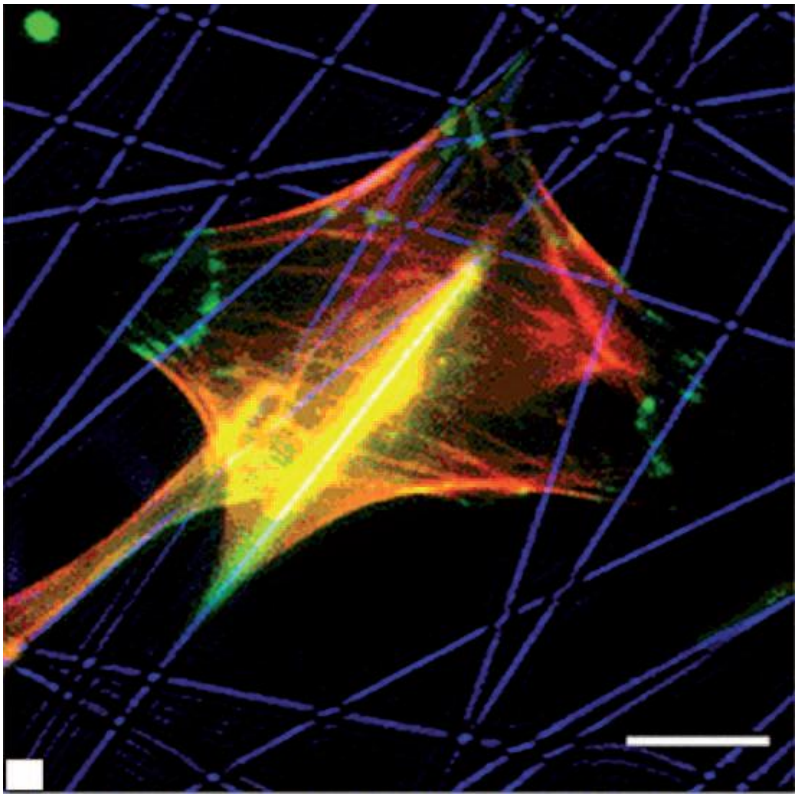

Figure 2-3 Immunofluorescent staining of adherent MC3T3-E1 cells has been super-imposed onto a phase contrast image of PDLLA fibers (red). The green corresponds to vinculin and the blue is the actin.

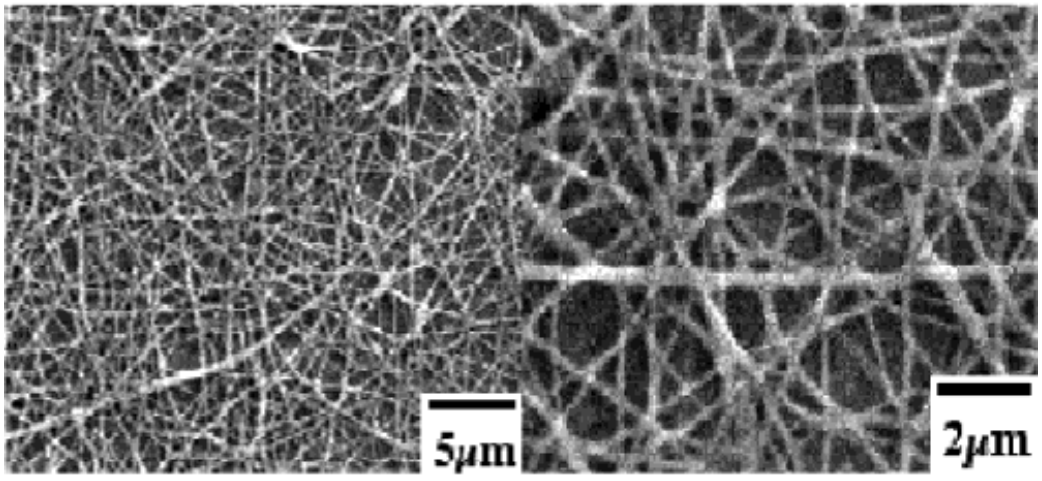

Figure 2-4 SEM images of electrospun nanofibrous membrane as highly sensitive detectors [8].

Electrospinning fibers have also been successfully applied in drug release area. Polymeric drug delivery systems have numerous advantages compared to conventional

www.manaraa.com

dosage forms, such as improved therapeutic effect, reduced toxicity, convenience and etc. Bio-degradable polymers provide sustained release of encapsulated drugs and degrade in the body to nontoxic, low molecular weight product that is easily eliminated. However, there are still many problems to be solved, such as the low efficiency of preparing nano and micro particles and vesicles is not high, and the control and regulation of the drug release profile. Recently, researches have shown that drugs can be encapsulated directly into electrospun fibers and these systems showed nearly zero order kinetics of drug release. In some applications, poly(L-lactide acid) (PLLA) was used as a carrier to contain drugs, additional surfactant might be added to change the diameter of the fibers in order to regulate the dynamics parameter as well as degradation time of the drug release systems. Drugs are mixed with the carrier and produced in the form of nano and micro fibers and are released from the fibrous membranes. The drug release profile and polymer matrix degradation profile are functions of electrospun fiber characteristics and carrier properties. Due to the cost-effective high yield nature of electrospinning process, electrospinning seems to be the only method which can be further developed for large scale production of continuous nanofibers for industrial applications.

Another area nanofibers involve in is filtration which is very necessary in many engineering fields [9]. Fibrous materials used for filter media provide advantages of high filtration efficiency and low air resistance (Figure 2-5). Filtration efficiency associates closely with the fiber fineness, which is one of the most significant factors in filter performance. Beside the applications mentioned above, electrospinning products have a

www.manaraa.com

broad range of applications, such as materials science and engineering, textile engineering, biomedical engineering, electrical engineering and etc.

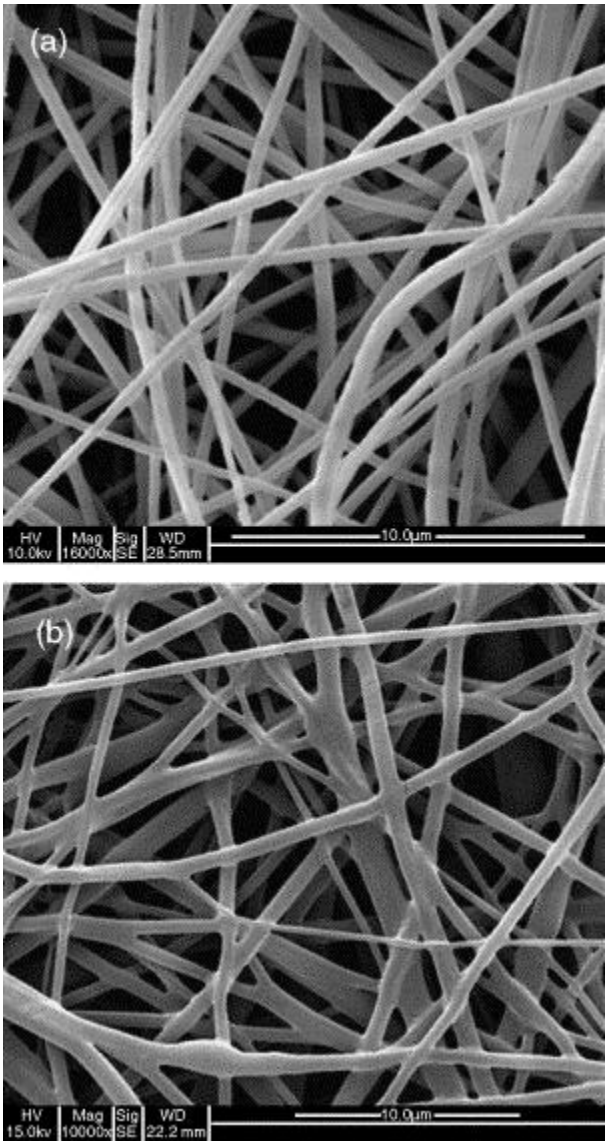

Figure 2-5 FESEM micrographs of electrospun PVDF membrane (a) before and (b) after heat treatment.

www.manaraa.com

2.3 Co-axial Electrospinning

Core-shell fibers, as another one dimension nanostructure start to draw interests, since core-shell structures could further enhance material properties for the single layer fiber applications. There exist multiple fabrication technology to fabricate core-shell nanofibers, including template coating, laser ablation and etc. Another powerful feature of electrospinning is the ability to produce core-shell structures. Sun *et al*. reported their work of using co-axial electrospinning (co-electrospinning) to produce core-shell fibers of two types of polymers. With co-electrospinning, two components can be coaxially and simultaneously electrospun through different feeding capillary channels to generate composite nanofibers in the form of core-shell structure. In their research, nanometer core-shell fibers made of two polymers poly (ethylene oxide) (PEO) and polysulfone (PSU) were fabricated using co-electrospinning [10].

Another successful application of using co-electrospinning is to fabricate hollow fibers. It has been demonstrated that a variety of materials such as polymers, ceramics and carbon could all be prepared as uniform fibers by electrospinning, with controlled size, compositions and morphologies. McCane *et al.* shows that with the use of a coaxial, dual capillary spinneret hollow titania fibers could be fabricated using co-electrospinning. Fabrication of hollow fibers by co-electrospinning a poly (vinvy pyrrolidone) (PVP) solution containing a titanium alkoxide and mineral oil, followed by selectively removal of the liquid core and calcination. The inner diameter and wall thickness of these hollow fibers could be readily varied from tens nanofibers to several hundred of nanometers by controlling the experimental parameters.

www.manaraa.com

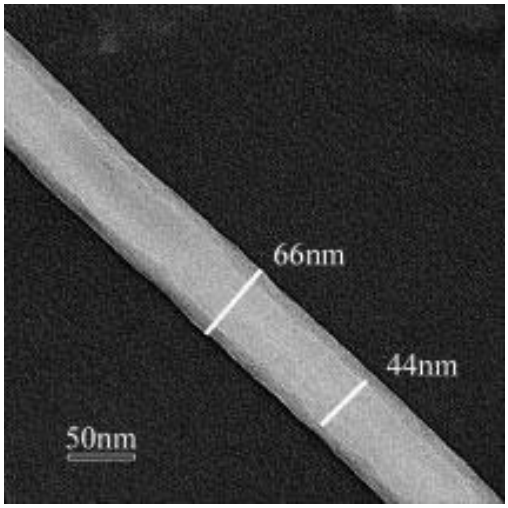

Figure 2-6 TEM of compound nanofibers. Core and shell solutions are PSU and PEO respectively [10].

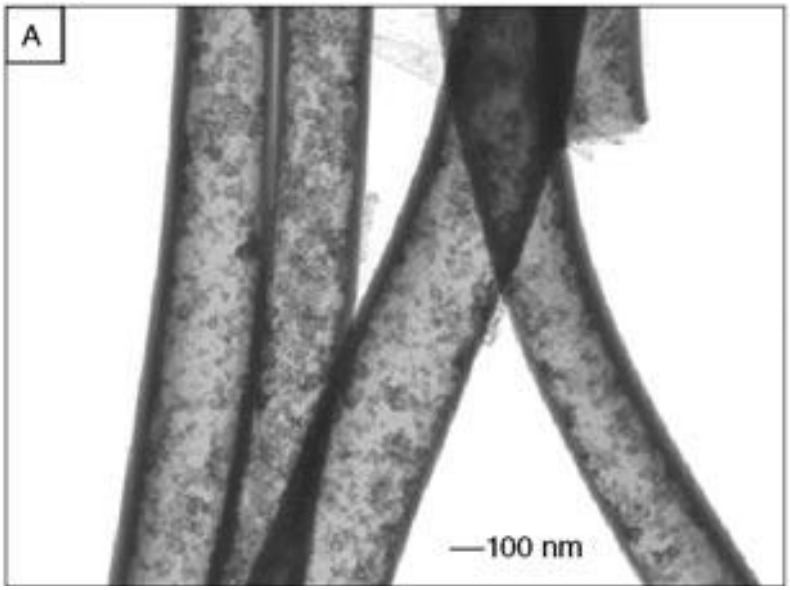

Figure 2-7 Hollow fibers fabricated by co-electrospinning [14].

www.manaraa.com

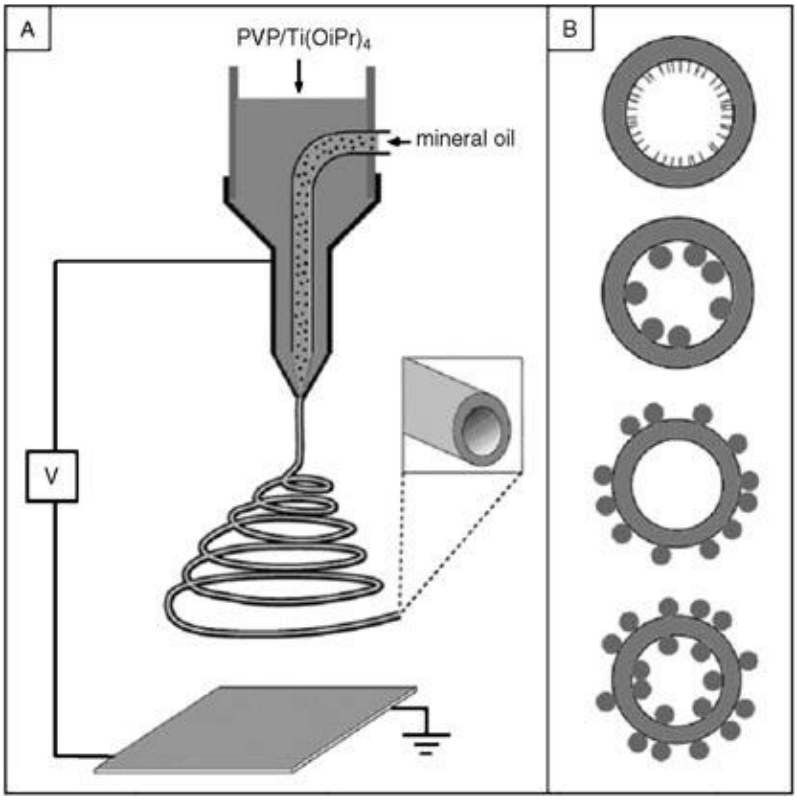

Figure 2-8 Schematic illustration of the setup that used a dual-capillary spinneret to directly electrospun hollow fibers [14].

Encapsulation is a common approach for protecting substances of interest from harsh environments. Within this broad setting, there are situations in which it is important that the encapsulated materials are divided into tiny quantities with characteristic sizes in the micro or nanometer range. Examples can be found in drug delivery, where, in order to survive and overcome biological barriers, capsules carried in the blood stream need to have diameters smaller than a certain threshold, usually below a few hundred nanometers. There are many different methods in which the final product consist of clusters of micro or nanocapsules in the form of powder, or dispersed in the form of an emulsion. The framework of encapsulation has been broadened by the use of electrified coaxial micro and nanojets for coaxial electrospinning of two different liquids. This method allows one step fabrication of

www.manaraa.com

micro and nano tubes. The products of co-electrospinning are all structures with radial anisotropies. Co-electrospinning has been used to encapsulate labile materials other than polymers within fibers. However, there are many situations in which hydrophobic materials need to be encapsulated by hydrophilic polymers in the form of fibers. There requirements exist in drug delivery and cosmetics. Co-electrospinning provides a simple solution for such a complicate structure which would have applications in various technological fields, such as drug delivery [11].

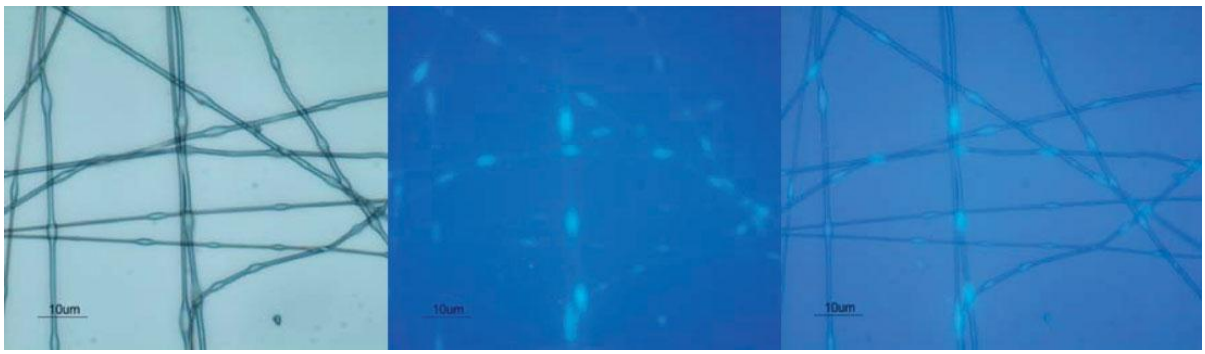

Figure 2-9 Optical Images of PVP-oil fibers.(a) visible light (b) UV light (c) overlap of (a) and (b).[11]

www.manaraa.com

CHAPTER 3. SELECTIVE DEPOSITION OF ELECTROSPUN NANOFIBERS USING MICROFLUIDIC CONFINEMENT APPROACH

3.1 Introduction to Electrospun Fiber Patterning

Electrospinning is an economical and versatile technique to fabricate continuous nanofibers [12]. The basic principle of electrospinning is that a Taylor cone of a polymer solution is formed at the tip of a metallic spinneret by applying a high voltage between the spinneret and a grounded collector. When the electrostatic repulsion within the charged polymer solution overcomes the surface tension, a charged fluid jet is ejected out of the spinneret, traveling through the air with solvent evaporation. Finally, nanofibers are deposited on the collector. A number of polymeric, metallic, and ceramic nanofibers have been realized through electrospinning [13,14]. Among them, electrospun nanofiber biomaterials possess highly porous structures with numerous interconnected nanopores, resembling the architecture of natural extracellular matrix (ECM). Therefore, nanofiber-based artificial ECM scaffolds have recently attracted much attention and have shown great promises for musculoskeletal, skin, vascular, and neural tissue engineering applications, where they serve as excellent frameworks to improve cell adhesion, proliferation, and differentiation [14-21].

To maximally mimic natural ECM scaffolds, it is crucial to develop the ability of creating structurally complex and high-definition shapes of nanofibers on substrates. For example, research on regenerative medicine has revealed that tissue formation relies considerably on the spatial orientation and distribution of the artificial scaffolds that control

www.manaraa.com

and guide cell growth and proliferation [22]. However, achieving micro-sized, structurally accurate, arbitrary-shaped patterns of nanofibers remains challenging. Current research to this topic is carried out in three major areas. The first area is to control the spatial orientation of nanofibers on collectors by overcoming the random deposition process of conventional electrospinning [23-33]. In this area, nanofiber alignment has been successfully accomplished by manipulating the applied electrostatic field through various modifications to collectors, including using paired conductive silicon strips separated by a void gap [23], multiple metal electrodes with particular configurations formed on an insulting substrate [24], and two pieces of conductive blades placed in line with a gap in between [25]. Other interesting fiber alignment strategies include the use of a rotating collection drum, a wheel-like bobbin or metal frame, and near-field electrospinning [26, 27]. The second area aims at forming patterned electrospun mats to realize controlled spatial distribution of nanofibers. To this end, many important and promising technologies have been reported. For example, conductive collectors with insulating regions of different areas and geometric shapes [30], woven wire fabric substrates [31], and enamel-coated steel sheets [32] have been employed to obtain electrospun mats with different patterned architectures. The third area is related to the selective deposition of nanofibers in discrete regions on collectors [33-39]. In this direction, movement of a collector during electrospinning provides a straightforward approach to discrete placement of nanofibers [34]. The resulting nanofiber patterns, however, have a low definition of shapes at the millimeter scale. Although electrodynamic focusing of nanofibers has been demonstrated to achieve micro-spots of nonwoven nanofibers on a collector, this technology requires a secondary electric field created by a specially designed electrostatic lens [35], or a metal-coated shadow mask [36]. Recently, conventional

www.manaraa.com

photolithography has also been utilized to form discrete nanofiber patterns, although maintaining the morphological appearances and material properties of electrospun mats after multiple processing steps (spin coating of photoresist, soft baking, exposure, development, dry/wet etching) still remains a challenge. Other technologies for selective formation of nanofibers include using electrical discharge and femtosecond laser micromachining. We present a simple and versatile method for selective deposition of nanofibers using a unique microfluidic collector, allowing formation of high-definition micro-patterns of nanofibers on a glass substrate for cell biology and tissue engineering. This research falls in the third area mentioned above.

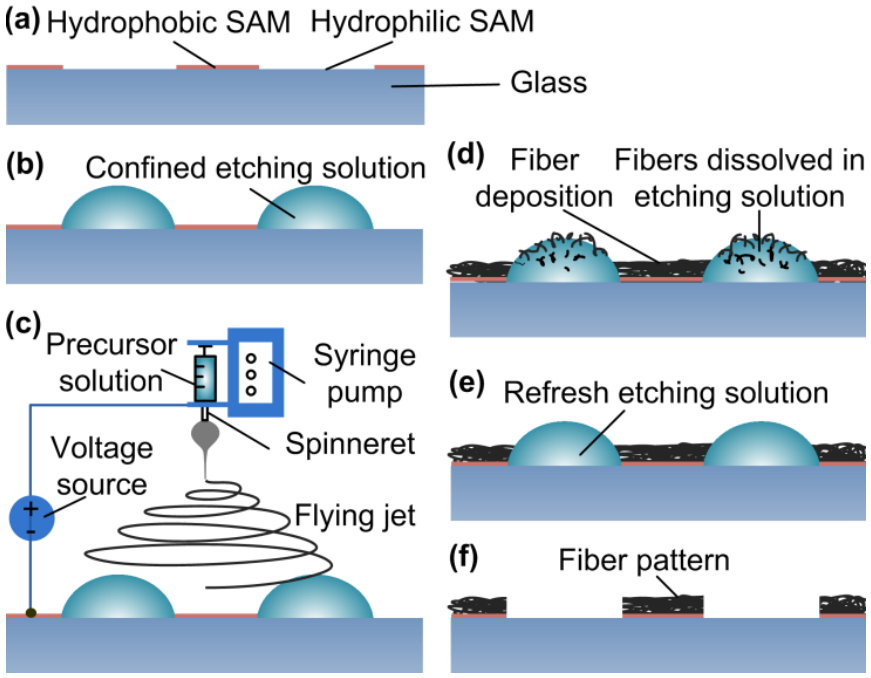

Figure 3-1 Process for selective fiber deposition. (a) The hydrophilic and hydrophobic regions are selectively patterned on the fiber collector surface using the photocleavable SAM technology. (b) The water-containing fiber etching solution is flowed to t the hydrophilic region via microfluidic filling, and is confined to that region due to the surrounding hydrophobic surface. (c) The fibers are deposited onto the modified fiber collector using electrospinning. (d) The etching solution dissolves the fibers in the hydrophilic region. (e) Polymer residue from the hydrophilic region is washed away by flowing the refresh etching solution into that region. (f) The fiber patterns are formed.

www.manaraa.com

3.2 Concept of Microfluidic Patterning of Electrospun Fibers

Figure 3-1 illustrates the principle and process of the proposed technology for selective deposition of nanofibers. The method is to selectively pattern the affinity of different regions of the collector surface for appropriate water-containing fiber etching solution. The pattern region is hydrophobic that repels the etching solution; while its peripheral region is hydrophilic that attracts the etching solution (Fig. 3-1a). These regions are patterned by means of photocleavable self-assembled monolayer (SAM) technology that allows transferring hydrophobic/hydrophilic patterns from a photo mask to the fiber collector surface (*described in the Experimental Section*) [41]. The fiber etching solution used here is either pure water or a mixture of water and suitable organic solvent that is fully miscible with water or has an acceptable solubility in water (SW). The water-containing etching solution is flowed to the hydrophilic (wet) region through a simple microfluidic capillary filling process, and is stably confined to the hydrophilic region without crossing the hydrophilic-hydrophobic line to the hydrophobic (dry) region (Figure 3-1b). Therefore, a unique microfluidic collector is formed, where the dry pattern region is separated from the wet etching region. During electrospinning, the fibers pile up on the dry surface, while all other fibers are dissolved by the etching solution on the dry surface (Figures 3-1 c-d). Finally, the polymer residue from the wet surface is washed by the refresh etching solution carefully, leaving the nanofiber patterns in the dry region (Figures 3-1 e-f). In this method, the pattern definitions are determined by the predetermined patterns on the photo mask and by the lateral over-etch at the edges of the nanofiber patterns. By defining the shape of the patterns on the

www.manaraa.com

photo mask, it is possible to realize arbitrary-shaped patterns of nanofibers. It should be noted that because a rather wide variety of organic solvents are available to mix with water to obtain proper water-containing etching solution (*described in the Results and Discussion section*), the presented selective deposition technique is applicable to a broad range of nanofiber materials.

3.3 Experimental Section

Materials: Two typical biomaterials are used to demonstrate the method: water-soluble polyethylene oxide (PEO), and water-insoluble poly-DL-lactic acid (PDLLA). PEO (M.W. = 1,000,000), chloroform (HPLC grade, 99.9 %), fluorescein (pure, M.W. = 332.3), ethanol (100 %), are obtained from Sigma Aldrich (St.Louis, MO). Hydrofluoric acid (49 %) and acetone are obtained from Fisher Scientific (Pittsburgh, PA). PDLLA (i.v. = 0.69) is obtained from Lactel Polymers (Birmingham, AL). All reagents are used as received without further purification.

Precursor Preparation: 30 wt/wt % PEO in ethanol is prepared by dissolving appropriate amounts of PEO powder in 70 % ethanol. The resulting mixture is further stirred by ultrasound for 6 hours at room temperature to obtain homogeneous and clear solutions without particulate materials. 12 wt/wt % PDLLA precursor is prepared by dissolving appropriate amount of PDLLA pellets into chloroform. The mixture is vigorously stirred after 24 hours at room temperature when the PDLLA pellets are fully dissolved in chloroform.

Selective Surface Patterning of SAM: The photocleavable SAM technology is used to pattern the hydrophobic and hydrophilic regions on the fiber collector surface (Figures 3-2a-

www.manaraa.com

d). Briefly, a glass slide surface is flushed with a mixture of 0.5 wt% octadecyltrichlorosilane (OTS) in hexadecane to form a hydrophobic SAM. The SAM surface is rinsed with hexane and methanol sequentially, and then is dried using nitrogen. Ultraviolet (UV, 365 nm) light is used to expose the SAM surface through the photo mask in the pH = 11.6 NaOH environment for 85 mins. The UV irradiated surface becomes hydrophilic, while the unirradiated one remains hydrophobic. As a result, water-containing etching solution can be confined to the hydrophilic region (Fig. 3-2f).

Microfluidic Capillary Filling and Confinement of Fiber Etching Solution**:** De-ionized (DI) water is chosen to etch unwanted PEO fibers in the hydrophilic region. A number of organic solvents can dissolve water-insoluable PDLLA, but these solvents themselves generally can *not* be confined to the hydrophilic region. To solve this problem, a mixture of water and water-soluble organic solvent with the mixing ratio of water/acetone (or W/A) = 50/50 wt/wt is used to etch unwanted PDLLA fibers (*optimization of W/A is described in the Results and Discussion section*). The filling of the etching solution to the hydropilic region is realized through microfluidic filling (Fig. 3-2). Placing a droplet of the etching solution at the liquid access port of the hydrophilic region with a conventional pipette is all that is needed to flow and confine the solution to that region. The microfluidic capillary force of the etching solution drives the fluid along the hydrophilic pathway. By placing the droplet of the etching solution with a proper volume, adequate filling pressure can be achieved to allow driving the fluid through the hydrophilic region. Figure 3-2e shows the flowing and confining process of the etching solution on the collector surface.

www.manaraa.com

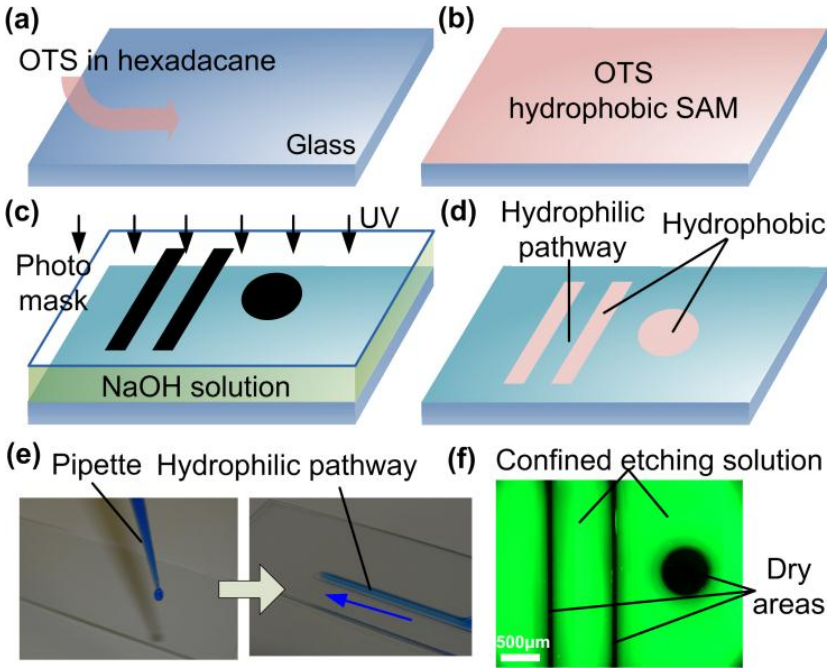

Figure 3-2 Process for modifying the fiber collector surface using the photocleavable SAM technology and microfluidic filling of etching solution. (a-b) The OTS hydrophobic SAM is formed on the glass surface. (c-d) The hydrophilic regions are patterned under the UV light through a photo mask. The gap between the glass surface and the photo mask is filled with the NaOH solution. (e) The water-acetone mixture is flowed into the hydrophilic region via the microfluidic capillary filling. (f) Fluorescence image of the water-acetone mixture (W/A = 50/50 wt/wt) confined to the hydrophilic region.

Electrospinning of Fibers: The PEO and PDLLA precursor solutions are loaded into 10 mm-diameter syringes A and B, respectively. A #30 gauge stainless steel needle (Howard Electronic Instruments Inc., KS) is electrically connected to a D.C. high voltage supply (Gamma High Voltage Research Inc., FL). A syringe pump (model KDS210, Kd Scientific Inc., MA) is used to deliver the precursor solution to the needle with a certain distance between the needle tip and the collector surface. The electrospinning conditions for PEO are in the following: the voltage applied between the spinneret and fiber collector VSC = 6 kV, the distance between the spinneret and fiber collector D = 10 cm, and the flow rate of precursor solution FR = 0.2 ml/h. For electrospinning of PDLLA, the following process conditions are used: VSC = 9 kV, D = 12 cm, and FR = 0.5 ml/h.

www.manaraa.com

Characterization: The diameter of electrospun nanofibers and thickness of fibrous mats are characterized using Scanning Electrons Microscope (SEM-JEOL JSM 606LV). Samples are sputtered with gold before inspection. The distribution of fiber diameter is analyzed by randomly sampling 100 individual fibers. The thickness of electrospun fiber mat is measured by tilting the sample stage 45^{o} to get a side view. For each thickness, 10 samples were inspected to obtain a statistical value. Fiber diameter and mat thickness are given as the mean diameter ± standard deviation.

3.4 Results and Discussion

The resulting PEO and PDLLA fibers are 500 ± 120 and 930 ± 196 nm in diameters, respectively. As expected, the fibers deposited in the hydrophilic regions are dissolved by the confined etching solutions. To remove the polymer residues from the hydrophilic surface, the surface is gently washed through the careful flowing and withdrawing process of the corresponding etching solutions again (DI water for cleaning PEO residue, and a mixture of acetone and water with W/A = 50/50 wt/wt for cleaning PDLLA residue).

Figure 3-3 shows the obtained fibrous patterns using the proposed selective nanofiber deposition method. A small amount of fluorescein dye is pre-added to the fiber precursor solutions to improve the visualization of the microstructures. Almost all the PEO and PDLLA residues are removed from the hydrophilic surfaces because no fluorescence is observed from the peripheral regions of the patterns. These patterns have high definition and their feature sizes are several tens of micrometers, almost one order higher than those obtained using most other methods and comparable to that achieved using the femtosecond laser.

www.manaraa.com

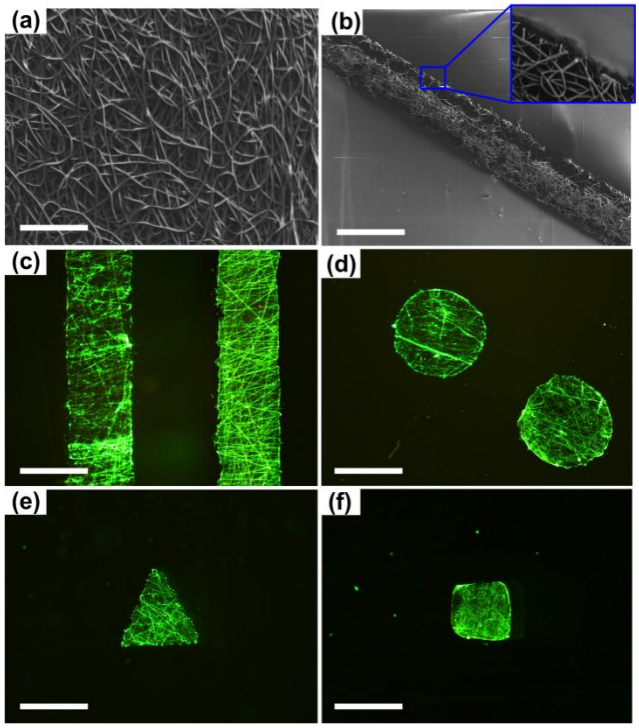

Figure 3-3 (a) Scanning electron microscope (SEM) image of as-electrospun PDLLA fibers. Scale bar represents 10 μm. (b) SEM image of the patterned PDLLA fibrous belt. The inset shows the edge of the pattern. (c-f) Fluorescence images of the PDLLA (c, d) and PEO (e, f) nanofibrous patterns with various shapes. Scale bars in (b-f) represent 50 μm.

The selective nanofiber deposition method can incorporate with some nanofiber alignment methods to obtain micropatterns in well-aligned nanofibrous mats. We have demonstrated the selective deposition of aligned nanofibers by using a pair of electrodes[1] on the microfluidic patterned fiber collector surface. As shown in Figure 3-4, two parallel gold electrodes are first formed on the glass slide surface using the conventional microfabrication technology [40]. The hydrophobic and hydrophilic regions are then created between these two electrodes, followed by the microfluidic filling of the fiber etching solution in the hydrophilic region, as described above. Such a spatial configuration results in suitable electrostatic forces that stretch the charged polymer jet to span across the gap and align perpendicular to the electrodes during electrospinning. Therefore, the aligned nanofibers are

www.manaraa.com

deposited selectively in the hydrophobic regions using the same method as that for the non-woven fibers, expect for using of the paired electrodes. The aligning direction of the nanofibers can also be readily adjusted by changing the angle of the parallel electrodes with respect to the hydrophobic and hydrophilic patterns (Figure 3-4). These micropatterns with high-definition shapes of aligned nanfibers may be used to define the preferred direction of cell motion further.

Due to the inherent porous structure and large surface area of the electrospun mat, the confined water-containing etching solution has a fairly high chance to *laterally* penetrate and over-etch the nanofibers selectively deposited in the hydrophobic region. Although the obtained patterns always have smaller dimensions than those designed on the photo-mask, the amount of the lateral over-etch can be compensated by an increase in the dimensions of the pattern designed on the photo mask. Therefore, it is important to identify and understand the possible major factors that control the lateral over-etch process. In the following section we will discuss the influences of the composition of etching solution, electrospinning condition, fiber and mat structure and morphology on the level of the lateral over-etch and the pattern definition.

The introduction of water into proper organic solvent allows confining the mixture to the hydrophilic region for patterning water-insoluble fibers, but at the same time decreases the etching ability of the mixture. Therefore, a tradeoff exists between the confining property and the etching ability of the etching solution. In this study, the former is characterized by the contact angle of the mixture on the hydrophilic surface, while the latter is characterized by the etching time that refers to the time from completing electrospinning to a visual clearance of the PDLLA fibers in the hydrophilic region. Figure 3-5 shows the contact angles θ and the

www.manaraa.com

corresponding etching times of water-acetone mixtures with different mixing W / A ratios. The θ increases linearly with increasing the W / A ratio. The weak confinement associated with the small θ is the possible source of instability under slight perturbations (e.g., the impingement of the flying fiber to the etching solution): the etching solution may cross the hydrophobic-hydrophilic contact line and then over-etch the fibers in the pattern region. Thus, the actual pattern area is reduced significantly (see the image at the upper right corner of Figure 3-6). As the θ increases with reducing the acetone content, the etching time becomes longer. The optimum W / A ratio and the corresponding θ range from 40 / 60 to 60 / 40 wt / wt and from 65 to 80 degrees, respectively. Specifically, at W / A = 50 / 50 wt / wt, the time for etching the PDLLA fibers is about 17 s, with the lateral over-etch of 3 μm only (see the image at the bottom right corner of Figure 3-6).

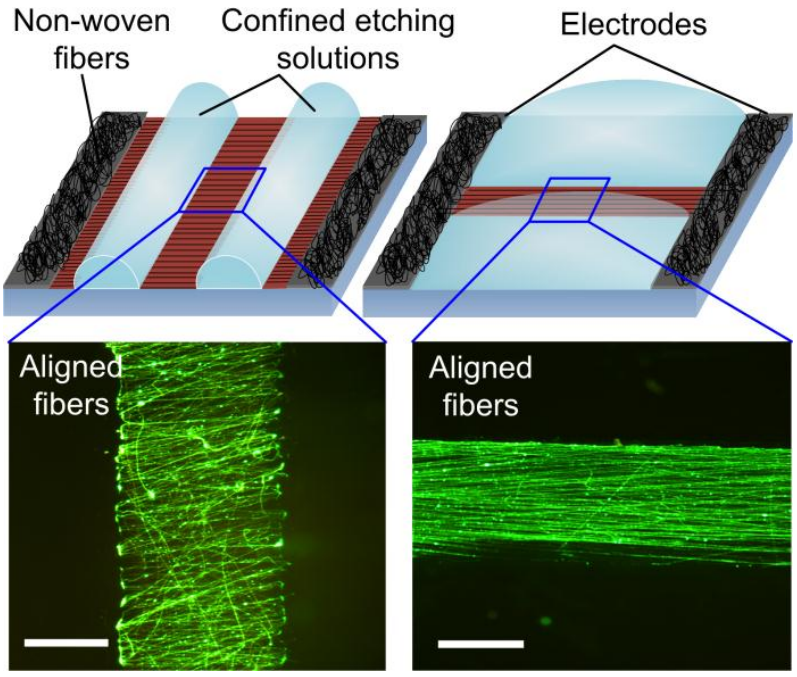

Figure 3-4 Selective deposition of aligned nanofibers on the collector surface. The hydrophilic and hydrophobic patterns are formed between two microfabricated parallel gold electrodes. Scale bars represent 50 μm.

www.manaraa.com

The voltage potential V_{SC}, applied between the spinneret and the collector, is another important factor to influence the lateral over-etch. As the charged fluid jet moves closer to the collector during electrospinning, it achieves acceleration due to the increasing electrostatic force. At a high voltage V_{SC}, the impingement force from the flying jet onto the etching solution surface could destroy the liquid confinement. Consequently, the etching solution may invade into the pattern region, resulting in poor pattern definitions. Figure 3-7 shows the lateral over-etch of the PDLLA fibrous patterns as a function of the V_{SC}. At V_{SC} = 20 kV, the lateral over-etch is pronounced. Lowering V_{SC} to 8 kV reduces the over-etch effect.

Both the fiber diameter and mat thickness also affect the lateral over-etch at the edges of the fiber patterns. It is observed that in the case of patterning large-diameter fibers, the etching solution permeates deeply to the pattern region along the fibers that do not melt immediately, causing a severe over-etch of the fibers. The fiber diameter d relies significantly on the polymer concentration in the precursor solution. As the PDLLA concentration changes from 7.5 to 20 %, d is increased linearly from 500 ± 110 to 1920 ± 395 nm. The fibers with d = 500 ± 110, 930 ± 196, 1210 ± 258, 1550 ± 320, and 1920 ± 395 nm are electrospun onto five microfluidic collectors, respectively. The etching solution used here has a mixing ratio of W/A = 50/50 wt/wt. The result shows that the lateral over-etch increases linearly with the fiber diameter (Figure 3-8). The plausible explanation to the result is as follows: i) larger diameters fibers require longer time to melt completely than small diameters fibers under the same etching condition, and thus more etching solution penetrates into the dry hydrophobic region along the larger diameter fibers, causing more lateral over-etch; ii) large diameter fibers carry more weight and hit the etching solution harder than

www.manaraa.com

small diameter fibers, and hence, interrupting the equilibrium state of the etching solution. The resulting vibration of the etching solution will give rise to a large amount of lateral over-etch. As for the mat thickness, the PDLLA fibrous mats with their thicknesses of 18 ± 4, 30 ± 7, 44 ± 12, 60 ± 16, 75 ± 19 and 90 ± 23 μm are formed on six microfluidic collectors, respectively. They are patterned using the water-acetone mixture (W/A = 50/50 wt/wt). Figure 3-9 shows that the amount of the lateral over-etch is also almost linear to the mat thickness. It is easy to imagine that the thicker the fiber mat, the larger contact area between the mat and etching solution in vertical direction, and thus, the more the etching solution violates the deposition region laterally, a higher level of lateral over-etch.

The selective nanofiber deposition method presented here is fairly simple and the minimum requirements are the creation of hydrophilic and hydrophobic regions on the collector surface and the confinement of water-containing organic etching solution in the hydrophilic region. Besides the PEO and PDLLA, many other nanofibers (polymethylmethacrylate, polydimethylsiloxane, polyvinylchloride, polystyrene, and etc) can be selectively deposited on glass substrates using this method. Water-miscible polar organic solvents (acetonitrile, acetic acid, ethanol, dimethylformamide, ethanol, 2-propanol, and etc) are preferred to prepare the aqueous fiber etching solutions; some non-polar organic solvents with acceptable SW (dimethylsulfoxide: SW = 25 g / 100 g; tetrahydrofuran: SW = 30 g / 100 g; 2-butanone: SW = 26 g / 100 g, and etc) can also be used.[31] Therefore, the wide selection of the organic solvents ensures that selective deposition of a broad range of nanofibers can be processed on glass substrates with a minor modification to the composition of fiber etching solution.

www.manaraa.com

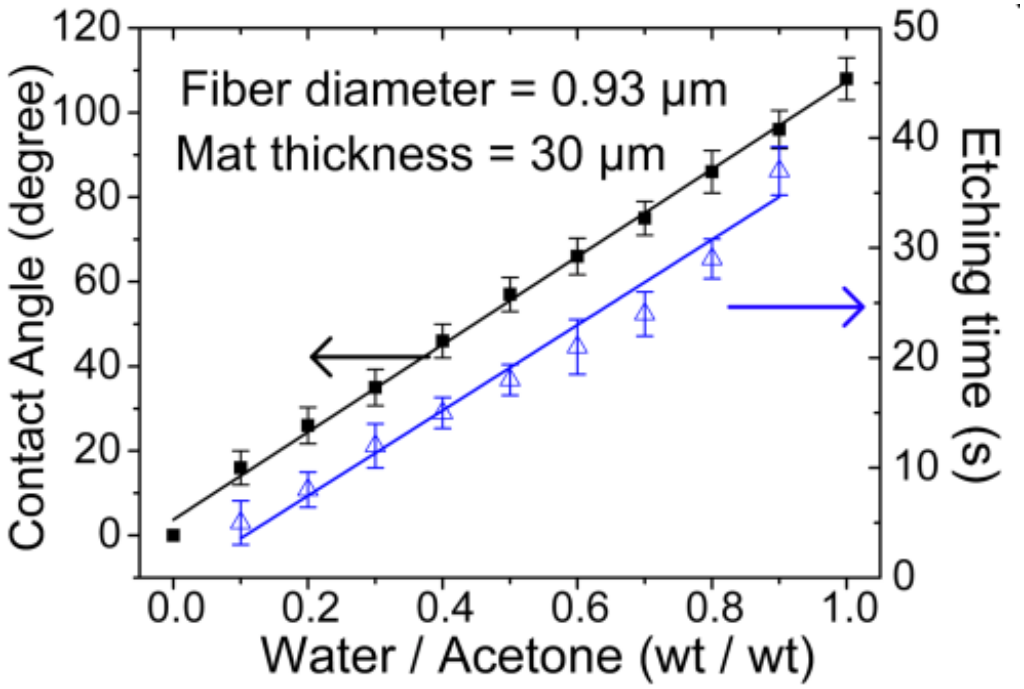

Figure 3-5 Dependences of the contact angle of water-acetone mixture (left-axis) and the time for etching PDLLA fibers (right axis) on the W/A mixing ratio, respectively.

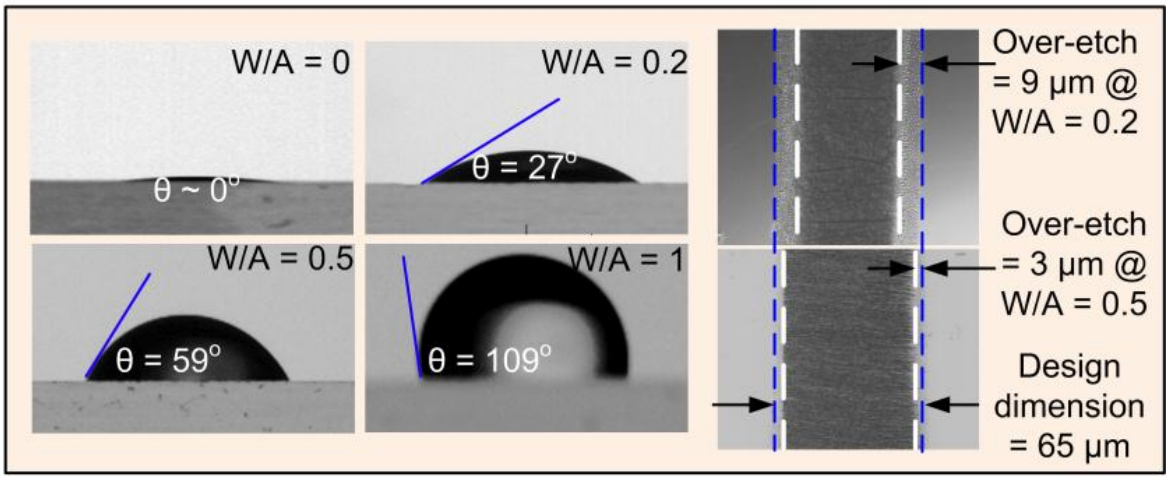

Figure 3-6 The left and middle columns show the optical images of the water-acetone droplets with W/A = 0, 0.2, 0.5 and 1, respectively, placed on the hydrophilic surface formed via the photocleavale SAM technology. The right column shows the lateral over-etch effects at the edges of the PDLLA patterns (fiber diameter: 0.93 μm; mat thickness: 30 μm).

www.manaraa.com

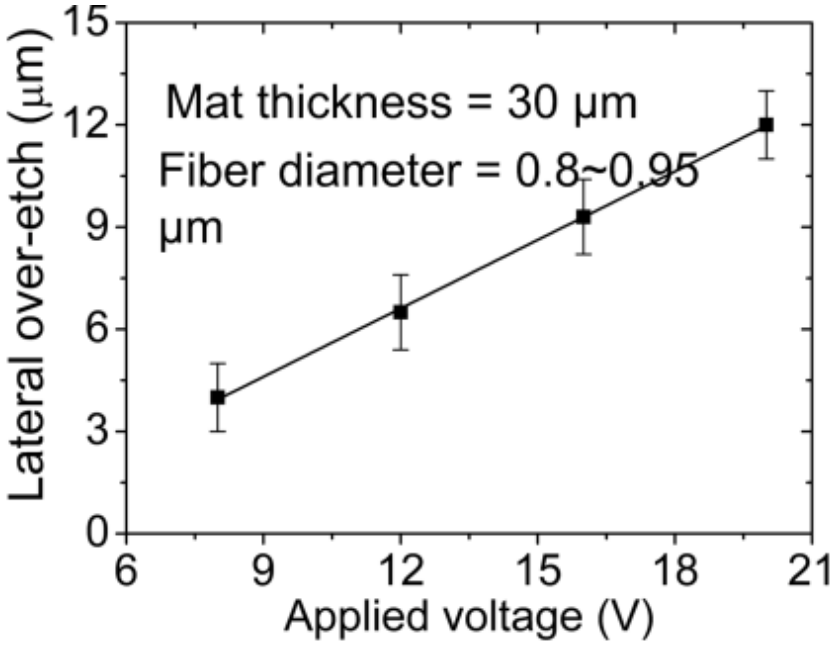

Figure 3-7 Dependence of the lateral over-etch of the PDLLA pattern on the voltage applied at the spinneret.

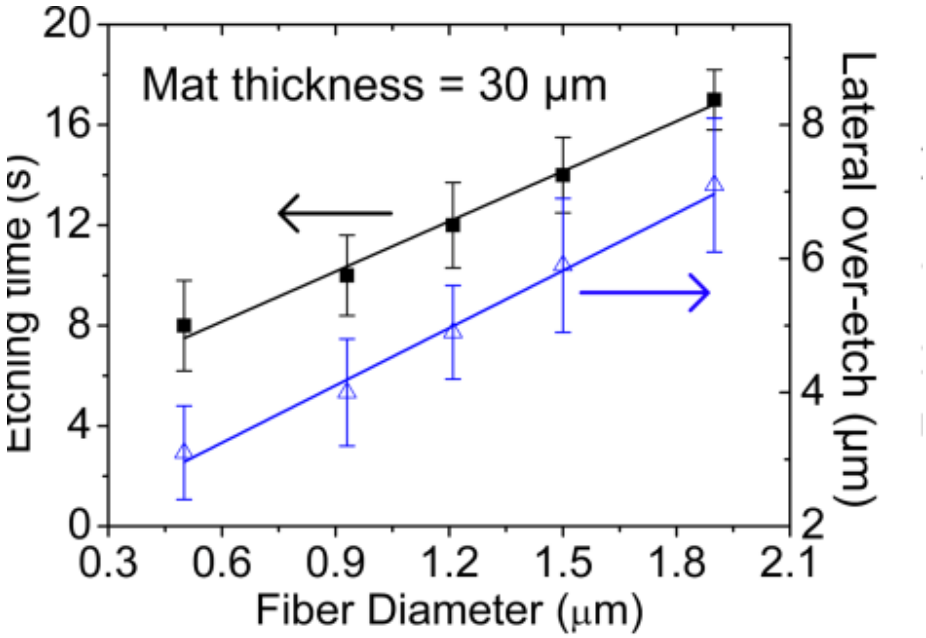

Figure 3-8 Dependences of the etching time and the lateral over-etch on the PDLLA fiber diameter. Error bars, ± s.d.

www.manaraa.com

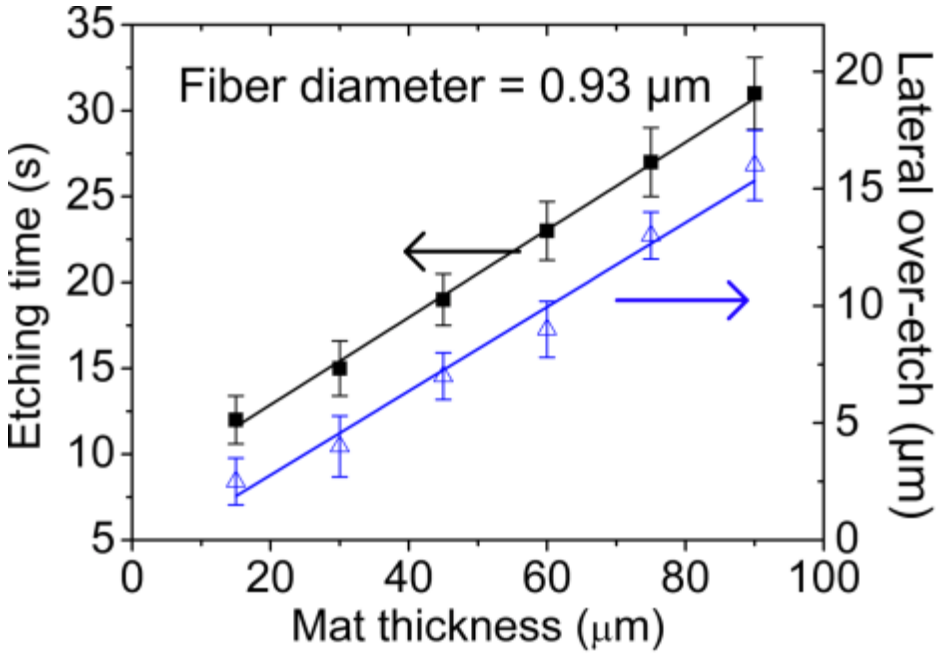

Figure 3-9 Dependences of the etching time and the lateral over-etch on the mat thickness. Error bars, ± s.d.

3.5 Conclusion

In conclusion, we have achieved micro-sized, structurally accurate, arbitrary-shaped patterns of both random and aligned electrospun nanofibers by etching away unwanted nanofibers from the wet hydrophilic region and leaving desired nanofibers in the dry hydrophobic region on a microfluidic collector surface. The photocleavable SAM technology offers apparent simplicity and flexibility to define the hydrophilic and hydrophobic regions to confine water-containing liquid. Thanks to the microfluidic filling technology, the fiber etching solution can be flowed into the hydrophilic region on the collector surface without

www.manaraa.com

using *actual* microfluidic channels (generally having walls and cover). Considering the general difficulties in patterning electrospun fibers that have hindered the fiber's applications in cell biology and tissue engineering, this method reported here could open up some new application opportunities by providing arbitrary-shaped, structurally accurate, micro-sized, and aligned/random nanofibrous ECM scaffolds.

www.manaraa.com

CHAPTER 4. HOLLOW POLYMERIC MICAOCAPSULES EMBEDDDING ACTUATORS FOR CONTROLLED RELEASE OF ENCAPSULANTS

4.1 Introduction to Controlled Encapsulation

Controlled encapsulation and release of biological and chemical agents and species (e.g., drugs, proteins, vitamins, cells, fragrances, and flavors) is of great importance to many applications, ranging from food and pharmaceutical industries to inkless paper [43-46]. Particularly, liquid core-polymer shell hollow microcapsules have attracted much attention. The polymer shells make microcapsules more stable and robust, not only protecting sensitive ingredients against denaturing environments, but allowing for easy handling of liquids [47-50]. By controlling the thickness, porosity, and/or mechanical strength of the polymer shells, it is possible to release the encapsulated ingredient in a controlled manner [51]. From the perspective of microcapsule preparations, many methods have been investigated to realize different types of hollow polymeric microcapsules such as polymersomes, multilayered capsules, and hollow microspheres. The methods include self-assembly of microgels in droplets [52], layer-by-layer polyelectrolyte deposition [53], interfacial polymerization [54] precipitation by phase separation [55], surface polymerization [56], copolymer vesicles [57], multiphase microfluidics [58], and combination of molecular self-assembly and precipitation [59]. These methods have led to substantial progress in manufacturing different kinds of hollow microcapsules, but have often required relatively non-trivial and complex chemical strategies [47]. From the perspective of release mechanisms, presently three major methods exist for releasing encapsulated ingredients out of hollow microcapsules [60,61]. The first method involves shell rupture through applied pressure, where a critical pressure was

www.manaraa.com

determined by the shell material and thickness [62,63]. The second scheme relies on dissolving shell material by melting, enzyme attack, or chemical reaction, where molecular release over a desired period of time was realized through a slow diffusion process [64-66]. The last scheme uses a swellable polymer shell. The mechanical strength of the polymer shell could be tuned by external stimuli such as electric fields, pH, temperature, or biochemical reaction. This, in turn, changes the diffusion rate of the encapsulated molecules from the microcapsules [67-70].

Electrospinning is a popular, simple, and versatile technique to generate micro/nanofibers from a wealth of materials. It utilizes a high strength electric field to draw a charged solution into a liquid jet from a nozzle [71]. Electrospray is similar to electrospinning, except that the ejected liquid jet breaks up into small droplets when the charged solution has a low viscosity or concentration. New applications of these manufacturing techniques are continuously being developed for energy storage, catalysis, sensors, and drug delivery, particularly as many interesting complex micro/nanostructures (e.g., hollow interiors, core-sheath complexes, and multicompartments [51,72-75]) can be realized by using modified electrospinning/spray processes (e.g., coaxial and multijet electrospinning/spray).

We report on the development of a new class of core-shell microcapsules capable of regulating the release profile of encapsulated molecules. The uniqueness of the microcapsules laid in embedding miniature actuators into their interior (Figures 4-1). The embedded actuators were made of electrically-sensitive hydrogel beads that could swell and contract by external electric fields. This allowed us to regulate the internal pressure of the

www.manaraa.com

liquid core, and thus, the diffusion rate of the encapsulated molecules from the microcapsules.

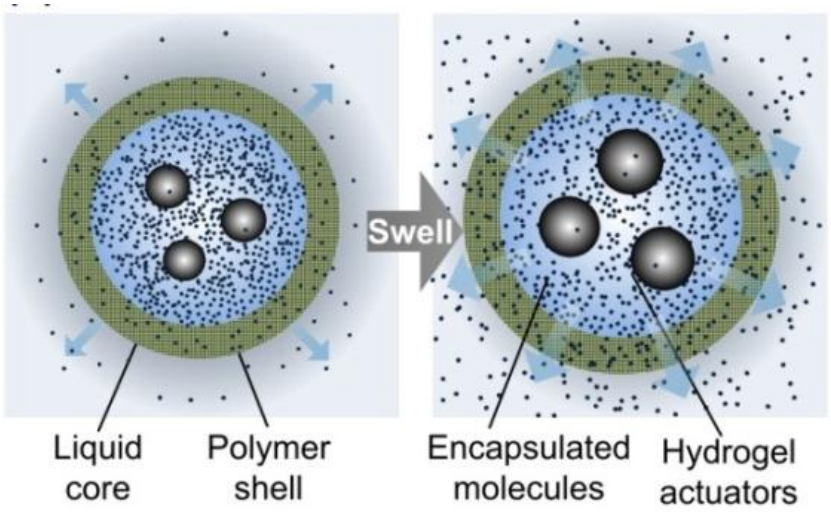

Figure 4-1 Schematic structure and mechanism of the liquid core-polymer shell microcapsule for regulated release of encapsulated molecules. The microcapsule contains electrically-sensitive hydrogel beads in its liquid core. The hydrogel beads expand by external electric fields. This causes to increase the internal pressure of the liquid core, regulating the release of the encapsulated molecules

Basically, changing the electric field strength applied to the embedded hydrogel beads caused redistribution of mobile ions inside the beads. This led to imbalanced osmotic pressure, and thus the swelling of the hydrogel beads [76]. It is believed that the hydrogel beads had a positive excess volume: the total volume of the hydrogel beads-solution system of the microcapsules increased when more water was imbibed in the hydrogel network [77]. The excess volume increased the internal pressure of the microcapsule, thinned the polymer shell (and possibly increased its permeability), and thus, regulated the releasing flux of the encapsulated molecules. Therefore, the embedded actuators provided an internal control variable to a conventional diffusion-based molecule release process, making it possible to regulate the release characteristic of the encapsulated molecules from the microcapsules. The

www.manaraa.com

microcapsules had the MEMS-like structures and functions [78], and were manufactured by the coaxial electrospray or co-electrospray process [79]. This technique allowed us to integrate the hydrogel beads, form the polymer shell, and load the releasable molecules in a single step.

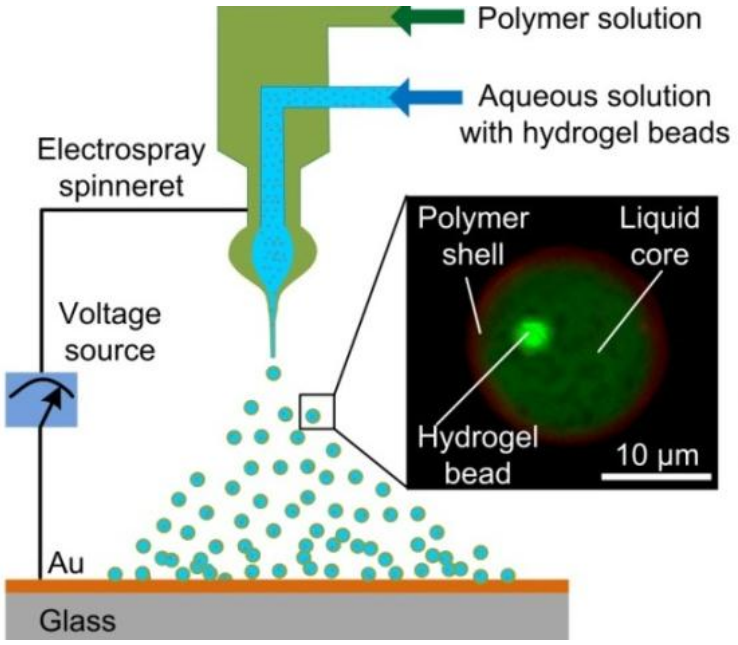

Figure 4-2 Schematic setup of co-electrospray for fabricating the microcapsules embedding hydrogel beads.

4.2 Fabrication of Liquid Core-Polymer Shell Microcapsules

Co-electrospray Setup: Figure 4-2 shows the co-electrospray setup for fabricating the microcapsules. As a critical component, a coaxial spinneret was formed by inserting a 21-guage needle into a 23-guage needle (BD Biosciences). The spinneret allowed delivery of the inner and outer flows independently by two individual syringe pumps (KDS 2000, Kd Scientific). The outer flow contained a polymer solution for forming the shell of the microcapsules. The inner flow contained an aqueous solution of hydrogel beads and

www.manaraa.com

releasable molecules of interest. A high voltage (Gamma High Voltage Research) was applied between the spinneret and a collector. The collector was a grounded conductive substrate (a gold-coated glass)

Polymer Shell and Liquid Core Materials: PDLA solution (solvent: chloroform) was used as the outer flow of the co-electrospray process. The hydrophobic property of PDLA satisfied a prerequisite for encapsulating aqueous liquids into a polymer shell using co-electrospray [80-82]. PDLA precursor solutions with different concentrations were prepared by mixing PDLA pellets (molecular weight 41000; Lactel Polymers) and chloroform (Sigma-Aldrich) in appropriate weight ratios. The solutions were stored at 4 ^{o}C for 24 h to dissolve these pellets and then stirred at room temperature to obtain a transparent, homogeneous solution. Deionized (DI) water containing hydrogel beads and releasable molecules were used as the inner flow of the co-electrospray process. 10 mg BBG dyes were mixed into 10 mL DI water and then stirred at room temperature to obtain the BBG solution with the concentration of 1 mg/mL.

Preparation of Electrically Sensitively Hydrogel Beads: There are a lot of different hydrogels available sensitive to different external stimuli such as infrared light [83], visible light [84], ultrasound [85], temperature [77], and magnetic fields [86]. Here in this work, home-made electrically-sensitive hydrogel was used as a model hydrogel. The diameter of the hydrogel beads was 3.2 ± 2.1 μm (the mean ± standard deviation obtained from ~200 hydrogel beads). Different hydrogel bead suspensions were prepared, with the bead concentration C_{bead} ranging from 2×10^6 to 2×10^8 / mL. The hydrogel precursor solution was formed by mixing acrylic acid (Sigma-Aldrich) and 2-hydroxyethyl methacrylate

www.manaraa.com

(Sigma-Aldrich) in a molar ratio of 1:4.2, ethylene glycol dimethacrylate (1.2 wt%, Sigma-Aldrich), and 2, 2-dimethoxy-2-phenyl-acetophenone (1.9 wt%, Sigma-Aldrich). Preparation procedures of electrically-sensitive hydrogel beads were described in the following: (a) The prepared hydrogel precursor solution was mixed with light mineral oil (NF/FCC, Fisher Scientific) in a volume ratio of 1 : 1. (b) The mixture was stirred by a vortex mixer (2000 rpm; Fisher Scientific) for 20 s and then exposed under ultraviolet (UV) irradiation (intensity: 27.5 mW/cm^2) for 20 s. (c) After the stirring and UV exposure steps in (b) were repeated for six times, a mixture of hydrogel beads and mineral oil was obtained. (d) To separate the hydrogel beads from the mineral oil, the mixture (3 mL) was added to 2 mL methanol (Sigma-Aldrich) in a vial, and then, agitated in an ultrasonic mixer (B2510-MT, Branson) for 5 mins. (e) After the resultant mineral oil droplets deposited on the bottom of the vial, the mixture of the methanol and hydrogel beads was taken by a pipette and then put in a new vial. (f) To separate the methanol from hydrogel beads, the mixture was centrifuged in the new vial at 1000 rpm for 5 mins, (g) After the upper methanol was thrown away, chloroform (2 mL; Sigma-Aldrich) was added to the vial, to remove the remaining mineral oil droplets. (h) After the chloroform evaporated away, methanol (2 mL) was added again to re-suspend the hydrogel beads. (i) After the mixture was centrifuged at 1000 rpm for 5 mins, the upper methanol was thrown away. (j) The hydrogel beads (diameter: 3.2 ± 2.1 μm) were finally obtained after dried in air.

4.3 Testing of Release Device and Results

The concentration of PDLA polymer solution was first optimized to form independent hollow microcapsules by the co-electrospray process. A voltage of V_{sc} = 9.5 kV

www.manaraa.com

was applied between a spinneret and a collector (a gold coated glass cove slip) with a distance of D_{sc} = 10 cm (Figure 4-2). The flow rate or FR for delivering the outer PDLA solution and the inner aqueous solution was set to be FR_{outer} = 8 mL/h and FR_{inner} = 0.4 mL/h, respectively. As the relative amount of PDLA with respect to the solvent (chloroform) decreased, the morphology of the co-electrospray products was found to change from a fibrous to spherical form. Figures 4-3 show the continuous core-shell microfibers and independent hollow microspheres formed with the critical PDLA-to-chloroform weight ratio of WR = 1 : 8 and 1 : 15, respectively. When the WR fell between these two critical ratios, the beaded fibrous structures (Figure 4-3) were emerged. When the WR < 1 : 18, the PDLA polymer solution was too thin to wrap the inner liquid which flowed out of the spinneret and fell onto the collector. Figure 4-4 shows an failure example in which the WR of polymer and its solvent is 1:20. This is because when the polymer is further diluted, the surface tension of the polymer solution is too low to wrap the inner fluids.

It was possible to tune the inner diameter ID of the microcapsules by adjusting the flow rate of the inner flow FR_{inner}. In this experiment, the WR of the PDLA solution was chosen to be 1 : 15. The FR_{inner} was varied from 0.08 to 0.8 mL/hr, while the FR_{outer} was fixed at 8 mL/hr. The upper limit of the FR_{inner} was set to be 0.8 mL/hr because above this limit, the jetted inner flow separated from the outer flow at the tip of a two-fluid Taylor cone. Figures 4-5a-c show that increasing the FR_{inner} ($\leq$ 0.8 mL/hr) had little influence on changing the OD (27.35 ± 2.2 μm) of the microcapsules (here, no hydrogel beads were introduced to the inner flow of the electrospray process). This was because the change of the FR_{inner} did not significantly affect the total flow rate of the two fluids. However, it was obvious that

www.manaraa.com

increasing the FR_{inner} gave rise to an increased ID of the microcapsules. Specifically, when the FR_{inner} was at 0.08, 0.4, and 0.8 mL/h, the resultant ID was found to be 8.1 ± 2.4 μm, 16.5 ± 3.5 μm, and 19.1 ± 3.8 μm, respectively. In the following sections, each measurement for the ID, OD, and shell thickness T_{shell} of the microcapsules was the mean ± standard deviation from ~200 microcapsules (the ID and T_{shell} were obtained based on their fluorescent images, and the OD based on their optical images).

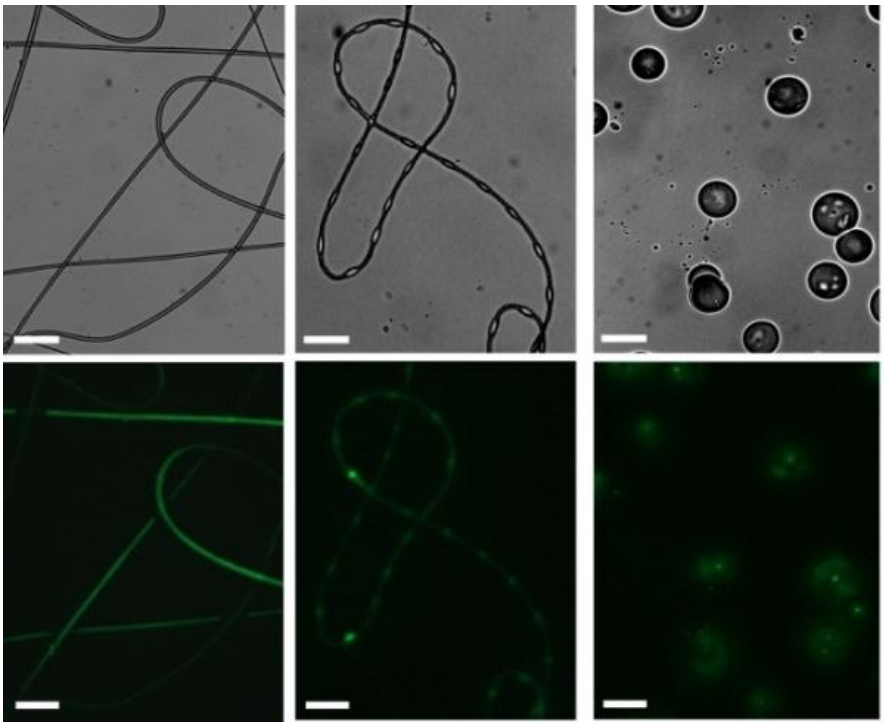

Figure 4-3 Morphological transition of co-electrospray products, obtained by adjusting the PDLA-to-chloroform weight ratio or WR from left to right column.Size bar: 10um.

We investigated controlling the quantity of hydrogel beads inside the microcapsules. By mixing a desired concentration of the hydrogel beads into the inner flow of the co-electrospray process, it was possible to obtain a statistical distribution of the number of the hydrogel beads encapsulated within the microcapsules. Basically, the encapsulation of hydrogel beads into the microcapsules was a stochastic process following the Poisson

www.manaraa.com

distribution function given by the formula $f(\lambda,k) = \lambda^k \exp(-\lambda)/(k!)$, where f is the probability of having k beads in a microcapsule, given an average loading number of λ beads per microcapsule [87,88]. Let's assume that the microcapsules have the ID of 16.5 μm (the experimental mean value). Theoretically, when $\lambda = 0.1$ ($C_{bead} = 2 \times 10^6$ / mL), 9.05 % of the microcapsules have 1 bead and 0.47 % have ≥ 2 beads, whereas 90.48 % contain no beads. When $\lambda = 1$ ($C_{bead} = 2 \times 10^7$ / mL), the possibility for a microcapsule to contain 0, 1, and ≥ 2 beads is 36.79, 36.79, and 26.42 %, respectively. When $\lambda = 10$ ($C_{bead} = 2 \times 10^8$ / mL), the possibility for one microcapsule to have ≥ 2 beads increases to be more than 99%. Figure 4-6 shows the fluorescent image of the microcapsules (ID = 16.5 ± 3.5 μm) with embedded hydrogel beads ($C_{bead} = 2 \times 10^7$ / mL; FR_{inner} = 0.4 mL/hr). Figure 4-7 shows the histogram of the number of hydrogel beads observed inside the microcapsules ($C_{bead} = 2 \times 10^7$ / mL). The statistical distribution of the hydrogel beads in the microcapsules were obtained by counting the hydrogel beads in ~500 microcapsules based on their fluorescent images. The experimental result was almost in agreement with the theoretical result estimated by the Poisson distribution formula.

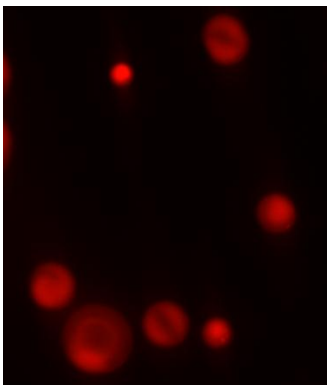

Figure 4-4 Failure encapsulation example when the WR is 1:20.

www.manaraa.com

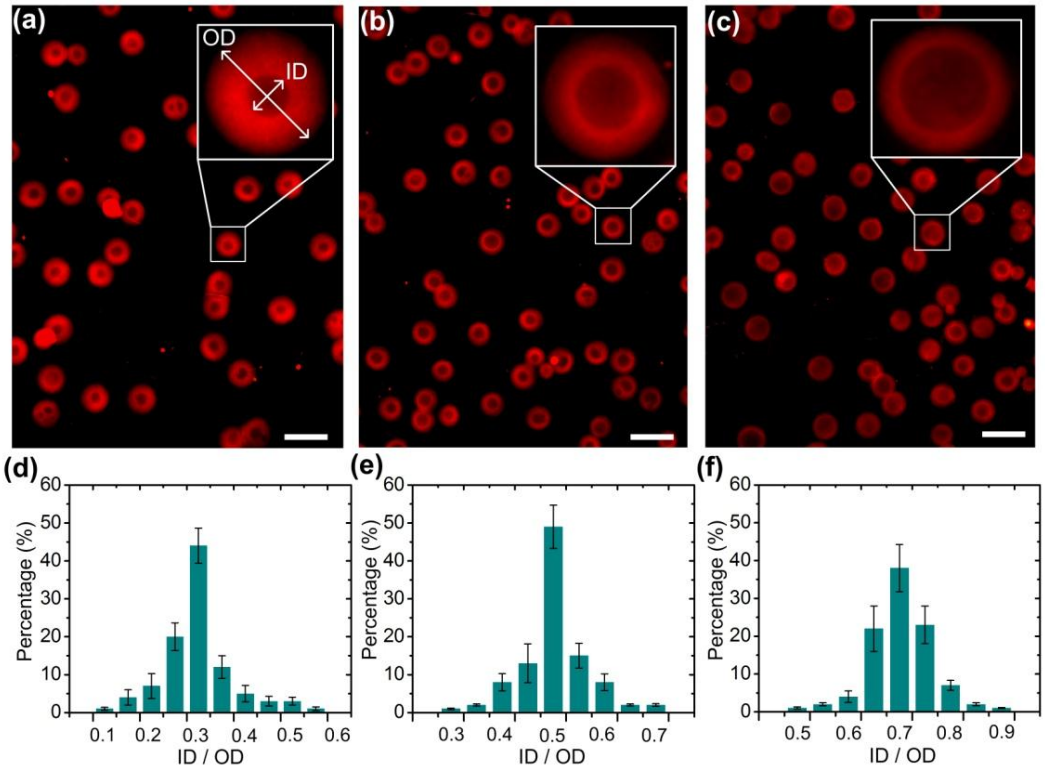

Figure 4-5 (a-c) Fluorescent images showing the liquid core-polymer shell microcapsules without hydrogel beads, fabricated at different inner flow rates: FR = 0.08 mL/h (a), 0.4 mL/h (b), and 0.8 mL/h (c). The outer flow rate was fixed at 8 mL/h. No hydrogel beads were introduced to the inner flow during the electrospray process. The scale bars represent 50 μm. (d-f) Histograms of the ratio of the inner to outer diameter (ID / OD) for the corresponding microcapsules shown in the same columns above in (a-c).

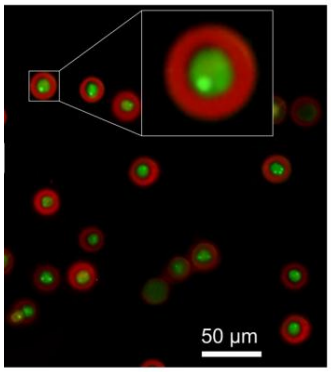

Figure 4-6 Fluorescence image showing the liquid core-polymer shell microcapsules with embedded hydrogel beads. Here, the concentration of the hydrogel beads used the inner flow of the electrospray process was $C_{bead} = 2 \times 10^7$ / mL. The flow rate of the inner flow was 0.4 mL/hr. The bright green spots indicate hydrogel beads. The red annular rings indicate the PDLA shells.

www.manaraa.com

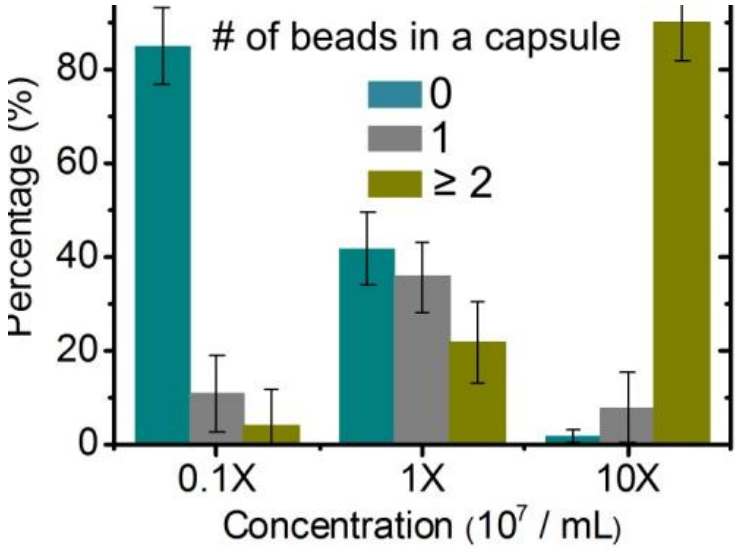

Figure 4-7 Histogram of the number of the hydrogel beads observed inside the microcapsules when C_{bead} = 2 × 10^6 / mL (left), 2 × 10^7 / mL (middle), and 2 × 10^8 / mL (right).

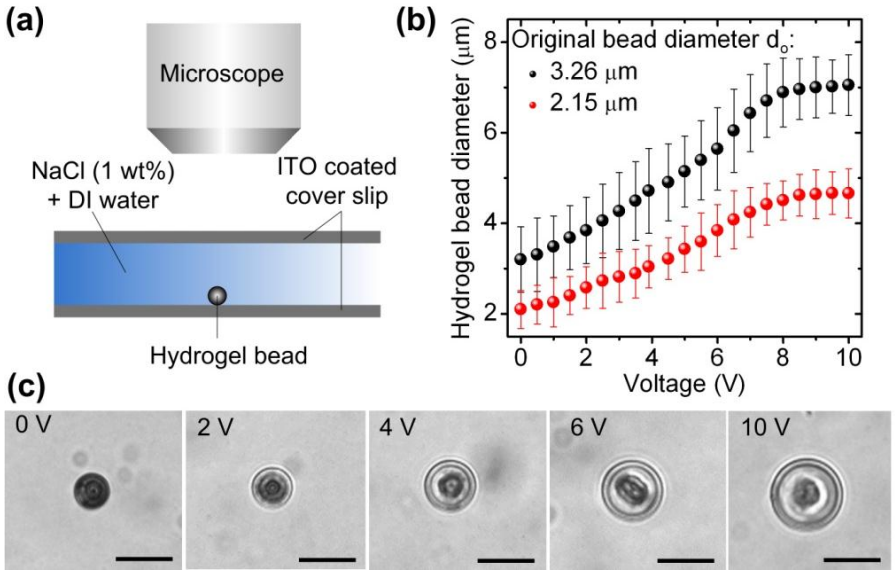

Figure 4-8 (a) Experimental setup for measuring the swelling characteristic of an electrically-sensitive hydrogel bead. (b) Size responses of two hydrogel beads as a function of an applied D.C. voltage. A low voltage was applied and remained on for 5 mins and then off for 5 mins before switching to a high voltage application. (c) Final morphologies of the hydrogel bead with the original diameter of 3.26 μm under different voltage conditions. The scale bars represent 5 μm.

www.manaraa.com

The swelling characteristic of the hydrogel beads was measured by exposing them to different electric fields. The hydrogel beads were placed in a 5 mm deep microfluidic channel containing DI water with 5 wt% NaCl. The channel was formed between two glass slides with conductive indium tin oxide (ITO) coatings. The shape change of the hydrogel beads was observed by a phase contrast microscope (DM2500, Leica) (Figure 4-8a). Different D.C. voltages (from 0.5 to 10 V with a step of 0.5 V) were applied between the two ITO glass slides. Here, a low voltage was applied and remained on for 5 mins, and then, off for 5 mins before switching to a high voltage application.

Figure 4-8c displays the expanded state of a hydrogel bead (original diameter: 3.26 μm) under different voltage applications. We found that it took ~15 s from a voltage application to an obvious expansion of the hydrogel bead, and then, ~18 s for the bead to reach a stable size. The response time was found to be independent of the applied voltage. This was because the movement of ions and water into and out of the hydrogel was mainly determined by diffusion, and the time scales for dimensional change depended on the size of the hydrogel structure. Figure 4-8b shows the dimension responses of two different sized hydrogel beads (original diameter: 3.26 μm, and 2.15 μm) as a function of an applied voltage. The size of the hydrogel bead reached an almost saturation value when the applied voltage was greater than 8 V. The data presented in Figure 4-8b was the mean ± standard deviation obtained from 10 measurements on each hydrogel bead.

To demonstrate the controlled release of encapsulated molecules from the microcapsules, dye brilliant blue G (BBG, 1 mg/mL) was mixed with DI water containing 1 wt% NaCl. The NaCl supplement was used to provide enough mobile ions when dissociated

www.manaraa.com

in water. A stock hydrogel bead suspension was diluted differently with the BBG-NaCl solution to obtain a desired C_{bead} for the inner flow of the co-electrospray process. To obtain enough microcapsules for test, the co-electrospray process was conducted for 2 hrs.

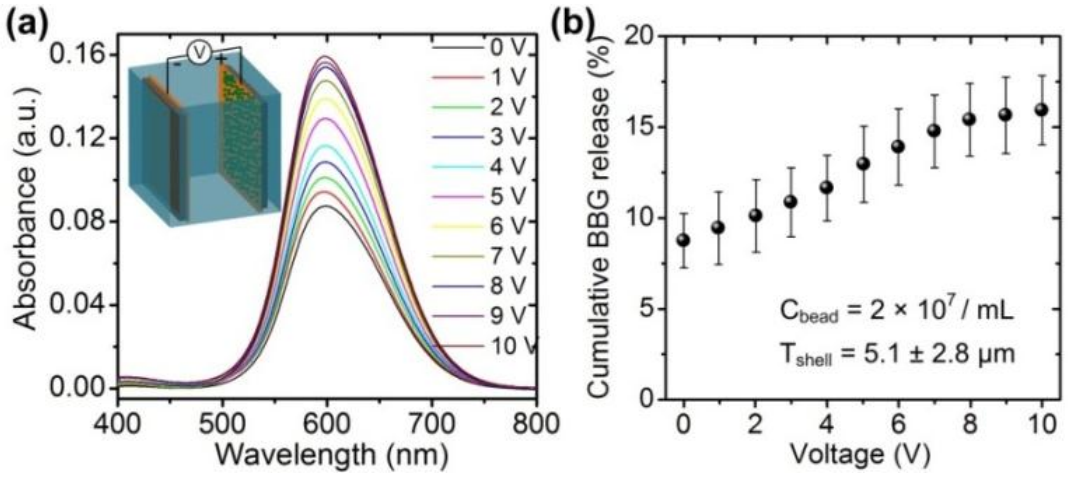

Figure 4-9 (a) Absorbance spectra of BBG molecules released from ten identical samples of the microcapsules (ID = 16.5 ± 3.5 μm; T_{shell} = 5.1 ± 2.8 μm; C_{bead} = 2 × 10^7 / mL) under different D.C. voltage conditions. A specific D.C. voltage was applied to a sample. All measurements were conducted 2 hrs after the voltage application. The inset shows an electric stimulation unit. (b) Cumulative BBG release from the samples measured in (a), as a function of the applied D.C. voltage.

The overall loading efficiency of the BBG molecules into the microcapsules was almost 100 % as the BBG solution was directly injected into the inner capillary of the spinneret by a syringe pump. The microcapsules were collected by the aforementioned gold-coated cover slip (1 cm^2). The collector served as the anode of an electric simulation unit shown in the inset of Figure 4-9a. The other gold-coated glass slide (cathode) was placed 5 mm away from and parallel to the collector. The two electrodes were immersed in a 1 mL quartz cuvette (BrandTech Scientific) containing DI water. The cumulative amount of molecule release was measured by monitoring absorbance at the characteristic absorption wavelength of molecules (for BBG, this is 600 nm) with a spectrometer (2800 UV/VIS,

www.manaraa.com

UNICCO). Prior to each measurement, the liquid in the cuvette was stirred gently by a glass rod to form a uniform distribution of BBG throughout the cuvette.

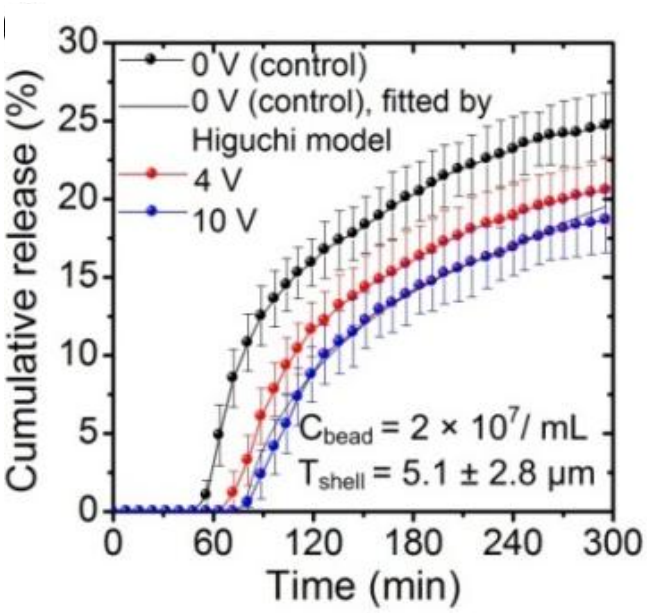

Figure 4-10 Transient responses of three identical samples of the microcapsules to different D.C. voltages: 0 V (control), 4 V, and 10 V. The black curve is obtained by fitting the Higuchi model to the BBG release data of the control sample.

It was found that as we increased the applied D.C. voltage to the microcapsules (ID = 16.5 ± 3.5 µm; T_{shell} = 5.1 ± 2.8 µm; C_{bead} = 2 × 10^7 / mL), the cumulative release of BBG molecules from the microcapsules increased (Figures 4-9 a-b). Here, each sample of the microcapsules was tested under an applied voltage at a specific value. The upper limit of voltage was set to be 10 V to prevent hydrolysis. Figure 4-9a shows the absorbance spectra of BBG molecules for different applied voltages, measured 2 hrs after each voltage application. The increase in absorbance peak intensity at the wavelength of 600 nm indicated that the BBG release increased with increasing applied voltage. Figure 4-9b summarizes and plots the BBG release as a function of the applied voltages. Interestingly, when the applied voltage was less than 8 V, the BBG release increased almost linearly with the voltage (Figure

www.manaraa.com

4-9b). But, at the higher voltages, the increasing rate of the BBG release, with respect to the voltage, decreased toward saturation. The explanation to this changing tendency is that the swelling of the hydrogel beads approached to an upper limit when exposed to the high electric fields as shown in Figure 4-8b. The transient responses of the microcapsules (ID = 16.5 ± 3.5 μm; T_{shell} = 5.1 ± 2.8 μm; C_{bead} = 2 × 10^7 / mL) were measured to investigate the release kinetics of the microcapsules under different voltage applications (Figure 4-10). Three identical samples were tested. Two of the samples were measured by applying the D.C. voltage of 4 V and 10 V, respectively, at time t = 0. Another sample served as the control sample with no applied voltage, providing the background molecule release from the microcapsules. As shown in the control experiment result (the blue dotted plot in Figure 4-10), the initial release from the sample was detectable by the spectrometer at t = 80 mins (representing the diffusion time of BBG molecules through the shell of the microcapsules). The cumulative release increased with time, while the increasing rate of release gradually decreased. We noted that the release characteristic of the control sample was fitted well by the Higuchi diffusion model ($Q \cong A\sqrt{t}$, where Q is the cumulative release, and A is the geometrical parameter) [89]. In contrast, the application of 4 V caused an earlier initial molecule release occurring at t = 72 mins (8 mins earlier than the control sample). As the applied voltage increased up to 10 V, the initial release occurred at t = 56 mins, 24 mins earlier than the control sample. By comparing the cumulative release of the microcapsules for the different applied voltages, we found that in the period of ~40 mins after the initial release, the cumulative release rose faster with the high voltage than it did with the low voltage (see the slope of each plot). Specifically, at the applied voltage of 0 (control sample), 4, and 10 V, the cumulative release was 8.7 ± 1.3, 10.4 ± 1.6, and 13.1 ± 1.7 %, respectively, measured 40

www.manaraa.com

mins after their respective initial release (t = 120, 112, and 96 mins). This provided quantitative evidence that the embedded hydrogel actuators not only triggered an earlier initial release, but enhanced the release rate in a few dozen minutes (~40 mins) after the initial release. The higher the voltage applied, the earlier the initial release observed, and the more molecules released within that period. This result was consistent with our observation in Figure 4-9b that applying a higher voltage increased the volume of the embedded hydrogel beads. We note that the regulation of the release profile was effective in a few dozen minutes (~40 mins) after the initial release. Afterwards, the molecule release with the applied voltage progressed in a similar way to the background release from the control sample (Figure 4-10). The explanation of this result is that as some of the encapsulated molecules were released from the microcapsules, the elevated internal pressure gradually reduced, and thus, the molecule diffusion became a dominating release mechanism. Nevertheless, the result demonstrated that the microcapsules were capable of regulating the release profile of the encapsulated molecules by changing the internal pressure to influence the regular diffusion-based release (background release).

Figures 4-11 demonstrate tuning the release profile of the microcapsules (ID = 16.5 ± 3.5 μm; T_{shell} = 5.1 ± 2.8 μm; C_{bead} = 2 × 10^7 / mL) by applying multiple electrical stimulations at different time instances. Specifically, the first sample was tested by applying identical square voltages (amplitude $V_{amp1,2,3}$ = 4 V; duration time $t_{dur1,2,3}$ = 30 mins) at t = 2, 3, and 4 hrs, giving rise to the net release of 2.15 ± 0.21, 2.24 ± 0.27, and 2.17 ± 0.24 %, respectively (see the three steps on the black dotted plot in Figure 4-4 left).

www.manaraa.com

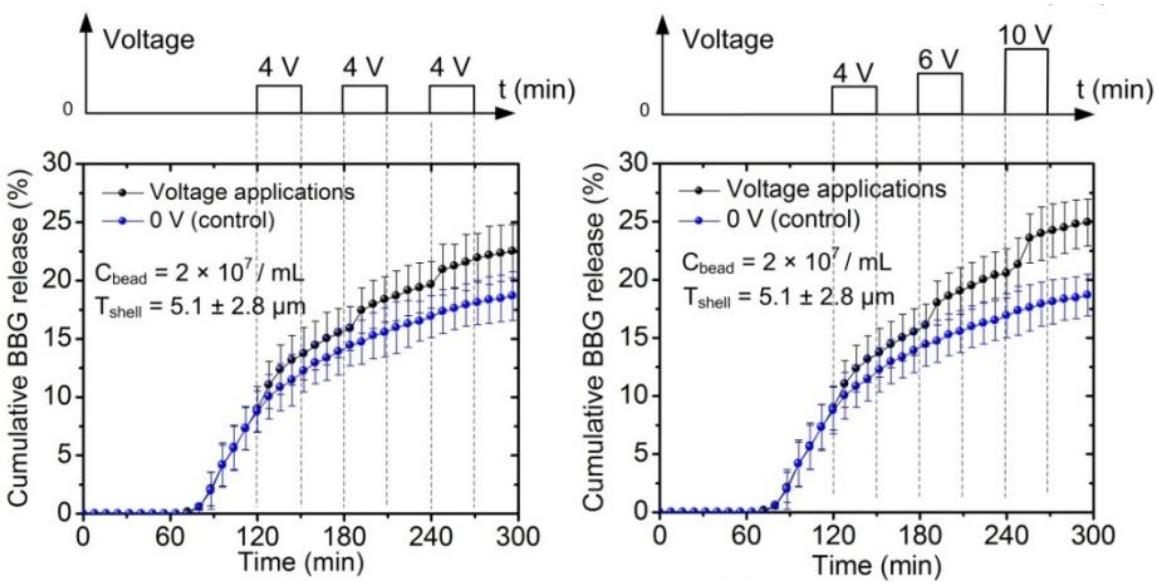

Figure 4-11 Cumulative BBG release from two identical samples of the microcapsules (ID = 16.5 ± 3.5 µm; T_{shell} = 5.1 ± 2.8 µm; C_{bead} = 2 × 10^7 / mL), responding to two different applied square voltages. The form of the applied square voltages is shown above the release profile.

Thus, the sample released almost equal amounts of BBG under the same voltage conditions at different time points and the resulting release profile (the black dotted plot) deviated from the background release profile (the blue dotted curve). In the second experiment, three different square voltages with increasing amplitude (V_{amp1} = 4 V; V_{amp2} = 6 V; V_{amp3} = 10 V; $t_{dur1,2,3}$ =30 mins) were applied to the sample at t = 2, 3, and 4 hrs, resulting in the net release of 2.15 ± 0.21, 2.69 ± 0.22, 3.37 ± 0.24 %, respectively (Figure 4-11 right). Thus, the higher the amplitude of the voltage, the more the BBG release occurred. To demonstrate the possibility of realizing a broad-range tuning of the release profile from the background release, we applied ten identical square voltages at different time points to the same type of the microcapsules. As shown in Figure 4-12, these square voltages had the same amplitude of 10 V and the same time duration of 30 mins. It was observed that each electrical stimulation triggered almost the same amount of net molecule release at ~3.4 % (see the ten

www.manaraa.com

steps on the plot in Figure 4-11). This allowed us to regulate the release profile of the microcapsules with relatively good accuracy. After the ten electrical stimulations, the resultant cumulative release was 65.2 ± 2.19 %, while the background cumulative release was only 32 ± 1.82 %. Thus, it was possible to realize a wide range regulation of the release profile by applying multiple electrical stimulations to the microcapsules.

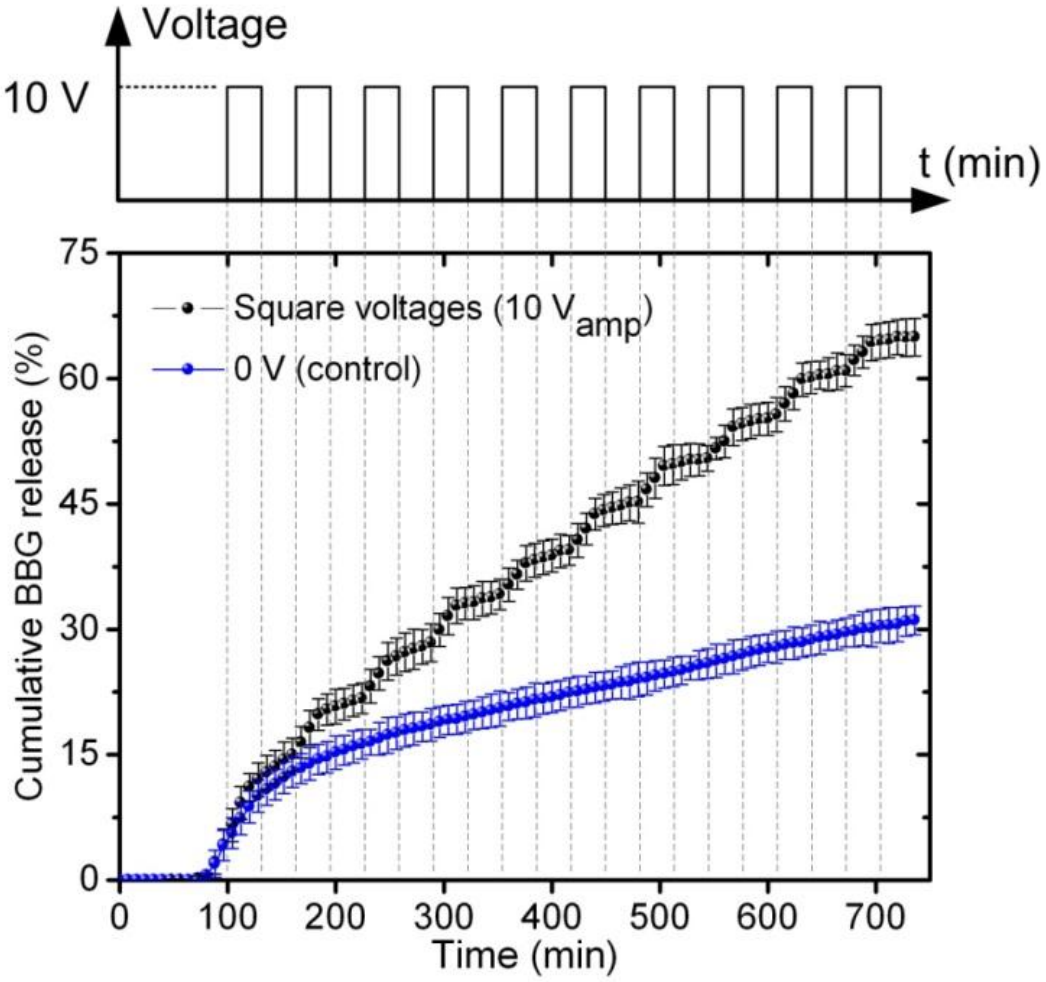

Figure 4-12 Cumulative BBG release of the sample of the microcapsules (ID = 16.5 ± 3.5 μm; T_{shell} = 5.1 ± 2.8 μm; C_{bead} = 2 × 10^7 / mL) under ten identical square voltage applications with the amplitude of 10 V and the duration of 30 mins.

www.manaraa.com

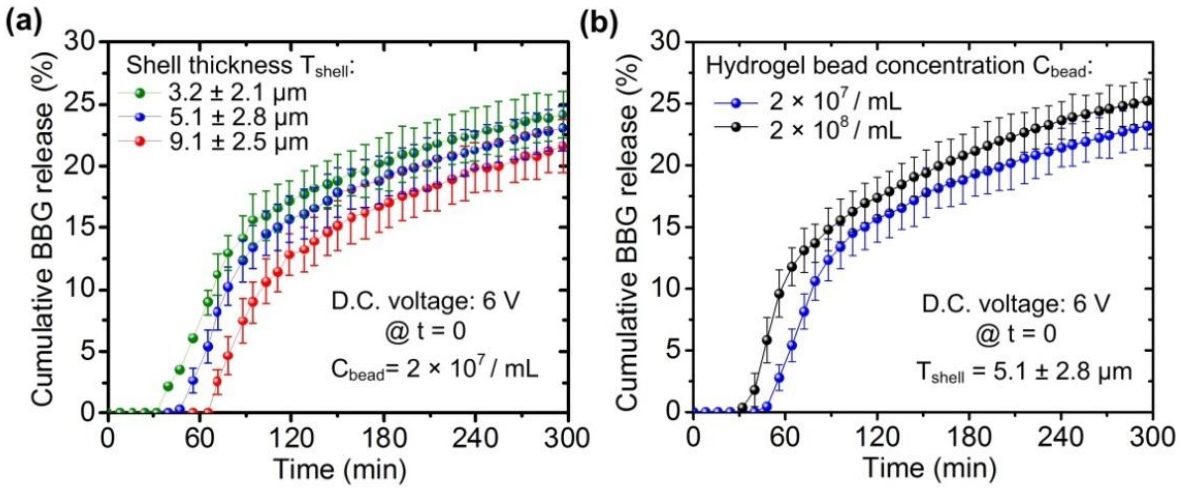

Figure 4-13 (a) Cumulative BBG release of three different samples. The samples were differentiated from each other by the shell thickness of the microcapsules (listed in the plot). OD = 27.35 ± 2.2 μm. C_{bead} = 2 × 10^7 / mL. The D.C. voltage of 6 V was applied to the three samples at t = 0. (b) Cumulative BBG release of two other samples. They were differentiated from each other by the concentration of hydrogel beads used in the outer flow of the co-electrospray process (given in the plot). The D.C. voltage of 6 V was applied to the two samples at t = 0.

To investigate how the shell thickness T_{shell} of the microcapsules influenced molecule release, three different samples (named sample S_1, S_2, and S_3) were prepared with the shell thickness of $T_{shell\text{-}S1}$ = 3.2 ± 2.1 μm, $T_{shell\text{-}S2}$ = 5.1 ± 2.8 μm, and $T_{shell\text{-}S3}$ = 9.1 ± 2.5 μm, respectively (note that $T_{shell\text{-}S1} < T_{shell\text{-}S2} < T_{shell\text{-}S3}$). The OD of the microcapsules in these samples was the same at 27.35 ± 2.2 μm. The concentration of the hydrogel beads used for all three samples was also the same at C_{bead} = 2 × 10^7 /mL. The D.C. voltage of 6 V was applied to the samples at t = 0. Figure 4-13a demonstrates that decreasing T_{shell} caused an earlier initial release from the microcapsules. Specifically, the initial release time of the sample S_1, S_2, and S_3 was found to be t_{S1} = 40, t_{S2} = 48, and t_{S3} = 64 mins, respectively. However, it is interesting to point out that after the initial release no obvious difference was observed in the cumulative release with time between the three samples. We believe that the

www.manaraa.com

reason is the following: Since the outer diameter of the microcapsules in the three samples was the same, their inner diameter had the relationship of $ID_{S1} > ID_{S2} > ID_{S3}$. The volume expansion of the hydrogel beads in the different samples was the same under the same voltage condition. This caused the internal pressure increase ΔP inside the microcapsules of the three samples to have the relationship of $\Delta P_{S1} < \Delta P_{S2} < \Delta P_{S3}$. Thus, the influence of decreasing the shell thickness on the release rate of the encapsulated molecules was largely counteracted by that of decreasing the internal pressure of the microcapsules. On the other hand, to demonstrate controlling the molecule release by changing the quantity of the hydrogel beads inside the microcapsules, two other samples (named sample N_1 and N_2) were prepared by using $C_{bead} = 2 \times 10^7$ /mL for N_1, and 2×10^8 / mL for N_2 (Figure 4-13b). Both of the samples had the same $T_{shell} = 5.1 \pm 2.8$ μm and ID = 16.5 ± 3.5 μm. The D.C. voltage of 6 V was applied to the samples at t = 0. Because the sample N_2 included more hydrogel beads than the sample N_1, the initial release from N_2 (t_{N2} = 32 mins) was detected earlier than that from N_1 (t_{N1} = 48 mins). Over the period of ~40 mins after the initial release, the cumulative release from the sample N_1 was 10.4 ± 1.51 %, less than that from N_2 of 13.34 ± 1.75 %. Afterwards, the release curves of the two samples had a similar changing tendency with time. Similarly, this was because after that 40-min period, the molecule release in both of the two samples was driven only by regular diffusion.

4.4 Discussions and Conclusions

To elucidate the underlying release mechanism of the present microcapsules, we constructed a model of the tri-layer core-shell structure and carried out a numerical simulation of the swelling process after a stimulus. According to the experimental result

www.manaraa.com

shown in Figures 4-13b, c, the outer diameter of the microcapsules (ID = 16.5 ± 3.5 μm, T_{shell} = 5.1 ± 2.8 μm, and $C_{bead} = 2 \times 10^8$ /mL) increased by 8.5 % as we increased the applied D.C. voltage from 0 to 10 V. Thus, the total volume of the hydrogel beads-solution system inside of the microcapsules increased as the hydrogel absorbed water. Given the low permeability of the PDLA shell, the volume increase was likely caused by the positive excess volume when mixing water and polymer in the hydrogel, as has been observed in similar systems. The positive excess volume may be related to voids in the gels or to the different spatial arrangement of water molecules in the gels. To account for such an effect, we modified the classic Flory-Rehner theory [90, 91], by assuming that each water molecule occupied a volume twice as large as the volume it occupies in a pure liquid phase. The static behavior of the liquid layer was modeled by an incompressible solid of negligible shear modulus, with its volume decreasing as the gel core swelled. The outer PDLA shell was modeled as a neo-Hookean solid with an elastic modulus 3 orders of magnitude higher than that of the hydrogel when dry.

For illustration purposes, we took the representative values of the experiments and set the initial diameter ratio of the gel core, liquid layer, and PDLA shell as 1:2:3.2 as in Figure 4-14a. Although in the experiments each microcapsule often contained different numbers of hydrogel bead, in the simulation we lumped the volume of multiple beads into one to maintain a simple symmetric structure.

www.manaraa.com

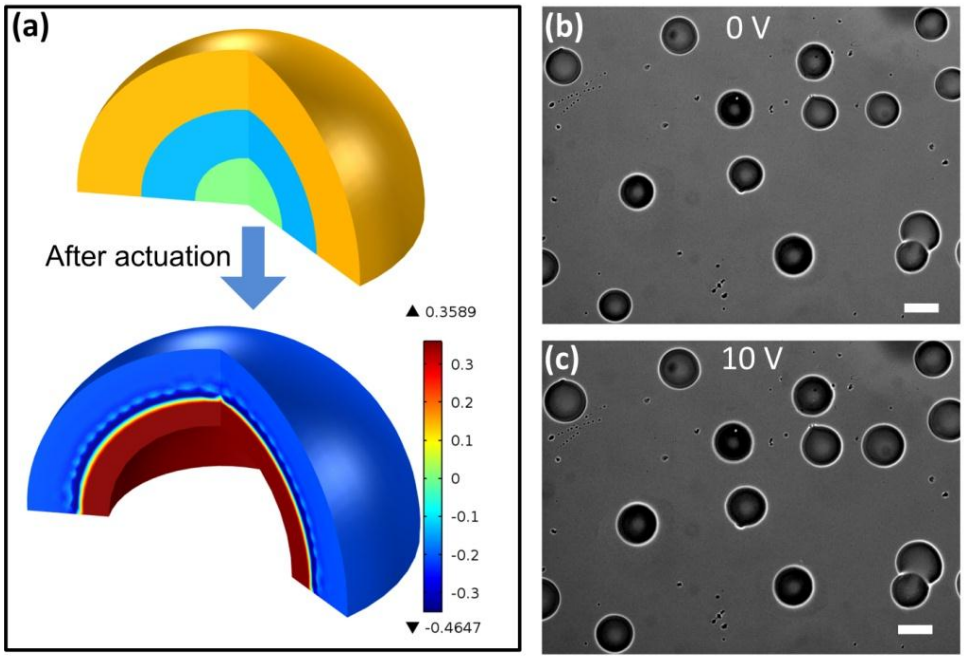

Figure 4-14 (a) Simulation result of the deformation of a microcapsule before (upper panel) and after (lower panel) a stimulus. The color scale in the actuated state indicates the distribution of pressure, normalized by the elastic modulus of the polymer shell. The hydrogel bead was removed to show the deformed structure (the pressure in the gel core was identical to that in the liquid layer). It was assumed that the volume occupied by each water molecule in hydrogel gel was larger than that in liquid water. The swelling of the hydrogel bead caused the volume increase of the water-hydrogel system inside, and consequently the expansion of the entire microcapsule. (b-c) Optical images showing the increase in the outer diameter of the microcapsules (ID = 16.5 ± 3.5 μm, T_{shell} = 5.1 ± 2.8 μm, and C_{bead} = 2×10^8 /mL) at three applied D.C. voltages: 0 V (b) and 10 V (c). The scale bars represent 20 μm.

As the actuation mechanism was coupled through a liquid layer, the actual shape and number of the gel beads should not affect the overall volume expansion. The gel core was initially in equilibrium with the liquid water. To model the effect of the stimulus, we reduced the Flory-Huggins parameter from 0.5 to -0.1. Such a change made the hydrogel more hydrophilic, so that it would take in more water and swell. The parameters were chosen so that the hydrogel beads increased in diameter approximately by a factor of 2 when unconstrained, as shown in Figure 4-14. Inside the liquid-filled microcapsule, the bead swells

www.manaraa.com

at the expense of the water from the liquid layer. The positive excess volume caused the bead-liquid system to expand, resulting in a ~8 % increase in the diameter of the microcapsule, and an increased pressure in the liquid layer, as shown by Figure 4-14a (lower panel). The calculated increase of diameter was comparable to that observed in Figures 4-14b, c. Taking a representative value for the modulus of PDLA, ~2 GPa, we estimated the peak internal pressure to be ~600 MPa. For molecules of size ~10^{-28} m^3, the internal pressure provided a chemical potential of ~10 k_BT, which was much higher than the entropic driving force of regular diffusion and thus dominated the release process. Other than the significantly increased driving force, the strain in the shell could also have increased the porosity and consequently the permeability of PDLA. However, we believe that compared to the increased internal pressure, the permeability change of PDLA was a relatively minor factor (due to the ~8% increase in outer diameter) in the experiment. To date, it was technically difficult to examine the pore size change of the PDLA shells with surrounding liquids. Nevertheless, the observed increase in the outer diameter resulted from the increased internal pressure of the liquid core, which could dominate the release process of the microcapsules.

It is known that degradation behaviors of PDLA are generally affected depending on the Mw of raw polymers used. Previous research demonstrated that low-Mw (e.g., 17,000) PDLA microstructures exhibited a significant degradation and water hydration in the low-Mw PDLA microstructures, while high-Mw (e.g., 41,000) microstructures showed little detectable degradation (until 53 days) [92]. Since our microcapsules used the high-Mw PDLA (Mw = 41,000) as the shell polymer, we believe that the influence of the polymer degradation on the release profile of the encapsulated molecules was negligibly small.

www.manaraa.com

There are several issues that remain. The distribution of hydrogel beads inside the microcapsules followed the Poisson distribution with a relatively low uniformity. Also, the size of our home-made hydrogel beads was not uniform either. To realize a more accurate and reliable release system, it is necessary to investigate how to prepare uniform-size hydrogel beads and disturb the natural Poisson distribution of the beads inside the microcapsules in the future. We note that the incorporation of the hydrogel beads into the interior of the microcapsules reduced the actual molecule loading capacity of the microcapsules. Also, hydrogel beads may absorb some of the encapsulated molecules. It is believed that optimization of the microcapsule dimensions and hydrogel chemistry can minimize the loading and release yield issues. However, handling of these issues is out of scope of this work.

We would point out that the present microcapsule scheme with the stimuli-responsive hydrogel bead actuators potentially can be relatively generic. By embedding other types of hydrogel into this microcapsule structure, it is possible to realize many other microcapsules remotely controlled by light, sound temperature,[1] and magnetic fields. This can provide more opportunities for developing controlled release microcapsules that can be interfaced to suitable external stimulation sources for delivery of chemical and biological species. However, it is important to investigate the workability of the microcapsules under medically safe doses of external stimuli that will likely trigger a significant clinical effect. Lastly, the internal actuation approach presented in this work potentially could be applied to many other existing controlled release mechanisms (e.g. shell rupture, shell dissolving by enzyme attract or chemical reaction, stimuli-responsive shell), having a broad impact on controlled

www.manaraa.com

encapsulation and release of biological and chemical agents and species (e.g., drugs, proteins, vitamins, cells, fragrances, and flavors) that are important to many applications ranging from food and pharmaceutical industry to inkless paper.

We have developed the MEMS-like liquid core-polymer shell microcapsules with embedded, electrically-sensitive hydrogel beads. The microcapsules were able to regulate the release profile of the encapsulated BBG molecules, by using external electric fields. The microcapsules were fabricated using a simple and single-step co-electrospray process. The statistical distribution of the number of hydrogel beads embedded in the microcapsules was adjusted by changing the concentration of the hydrogel beads in the inner flow of the co-electrospray process. The inner diameter of the microcapsules increased as the inner flow rate increased. We also have demonstrated that the BBG molecule release from the microcapsules started earlier for higher applied voltages. Additionally, higher applied voltages triggered the release of larger numbers of encapsulated molecules during the first several dozen minutes after the initial release. Furthermore, decreasing the shell thickness of the microcapsules caused an earlier initial release, while having little influence on the release rate (given that the outer diameter of the microcapsules was fixed). Lastly, increasing the number of hydrogel beads in the microcapsules resulted in not only an earlier initial release, but a faster release during a 40-min period after the initial release.

www.manaraa.com

CHAPTER 5. A CONTROLLED BIOCHEMICAL RELEASE DEVICE WITH EMBEDDED NANOFLUIDICS CHANNELS

5.1 Introduction to Controlled Release

Controlled release of active molecules (e.g., drug, gene, DNA, protein, and chemical agent) is highly desired for many applications in such diverse fields as pharmaceutical, agricultural, cosmetic, and food industries [93,94,95]. Polymeric micro/nanostructures such as spheres, tubes, fibers, and membranes play important roles in encapsulating and releasing these biomolecules [96-100]. Generally, biomolecules of interest are incorporated in either dissolved or dispersed form within a polymer matrix, and then, gradually diffuse out in a controlled manner by chemical and biological interactions between the polymer and the body environment. This type of controlled release devices often has no complex structures nor requires connecting to an external molecule source [96-100]. The other type of release devices is formed using micro-electro-mechanical systems (MEMS) technology. They can be reloaded with biomolecules of interest and can accurately control molecule release using relatively complex MEMS structures [101]. The controlled release device studied in this chapter falls in the former category.

Stimuli-responsive hydrogels are smart materials that can expand and contract, responding to environmental stimuli such as glucose, antigen, pH, temperature, light, electric field, and ionic strength [102]. Research and development of controlled release devices based on stimuli-responsive hydrogels have been attracting much attention [103-110]. However, almost all existing hydrogel-based release schemes require chemically incorporating eleasable molecules into hydrogel delivery matrices by molecular binding. Liberation of

www.manaraa.com

entrapped molecules relies on swelling polymer chains as hydrogels undergo a responsive swelling-driven phase transition, or cleaving polymer chains via hydrolytic degradation or enzyme attack [106]. Therefore, to realize controlled release of molecules from hydrogels, many factors and their interplays have to be taken into account, including polymer-molecule binding affinities and interactions, destruction of labile covalent bonds, release kinetics of entrapped molecules within hydrogel matrices, and swelling rate of polymer networks [107,108]. This may pose complexity and difficulty inndesigning hydrogel pharmacological formulations and associated delivery micro/nanocapsules. Electrospinning is a simple, effective, and versatile method for producing nanofibers from polymers or polymer blends. It utilizes a high electric field to draw a charged polymer solution out of a metallic needle into a liquid jet. The jet undergoes thinning, bending, and stretching in air. Finally, nanofibers fall onto a collector. Co-electrospinning is a relatively new technology with a coannular nozzle, for fabricating complex nanofibers encasing materials such as polymer and liquid crystal within a polymer shell. [110,111] New applications of co-electrospun nanofibers are expanding. For example, we recently developed flexible light-emitting nanofibers by encapsulating liquid metal into a polymer sheath of organic electroluminescent materials [112].

In this chapter, we report a controlled biochemical release device embedding nanofluidic channels into a polymer network of a stimuli-responsive hydrogel (Figure 5-1(a)). The nanofluidic channels serve as biomolecule reservoirs and are formed by multiple liquid core-polymer shell nanofibers. The core layer of the nanofibers contains an aqueous solution with biomolecules of interest. The outer layer is made of a hydrophobic polymer

www.manaraa.com

shell, functioning as a barrier to minimize lateral leakage of encapsulated biomolecules. The nanofibers are fabricated using co-electrospinning and then are embedded into a stimuli-responsive hydrogel membrane. Two ends of the nanofibers are open. Our hypothesis for controlled release of the device is based on buckling instability of the polymer shell of the nanofibers. Briefly, interactions between the hydrogel and a specific stimulus cause to change physical volume of the hydrogel. As a result, the embedded nanofibers carry a large compressive stress in both axial and radial directions, causing buckling of the shell of the nanofibers and extrusion of the encapsulated biomolecules. The present device decouples releasable biomolecules from a hydrogel polymer matrix, avoiding chemical interactions between the biomolecules and the hydrogel polymer chains, and thus, alleviating nontrivial chemical and biological engineering design of hydrogel formulations. Therefore, this method can make it easier and more accurate to tune and optimize release characteristic of the device.

5.2 Fabrication of Embedded Nanofluidics Device

To prepare the NIPAAm hydrogel solution, N-isopropyl acrylamide (NIPAAm), N,N'-methylenebisacrylamide, dimethyl sulphoxide, deionized water and 2,2-dimethoxy-2-phenylacetophenone are mixed in the weight ratio of 2.18 : 0.124 : 3.0 : 1.0 : 0.154 and then vigorously stirred for 30 mins at room temperature. The PDLA solution is prepared by mixing PDLA (i.v. = 0.69) pellets (Lactel Polymers) and chloroform in the weight ratio of 1:8. This mixture is stored at 4 ^{o}C for 24 hrs to dissolve these pellets and then vigorously stirred for 2 hrs at room temperature to obtain a transparent, homogeneous solution. All chemicals are purchased from Sigma-Aldrich unless otherwise stated and used as received without further purification. As an important component of the co-electrospinning setup, a

www.manaraa.com

coaxial spinneret is formed by inserting a 21-guage needle into a 23-guage needle (BD Biosciences). The spinneret allows delivery of the outer PDLA solution and the inner BBG solution independently by two individual syringe pumps (KDS 2000, Kd Scientific). The voltage of 9.5 kV (Gamma High Voltage Research) is applied to the spinneret. A collector is placed 10 cm below the spinneret and formed by patterning two parallel gold (Au) thin strips on a glass slide. The flow rate for the core and polymer shell layers is 0.4 and 0.6 mL/hr, respectively.

To embed the nanofibers into the NIPAAm hydrogel, another glass slide is placed 50 μm above the collector. Then, the hydrogel solution is flowed into the air gap between the two slides and then exposed under ultraviolet irradiations. The exposure time and light intensity is 12.5 s and 15.3 mW/cm^2, respectively. After that, the upper glass slide is removed. Finally, the hydrogel membrane embedding liquid core-polymer shell nanofibers is carefully peeled off from the lower slide and ready for test.

The device used in this example is structurally identical to that in Figures 5-1a-b. The temperature of the device is increased from 22 ^oC at t = 3 hr and stabilized at 28 ^oC after ~110 s. Then, the temperature is held for 40 s before the heater is turned off. BBG release is observed to increase distinctly from ~18.5 to ~28.6 % of the total loading amount (Figure 5-1a). Similarly, the control "A" device is identical to the actual device, but operates at 22 ^oC (constant). The control "B" device is also identical to the actual device, but has no surrounding hydrogel. Figure 5-5b shows the corresponding absorbance spectra of the three devices above.

To demonstrate the mechanism, N-isopropyl acrylamide (NIPAAm) temperature-sensitive hydrogel is used as a model hydrogel, which expands at low temperatures and

www.manaraa.com

shrinks at high temperatures. Hydrophobic poly (D, L-lactide) (PDLA; PDLA-to-chloroform weight ratio¼1:8) and aqueous Brilliant Blue G (BBG, 1mg/ml) solution are used as the polymer shell material and inner core liquid, respectively, of the nanofibers. Since interaction between water and PDLA is thermodynamically unfavorable, possible lateral leakage of BBG molecules through the shell is significantly reduced. Figures 5-1(b)–(d) show the brief device fabrication processes for the proposed release device. The fabrication involves using co-electrospinning to fabricate BBG liquid core-PDLA polymer shell nanofibers (Figure 5-1(b)) and using liquid phase photopolymerization to embed the nanofibers into a 50 lm thick NIPAAm hydrogel membrane (Figure 5-1(c)). A razor blade is used to cut a strip of the nanofiber-hydrogel membrane for testing (Figure 5-1(d)). Here, the BBG solution is automatically loaded into the core of the nanofibers during co-electrospinning. The spinning time is 1 h, resulting in multiple layers of stacking nanofibers (~45 lm thick in total). The nanofibers (liquid core diameter: ~680 nm; PDLA shell thickness: ~145 nm) are aligned perpendicular to two gold strip electrodes on a glass slide due to electrostatic interactions (Figure 5-1(e)).

www.manaraa.com

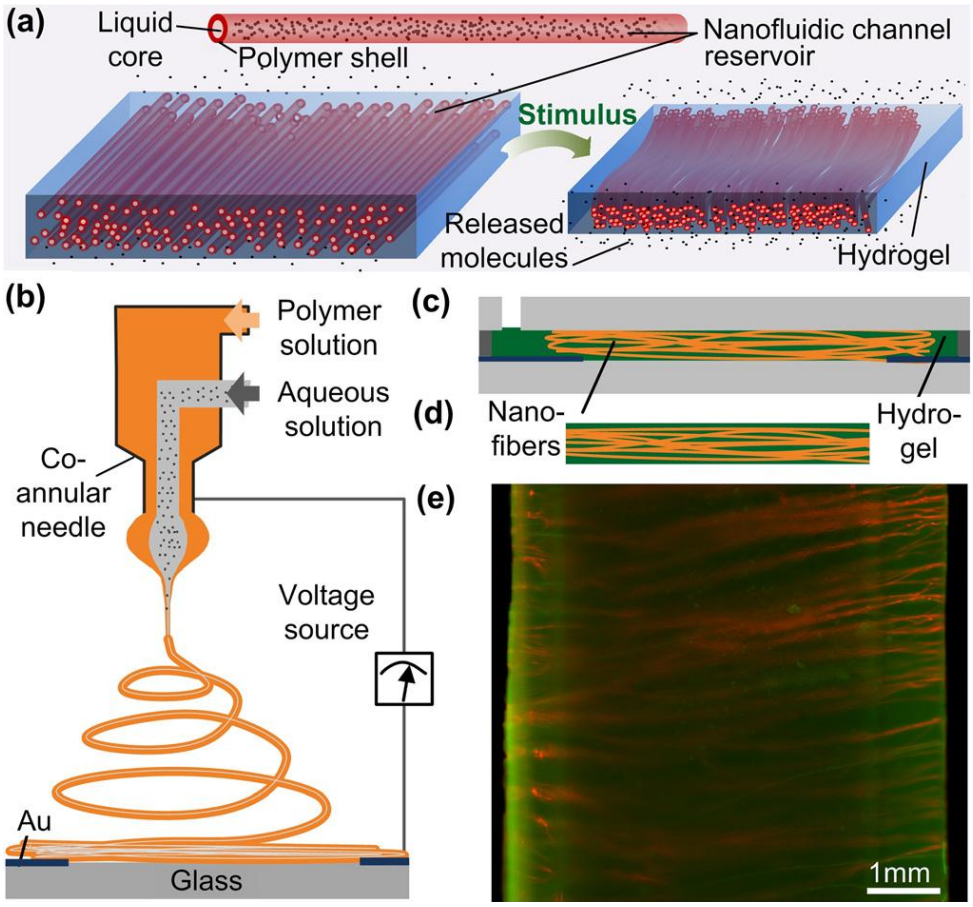

Figure 5-1 (a) Schematic for structure and mechanism of the controlled release device. Fabrication processes for the device: co-electrospinning liquid corepolyme shell nanofibers (b); flowing hydrogel solution into nanofiber interstitials and photopolymerization of hydrogel (c); cutting a strip of hydrogel membrane embedding nanofibers (d). (e) Fluorescent image for part of the fabricated device (green: hydrogel; red: nanofibers).

5.3 Theoretical Basis for Embedded Nanofluidics Device

We first conduct a theoretical study to elucidate the mechanism. The device is regarded as a composite with aligned PDLA nanofibers in a hydrogel matrix. We model PDLA as a neo-Hookean material, and NIPAAm hydrogel with the Flory-Rehner model [91,115]. The calculation is carried out using SIMULIA Abaqus 6.10 with the hydrogel model implemented through a user subroutine [115]. We assume the hydrogel to be in equilibrium with pure solvent and execute a static analysis disregarding the drug flow in the

www.manaraa.com

core. The Flory-Huggins parameter X is gradually increased from 0.1 to 0.5 to model the effect of the temperature-induced phase transformation [116, 117]. The increased hydrophobicity causes the hydrogel to shrink.

For simplicity, we neglect the interaction between nanofibers and only look at a single nanofiber in a large piece of hydrogel. The cross-sectional geometry of nanofiber is set to that measured, and the elastic modulus of PDLA is set to be 1000 times that of dry NIPAAm. The initial water concentration is set to be 97.5 vol. %. The simulated deformation pattern is shown in Figure 5-2. During the initial stage of deswelling, the nanofiber deforms uniformly (Figures 5-2(a) and (b)). When v further increases beyond a critical value, the uniform deformation loses stability, and the nanofibers buckles. The initial buckling is close to the Euler buckling of a beam, but as the amplitude increases, the circular cross section collapses (Figure 5-2(c)). The cross-sectional images shown in Figures 5-2(d) and 5-2(e) clearly illustrate this change. Before the onset of instability, the cross section of the nanofibers remains circular, with the diameter slightly increases due to the Poisson effect. As a result, the internal volume of the nanofiber is hardly changed, and the liquid drug is not released except by diffusion. It is shown that, after buckling, the cross section of the nanofiber is flattened, and the internal volume greatly reduced. The drug content is thus squeezed out from the nanofiber. Similar to the wrinkles in a hardfilm-soft-substrate system [118], the wavelength of buckling is set by the nanofiber geometry and the stiffness ratio between the nanofiber and the hydrogel membrane.

www.manaraa.com

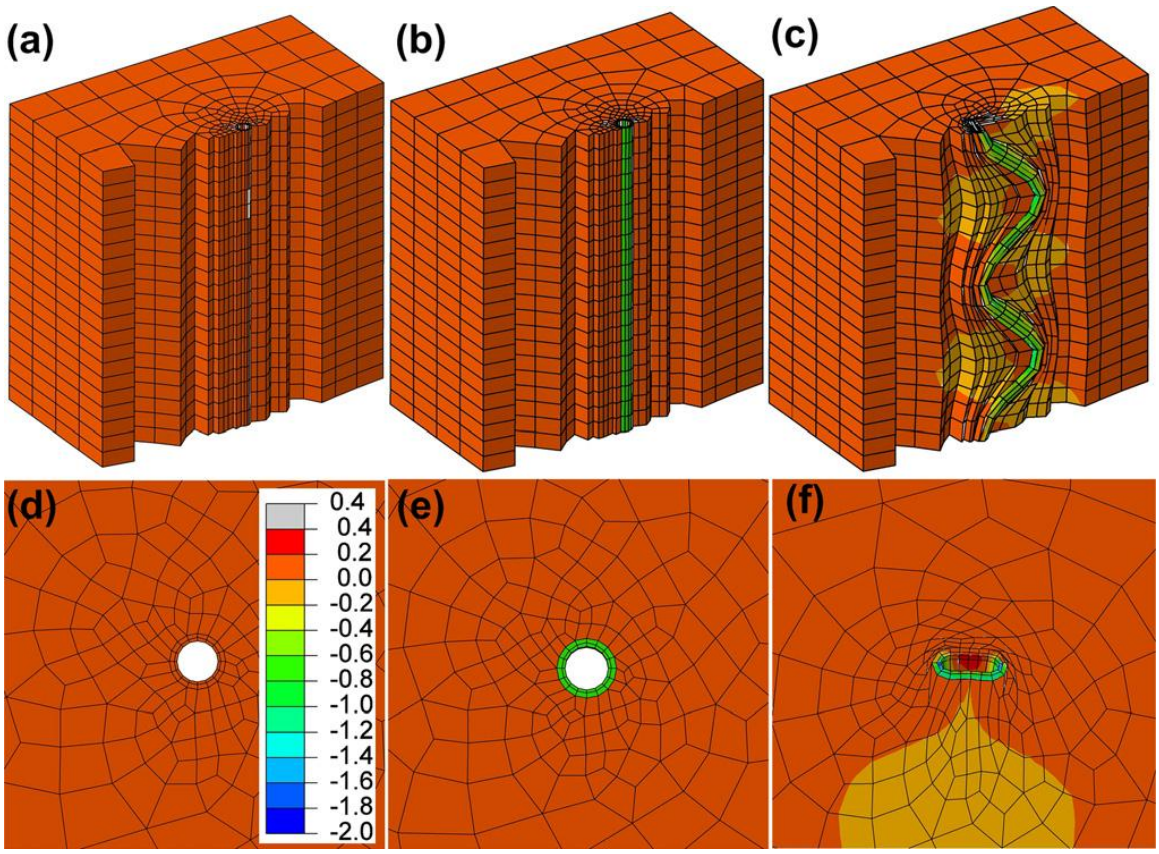

Figure 5-2 Calculated deformation of nanofiber-hydrogel system at (a) the initial (swollen) state, (b) the state before buckling, and (c) the post buckling state. Part of the model has been removed to show the fiber. (d) and (e) The cross-sectional view of the fiber at different stages. The colorscale shows the axial stress normalized by the modulus of PDLA.

5.4 Measurements of Embedded Nanofluidics Device

As a release indicator, BBG has a characteristic absorption peak at the wavelength of 600 nm. BBG release from the fabricated device is determined by measuring changes in absorption intensity with a spectrometer (2800 UV/VIS, UNICO). A nanofiber-hydrogel device is placed on the bottom of a quartz cuvette (BrandTech Scientific) containing deionized water. Local temperature of the cuvette is controlled by a Kapton heater, a Type-K thermocouple, and a thermostat. Prior to each spectroscopic measurement, the liquid in the

www.manaraa.com

cuvette is stirred gently for several seconds using a glass rod, to obtain a uniform distribution of BBG molecules within the cuvette. Each measurement cycle takes about 8 s.

Figures 5-3(a) and 5-3(b) demonstrate temperature response of the device to a temperature excitation. Here, the device temperature is increased from room temperature (22 ^{o}C) at ~1 h and stablized at 26 ^{o}C after 110 s, and then, it is held for 40 s before the heater is turned off (upper panel in Figure 5-3(c)). About 10 s after the temperature stablization, the hydrogel starts to shrink and then stops in 10 s. BBG release increases rapidly from 9.1 to 16.3 wt. % of the total loading amount in 8 s (Figure 5-3(a), and lower panel in Figure 5-3(c)). To confirm the role of the hydrogel in controlling the molecule release, two control experiments (controls "A" and "B") are conducted. The control "A" device is identical to the actual device having both hydrogel and nanofibers, but operates at a constant temperature of 22^{o}C. Thus, molecule release is governed by molecular concentration difference induced entropic driving force. It is obvious that the release profile of the actual device deviates from that of the control "A" device. We note that increasing temperature can not only trigger hydrogel contraction, but also cause to elevate diffusion rate of BBG from the core. It is thus necessary to find out how each of the two consequences contributes to regulating the release profile of the actual device. The control "B" device only has nanofibers but does not have surrounding hydrogel. Under the same temperature activation (upper panel in Fig. 5-3(c)), BBG release increases only slightly from 9.1 to 10.6 wt. % of the total loading amount. This release counts only a small portion of the total release from the actual device (from 9.1 to 16.3 wt. %). Response of the device to a different temperature excitation is demonstrated in

www.manaraa.com

supplementary material. Therefore, it is confirmed that the hydrogel volume change dominates the modulation of the molecule release in the present device.

We believe that the release action is mainly caused by buckling instability of the PDLA shell of the nanofibers. As shown in Figure 5-3(c), almost no BBG molecule is released after temperature increases, until a certain delay after which a large amount of drug is released. The delay followed by sudden release is an evidence of the buckling mechanism. Due to the huge difference in stiffness between the PDLA and the NIPAAm hydrogel, the shrinkage of the hydrogel initially would not induce a large deformation in the nanofibers. Instead, a hoop stress is developed in the hydrogel surrounding each fiber. With the thickness of the shell comparable to its inner radius, the radial collapse of the cylindrical shell may seem unlikely if only the hoop stress is present. In this system, the nanofibers also carry a large compressive stress in the axial direction, as shown in Figure 5-2(b). The combined axial and radial compression is expected to cause the buckling of the PDLA shells.

Figure 5-4 (left axis) displays net BBG releases from multiple similar devices under various temperature excitations. Each nanofiber-hydrogel device is heated up from 22 ^{o}C (at t~1 h) to a specific higher temperature. BBG release is monitored 10 s after a higher temperature is stabilized. The result shows that the devices with large temperature rises release more BBG than those with small temperature rises. A significant BBG increase occurs between 30 and 35 ^{o}C. A primary reason behind the observation is that the volume phase transition point of the NIPAAm hydrogel is around 32 ^{o}C, near which the hydrogel shrinks rapidly. Volume response of the hydrogel membrane embedding the nanofibers is shown in Figure 5-4 (right axis).

www.manaraa.com

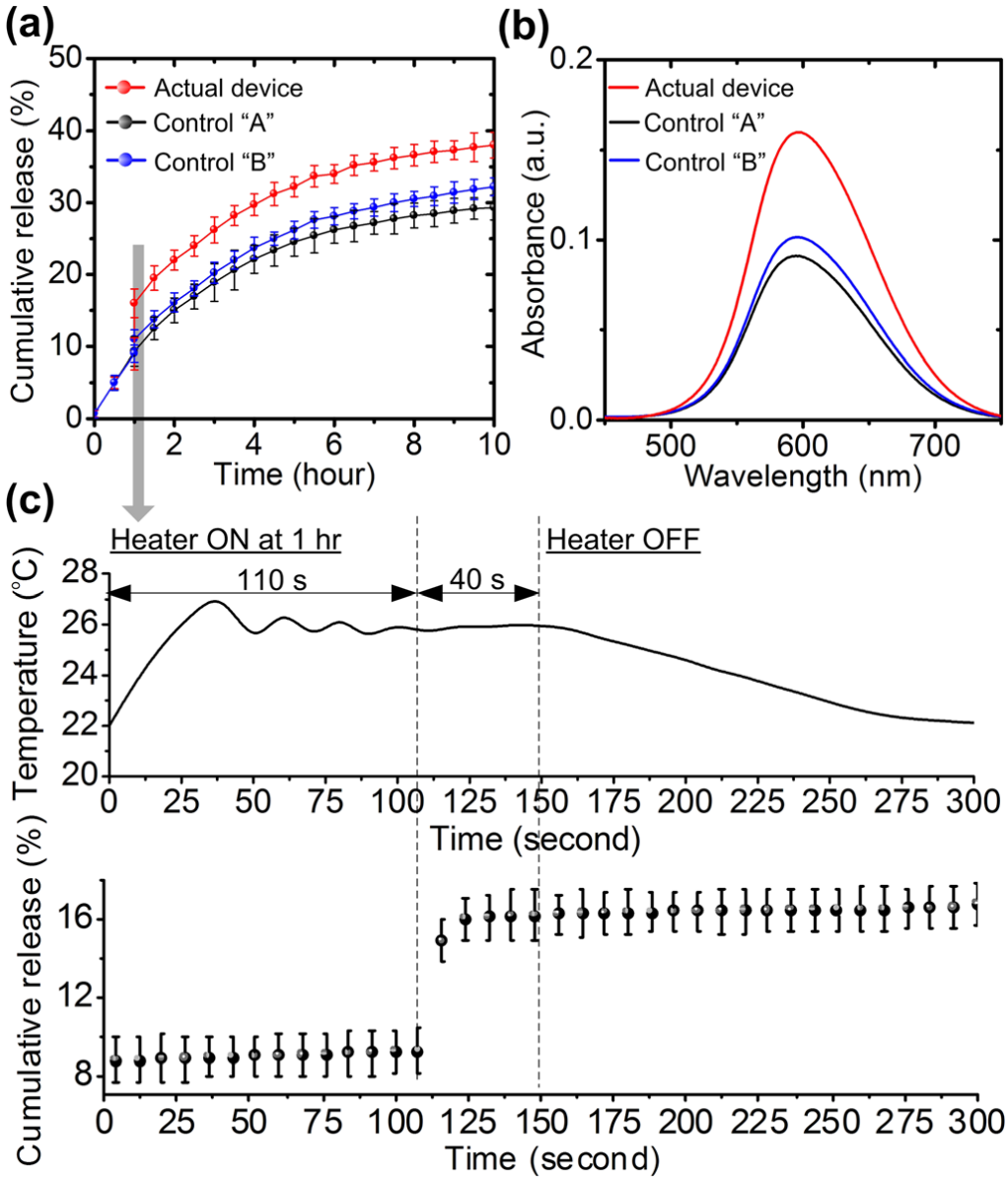

Figure 5-3 Cumulative release profiles (a) and corresponding absorbance spectra (b) of an acutal device, and control "A" and "B" devices. (c) A close-up cumulative release profile (lower panel) under a temperature excitation (upper panel) starting at t¼1 h over 300 s.

www.manaraa.com

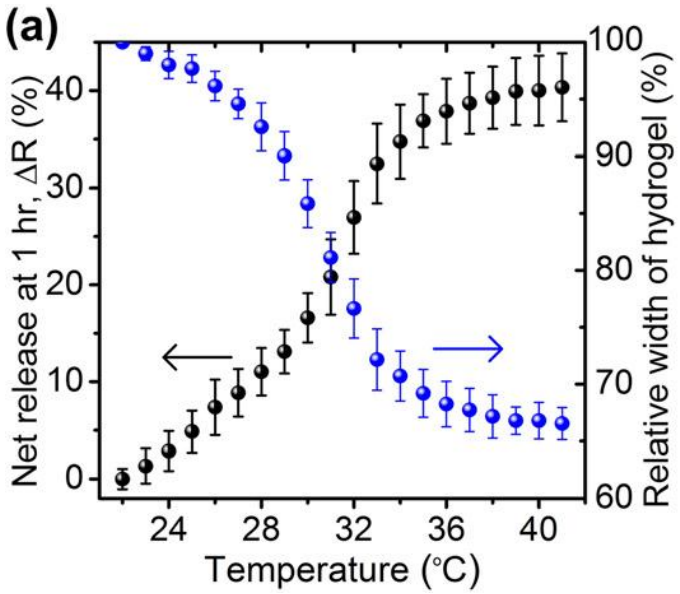

Figure 5-4 Net BBG release of different individual release devices as a function of temperature (left axis). The starting temperatures for the devices are all at 22 ^{o}C. The right axis shows dimension (width) change of the device shown in Figure 5-2(d), as a function of temperature. The highest value of 100% represents no change in hydrogel width at 22 ^{o}C.

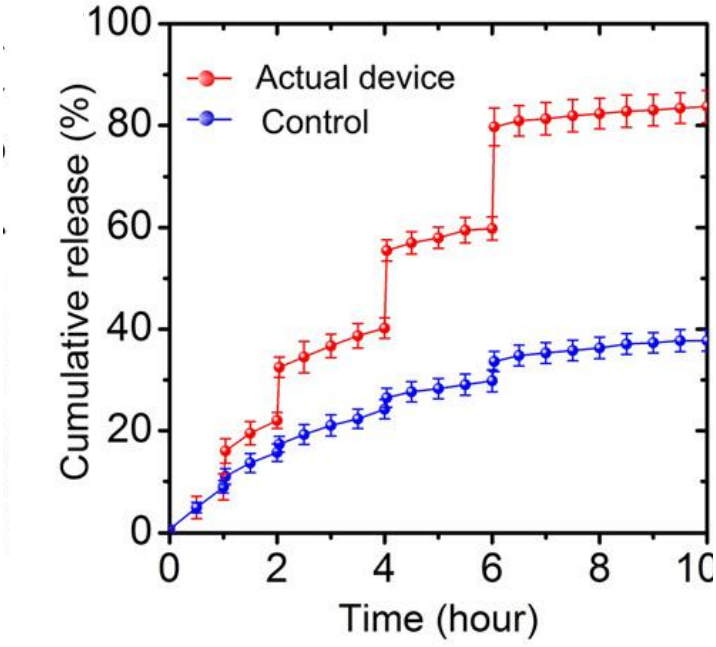

Figure 5-5 Cumulative release from an actual device (red dot) and a control device responding to multiple temperature excitations (blue dot). The control device is structurally the same as the actual device, except for having no surrounding hydrogel.

www.manaraa.com

Figure 5-5 demonstrates real-time regulating the release profile of a nanofiber-hydrogel device by applying multiple temperature excitations at different time instances. Here, the device is excited from 22 to 26 ^{o}C C at t~1 h, from 22 to 28 ^{o}C at 2 h, from 22 to 30 ^{o}C C at 4 h, and from 22 to 32 ^{o}C C at 6 h, giving rise to release 7.2, 10.5, 15.1, and 10.4 wt. %, respectively, of the total loading amount, whereas a control device releases 1.5, 1.9, 2.3, and 3.8 wt. %, respectively, under the same conditions. The result not only confirms further that the hydrogel functions to squeeze the encapsulated molecules out of the nanofibers, but also, more importantly, demonstrates the capability of tuning the release characteristic in a real-time manner.

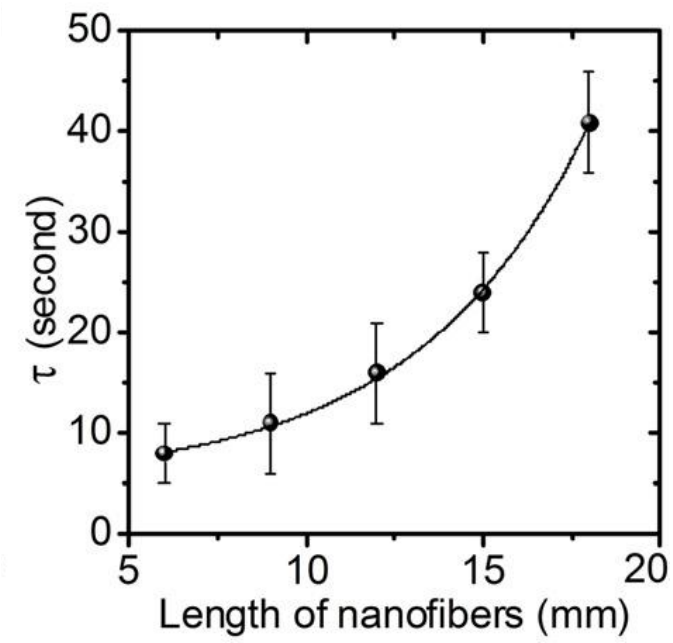

Figure 5-6 Time gap s between observing hydrogel contraction and observing abrupt BBG release, as a function of the length of the nanofibers.

To examine how the length of the nanofibers L affects a time gap s between observing hydrogel contraction and observing abrupt molecule release, we fabricate five nanofiber-hydrogel devices with different L. As L increases from 6 to 18mm (Figure 5-7), s

www.manaraa.com

increases from 8 to 41 s under the same temperature excitation (22 - 26 ^{o}C at 1 h). Also, the increasing rate of s is found to increase with increasing L. A possible explanation is as follows. As the nanofibers are being deformed by shrinking hydrogel, the encapsulated molecules in the liquid core experience acceleration. When the short nanofibers are used, BBG molecules in the deep central region of the liquid core can leave the nanofibers before the hydrogel contraction is completed. But, this is not the case when the long nanofibers are used: after the hydrogel contraction is completed, BBG molecules have not been away from the nanofibers. They continue moving inside the nanofibers mainly by inertia, but not by a squeezing force. Due to lack of further acceleration, a longer time is required for the encapsulated molecules to leave the nanofibers.

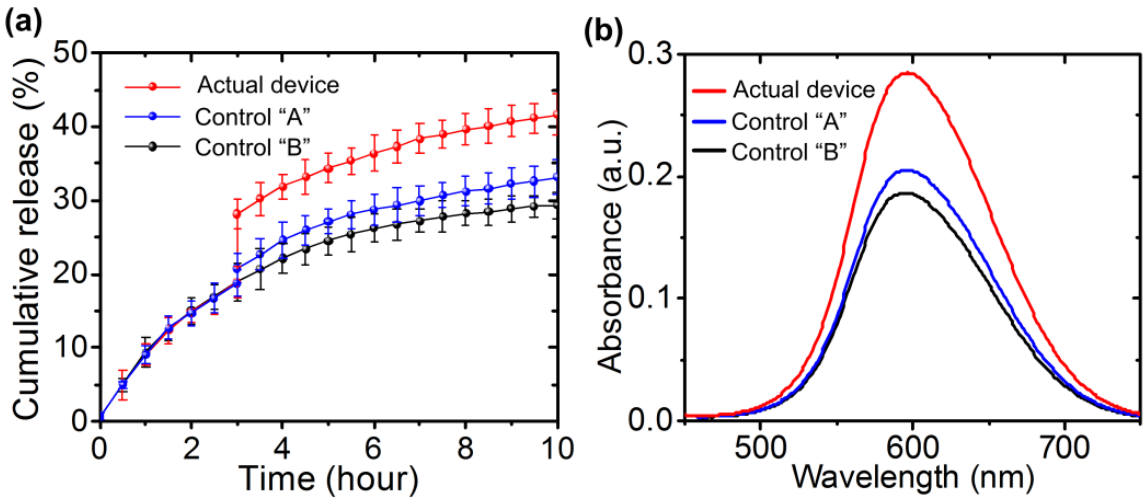

Figure 5-7 (a) Cumulative release profiles and (b) corresponding absorbance spectra of the release device, the control "A" device, and the control "B" device. Temperature excitation: 22 → 28 ^{o}C at t = 3 hrs.

The present work has demonstrated integrating co-electrospun nanofluidic channels into stimuli-sensitive hydrogels to realize controlled release of biomolecules. The device architecture allows isolating releasable molecules from responsive polymer matrices and, thus, minimizing complex chemical and biological engineering design effort of hydrogel

www.manaraa.com

formulations. The co-electrospinning process allows for flexible tuning of materials and dimensions of the polymer shell and liquid core of nanofibers [110, 111]. Also a wide variety of materials (e.g., neural probes, plastic, silicon) may be chosen to collect nanofibers. Further elaboration of the controlled release technology is possible by taking the following efforts. First, the present device is obtained by cutting from a hydrogel membrane embedding core-shell nanofibers.

To accurately control device dimensions, selective nanofibers patterning techniques can be adopted to pattern as-deposited nanofibers [118]. Second, the encapsulated molecules in the nanofibers initially diffuse out through the two side openings of the nanofibers. This issue could be alleviated by using an appropriate polymer-based molecule carrier in the core of the nanofibers. Finally, the simulation result presented here servers the purpose of demonstrating the mechanism. With more detailed material models, dynamic release process may be simulated. Nevertheless, by employing other specific stimuli-responsive hydrogels into the present device architecture, this approach can potentially herald a possible solution for controlled release of various biological species and chemical agents.

www.manaraa.com

CHAPTER 6. CONCLUSION AND FUTURE WORK

In this thesis, two smart controlled drug release system were developed employing electrospinning as the core fabrication technology. The high yield and cost effective property of electrospinning facilitate the fabrication of micro and nanofibers as well as spherical core-shell structures. Both electrospinning products, aligned core-shell fibers and core-shell microspheres, are developed and applied in smart biomolecule release systems. Environmental sensitive hydrogels are integrated in the two drug delivery systems as the sensing and actuation elements. In the MEMS-like liquid core-polymer shell microcapsules delivery system, electrically-sensitive hydrogel are fabricated as micron-sized beads. While in the embedded nanofluidics delivery device, temperature sensitive hydrogel acts as a bulk structure. Both systems are able to control and regulate the release profile of internal loadings.

Electrospinning is the major fabrication technology in this work. Selective deposition of electrospun nanofibers using microfluidics confinement method offers a technology platform for further applications of electrospinning in biomolecule release systems. A simple, versatile method for the selective deposition of nanofibers with high definition using a unique microfluidic fiber collector was presented. The collector contains fiber etching solutions that are selectively confined to defined regions by means of photocleavable self-assembled monolayer (SAM) technology and microfluidic capillary filling. The presented approach achieves arbitrarily shaped, microsized, structurally accurate architectures in both random and aligned nanofibers. Aligned and selected deposited core-shell electrospun fibers are successfully applied to fabricate the microfluidics drug reservoir. The electrospinning

www.manaraa.com

technology is highly versatile in adjusting the fiber parameters, such as inner and outer diameter as well as porosities. These freedoms further provide a method to adjust the loading ability and release rate of the system.

Core-shell microcapsules are developed capable of regulating the release profile of encapsulated molecules. These microcapsules uniquely contain embedded miniature actuators inside their liquid core. The internal actuators are made of stimuli-responsive smart hydrogel beads. The embedded hydrogel beads swell in response to external electric fields, regulating the internal pressure of the liquid core, and thus the diffusion rate, of the encapsulated molecules from the microcapsules. The incorporation of the actuators into the interior of the microcapsules provides an internal control variable to a conventional diffusion-based release process. The microcapsules, which behave much like micro-electro-mechanical systems (MEMS), are fabricated by a simple co-electrospray process. This fabrication technique allows integrating the hydrogel beads, forming the polymer shell, and loading the releasable molecules simultaneously in one step. The microcapsules were able to regulate the release profile of the encapsulated BBG molecules, by using external electric fields. The statistical distribution of the number of hydrogel beads embedded in the microcapsules was adjusted by changing the concentration of the hydrogel beads in the inner flow of the co-electrospray process.

A second controlled release device is developed by embedding nanofluidic biomolecule reservoirs into a polymer network of a stimuli-responsive hydrogel. The reservoirs are made of liquid core-polymer shell nanofibers using co-electrospinning technique. The mechanism of controlled release is based on buckling instability of the

www.manaraa.com

polymer shell under combined axial and radial compression, caused by volume changes of hydrogel responding to a specific stimulus. The device decouples releasable biomolecules from a hydrogel polymer matrix, avoiding chemical interactions between biomolecules and hydrogel polymer chains, and thus, alleviating nontrivial chemical and biological engineering design of hydrogel formulations. Temperature-sensitive hydrogel is used as a model hydrogel. The present work has demonstrated integrating coelectrospun nanofluidic channels into stimuli-sensitive hydrogels to realize controlled release of biomolecules. The device architecture allows isolating releasable molecules from responsive polymer matrices and, thus, minimizing complex chemical and biological engineering design effort of hydrogel formulations. The co-electrospinning process allows for flexible tuning of materials and dimensions of the polymer shell and liquid core of nanofibers. Also a wide variety of materials (e.g., neural probes, plastic, silicon) may be chosen to collect nanofibers. Further elaboration of the controlled release technology is possible by taking the following efforts. First, the present device is obtained by cutting from a hydrogel membrane embedding core-shell nanofibers.

Although we have extensively studied the fabrication process as well as the measurement of devices, there are still multiple tasks left to further explore in this area. The polymer material we used in this study is mostly a model polymer PDLA. However, the cost of PDLA is expensive comparing to other polymers. It would be very promising if a substitute polymer could be found to replace PDLA in this system with equal device performance to cut down the cost. Finding suitable substitutes will also widen the application of this work.

www.manaraa.com

A comprehensive theoretical release device model would be necessary to further understand the dynamics performance and make comparisons between the above two release devices in multi aspects. First, the two devices employ hydrogels in different format: bead structure and bulk structure. Although hydrogel performance with respect to its size and geometry is studied in other work previously. Hydrogel dynamics and its effect to drug release system were not particularly studied. Therefore, a theoretical analysis and experimental verification work of hydrogel dynamics at this particular situation will provide information on the hydrogel swelling and contracting dynamics, which is the most important part of understanding dynamic performance of the drug release system. This theoretical model would eventually guide the device design to search for optimum design parameters, such as the inner and outer diameters in the fibrous structure and spherical structure, size and number of hydrogel beads in each compartment, geometry information regarding the bulk temperature sensitive hydrogel. Besides, locating each drug release performance parameter with design parameter is highly necessary and desired to accurately define and design release systems.

Electrically sensitive and temperature sensitive hydrogels are used as two model hydrogels in this work. Other types of hydrogels are already available, such as photo-sensitive hydrogel, pressure sensitive hydrogel, pH sensitive hydrogel. Although hydrogel materials are bio-compatible, the actual effect of physiological environment to hydrogel and to the dynamics performance of the release system is not studied in this work. In the microcapsule release systems, hydrogel beads are fabricated in our lab since no commercial hydrogel beads in the range of micron are currently available to purchase. Although our

www.manaraa.com

hydrogel beads diameter distribution is acceptable to use as preliminary research, a highly uniform distributed hydrogel beads with small standard deviation value is necessary to accurately study the effect of size and number of hydrogel beads per microcapsule statistically.

www.manaraa.com

BIBLIOGRAPHY

[1] K. E. Uhrich, "Polymer Systes for Controlled Drug Release," *Chem.Rev*. 1999, vol. 99, pp. 3183-3198.

[2] W. Morris, M. C. Steinhoff and P. K. Russel, "Potential of polymer microencapsulation technology for vaccine innovation," *Vaccine*, 1994, vol. 12, pp. 5-11.

[3] R. A .Siegel, "Controlled Drug Delivery Challenges and Strategies," Park, K., Ed. 1997.

[4] O. Wichterle and D. Lim, "Hydrophilic gels for biological use," *Nature*, 1960, vol. 185, pp. 117-118.

[5] I. I. Slowing, J. L. Vivero-Escoto, C. Wu and V. Lin, "Mesoporous silica nanoparticles as controlled release drug delivery and gene transfection carriers," *Adv. Drug Delivery Rev*., 2008, vol. 60, pp. 1278-1288.

[6] R. Dersch, M. Sterinhart, U. Boudriot, A. Geriner and J. H. Wendorff, "Nanoprocessing of polymers: applications in medicine,sensors, catalysis, photonics," *Polym. Adv. Technol.*, 2005, vol. 16, pp. 276-282.

[7] D. H. Reneker and A. L. Yarin, "Electrospinning jets and polymer nanofiber," *Mechanics Research Communications*. 2000, vol. 27, pp. 37-42.

[8] X. Wang, C. Drew, S. Lee, K. J. Senecal, J. Kumar and L. A. Samuelson, "Electrospun Nanofibers Membranes for Highly Optical Sensors," *Nano Letter*, 2005, vol. 11, pp. 1273-1275.

[9] R. Gopal, K. Vermani and S. Garg, "Hydrogels: from controlled release to pH-responsive drug delivery," *Journal of Membrane Science*, 2006, vol. 281, pp. 581-586.

[10] Z. Sun, E. Zussman, A. L. Yarin, J. H. Wendorff and A. Greiner, "Compound Core-Shell Polymer Nanofibers by Co-electrospinning," *Adv. Mater., 2003*, vol. 22, pp. 1929-1932.

[11] J. E. Diza, A. Barrero, M. Marquez and I. G. Loscertales, "Controlled Encapsulation of Hydrophobic Liquids in Hydrophilic Polymer Nanofibers by Co-electrospinning," *Adv. Funct. Mater*., 2006, vol. 16, pp. 2110-2116.

[12] D. Li, and Y. Xia, "Electrospinning of Nanofibers: Reinventing the Wheel?," *Adv. Mater*., 2004, vol. 16, pp. 1151– 1170.

[13] B. Bognitzki, M. Becker, M. Graeser, W. Massa, J. H. Wendorff, A. Schaper, D. Weber, A. Beyer, A. Golzhauser, and A. J. Greiner, "Preparation of Sub-micrometer Copper Fibers via Electrospinning," *Adv. Mater.*, 2006, vol. 18, pp. 2384– 2386.

[14] D. Li, J. McCann, and Y. Xia, "Electrospinning: A Simple and Versatile Technique for Producing Ceramic Nanofibers and Nanotubes," *J. Am. Ceram. Soc*., 2006, vol. 89, pp. 1861– 1869.

[15] B. Min, G. Lee, S. H. Kin, Y. S. Nam, T. S. Lee, and W. H. Park, "Electrospinning of silk fibroin nanofibers and its effect on the adhesion and spreading of normal human keratinocytes and fibroblasts in vitro," *Biomaterials*, 2004, vol. 25, pp. 1289– 1297.

[16] F. Yang., R. Murugan, S. Wang and S. Ramakrishna. *Biomaterials*, 2005, vol. 26, pp. 2603– 2610.

[17] J. S. Choi, S. J. Lee, G. J. Christ, A. Atala, and J. J. Yoo, "Electrospinning of nano/micro scale poly(l-lactic acid) aligned fibers and their potential in neural tissue engineering," *Biomaterials*, 2008, vol. 29, pp. 2899– 2906.

www.manaraa.com

[18] G. E. Wnek, M. E. Carr, D. G. Simpson, and G. L. Bowlin, "Electrospinning of Nanofiber Fibrinogen Structures," *Nano Lett.*, 2003, vol. 3, pp. 213– 216.
[19] X., Zhu, W., Cui, X. Li, and Y. Jin, "Electrospun Fibrous Mats with High Porosity as Potential Scaffolds for Skin Tissue Engineering," *Biomacromolecules*, 2008, vol. 9, pp. 1795– 1801
[20] S. Srouji, T. Kizhner, E. Suss-Tobi, E. Livne, and E. *J.* Zussman, "3-D Nanofibrous electrospun multilayered construct is an alternative ECM mimicking scaffold," *Mater. Sci: Mater. Med.*, 2008, vol. 19, pp. 1249– 1255.
[21] A. Townsend-Nicholson, and S. N. Jayasinghe, "Cell Electrospinning: a Unique Biotechnique for Encapsulating Living Organisms for Generating Active Biological
[22] J. B. Recknor, D. S. Sakaguchi, and S. K. Mallapragada, "Directed growth and selective differentiation of neural progenitor cells on micropatterned polymer substrates," *Biomaterials*, 2006, vol. 27, pp. 4098– 4108.
[23] D. Li, Y. Wang, and Y. Xia, "Electrospinning of Polymeric and Ceramic Nanofibers as Uniaxially Aligned Arrays," *Nano Lett.*, 2003, vol. 3, pp. 1167– 1171.
[24] D. Li, Y. Wang, and Y. Xia, "Electrospinning Nanofibers as Uniaxially Aligned Arrays and Layer-by-Layer Stacked Films," *Adv. Mater.*, 2004, vol. 16, pp. 361– 366.
[25] W. E. Teo, and S. Ramakrishna, "Electrospun fibre bundle made of aligned nanofibres over two fixed points," *Nanotechnology*, 2005, vol. 16, pp. 1878– 1884.
[26] Z. M. Huang, Y. Z. Zhang, M. Kotaki, and S. Ramakrishna, "A review on polymer nanofibers by electrospinning and their applications in nanocomposites," *Compos. Sci.,, Technol.*2003, vol. 63, pp. 2223– 2253.
[27] J. Doshi, and D. H. *J.* Reneker, "," *Electrost.*, 1995, vol. 35, pp. 151– 160.
[28] Theron, A., Zussman, E. and Yarin, A. L. "Electrostatic field-assisted alignment of electrospun nanofibres," *Nanotechnology*, 2001, vol. 12, pp. 384– 390.
[29] D. Sun, C. Chang, S. Li, and L. Lin, "Electrospinning process and applications of electrospun fibers," *Nano Lett.*, 2006, vol. 6, pp. 839– 842.
[30] D. Li, M. Ouyang, J. T. McCann, and Y. Xia, "Collecting Electrospun Nanofibers with Patterned Electrodes," *Nano Lett.*, 2005, vol. 5, pp. 913– 916.
[31] D. Zhang, and J. Chang, "Patterning of Electrospun Fibers Using Electroconductive Templates," *Adv. Mater.*, 2007, vol. 19, pp. 3664– 3667.
[32] A. Zucchelli, D. Fabiani, C. Gualandi, and M. *J.* Focarete, "Patterning of Electrospun Fibers Using Electroconductive Templates," *Mater. Sci.*, 2009, vol. 44, pp. 4969– 4975.
[33] Z. Ding, A. Salim, and B. Ziaie, "Selective Nanofiber Deposition through Field-Enhanced Electrospinning," *Langmuir*, 2009, vol. 25, pp. 9648– 9652.
[34] P. D. Dalton, N. T. Joergensen, J. Groll, and M. Moeller, "Patterned melt electrospun substrates for tissue engineering," *Biomed. Mater.*, 2008, vol. 3, pp. 034109.
[35] M. Ikeuchi, R. Tane, M. Fukuoka, and K. Ikuta, "Nanofibrous Surface Patterning using Nano-Meshed Microcapsules Induced by Phase Seperation Assisted Electrospray," *IEEE 22nd Int. Conf. Micro Electro Mech. Syst.*, 2009, pp. 124– 127.
[36] A. Salim, C. Son, and B. Ziaie, "Selective nanofiber deposition via electrodynamic focusing," *Nanotechnology*, 2008, vol. 19, pp. 375303.
[37] J. Shi, L. Wang, and Y. Chen, "Microcontact Printing and Lithographic Patterning of Electrospun Nanofibers," *Langmuir*, 2009, vol. 25, pp. 6015– 6018.

www.manaraa.com

[38] H. Zeng, and Y. Zhao, "Creating microstructures in electrospun nanofibers using a micropatterned collector chip," *15th Int. Conf. Solid-State Sens. Actuators Microsyst.*, 2009, pp. 1099– 1103.
[39] H. W. Choi, J. K. Johnson, J. Nam, and D. F. J. Farson, "Structuring electrospun polycaprolactone nanofiber tissue scaffolds by femtosecond laser ablation," *Laser Appl.*, 2007, vol. 19, pp. 225– 231.
[40] S. Sengele, H. Jiang, J. H. Booske, C. L. Kory and R. L. Ives, "Microfabrication and Characterization of a Selectively Metallized W-Band Meander-Line TWT Cirtuit", *IEEE Transactions on Electron Devices*, 2009, vol. 56, pp. 730-737.
[41] B. Zhao, J. S. Moore, and D. J. Beebe, "Surface-Directed Liquid Flow Inside Microchannels," *Science*, 2001, vol. 291, pp. 1023– 1026.
[42] C. Reichardt, *Solvents and Solvent Effects in Organic Chemistry*, 3rd ed.; Wiley-VCH: Weinheim, Germany, 2003.
[43] C. Wang, Q. Ge, D. Ting, D. Nguyen, H.-R. Shen, J. Chen, H. N. Eisen, J. Heller, R. Langer, and D. Putnam, "Molecularly engineered poly(ortho ester) microspheres for enhanced delivery of DNA vaccines," *Nat. Mater*., 2004, vol. 3, pp. 190−196.
[44] G. Orive, R. M. Hernandez, A. R. Gascon, R. Calafiore, T. M. S. Chang, P. de Vos, G. Hortelano, D. Hunkeler, I. Lacik, A. M. J. Shapiro, and J. L. Pedraz, "History, challenges and perspectives of cell microencapsulation," *Trends Biotechnol*., 2004, vol. 22, pp. 87−92.
[45] T. Wang, I. Lacik, M. Brissova, A. V. Anilkumar, A. Prokop, D. Hunkeler, R. Green, K. Shahrokhi, and A. C. Powers, "An encapsulation system for the immunoisolation of pancreatic islets," *Nat. Biotech*., 1997, vol. 15, pp. 358−362.
[46] N. C. Bigall, A. Curcio, M. P. Leal, A. Falqui, D. Palumberi, R. Di Corato, E. Albanesi, R. Cingolani, and T. Pellegrino, "Magnetic nanocarriers with tunable pH dependence for controlled loading and release of cationic and anionic payloads," *Adv. Mater*., 2011, vol. 23, pp. 5645−5650.
[47] H. N. Yow and A. F. Routh, "Formation of liquid core-polymer shell microcapsules," *Soft Matter*, 2006, vol. 2, pp. 940−949.
[48] R. Atkin, P. Davies, J. Hardy, and B. Vincent, "Preparation of aqueous core/polymer shell microcapsules by internal phase separation," *Macromolecules*, 2004, vol. 37, pp. 7979−7985.
[49] K. Wygladacz, N. Ye, C. Xu, R. W. Retter, M. Bell, A. Hilgenbrink, and E. Bakker, "Uniform polymeric hollow microcapsules with controlled doping levels fabricated under nonreactive conditions," *Adv. Mater*.,. 2007, vol. 19, pp. 1059−1063.
[50] J. Wang, L. Sun, K. Mpoukouvalas, K. Lienkamp, I. Lieberwirth, B. Fassbender, E. Bonaccurso, G. Brunklaus, A. Muehlebach, T. Beierlein, R. Tilch, H.-J. Butt, and G. Wegner, "Construction of redispersible polypyrrole core-shell nanoparticles for application in polymer electronics," *Adv. Mater*., 2009, vol. 21, pp. 1137−1141.
[51] Y. Zhao and L. Jiang, "Hollow micro/nanomaterials with multilevel interior structures," *Adv. Mater*., 2009, vol. 21, pp. 3621−3638.
[52] A. D. Dinsmore, M. F. Hsu, M. G. Nikolaides, M. Marquez, A. R. Bausch, and D. A. Weitz, "Colloidosomes: Selectively permeable capsules composed of colloidal particles," *Science*, 2002, vol. 298, pp. 1006−1009.

www.manaraa.com

[53] D. O. Grigoriev, T. Bukreeva, H. Mohwald, and D. G. Shchukin, "New method for fabrication of loaded micro- and nanocontainers: Emulsion encapsulation by polyelectrolyte layer-by-layer deposition on the liquid core," *Langmuir*, 2008, vol. 24, pp. 999−1004.
[54] M. Kobaslija and D. T. McQuade, "Polyurea microcapsules from oil-in-oil emulsions via interfacial polymerization," *Macromolecules*, 2006, vol. 39, pp. 6371−6375.
[55] A. Shulkin and H. D. H. Stover, "Photostimulated phase separation encapsulation," *Macromolecules*, 2003, vol. 36, pp. 9836−9839.
[56] A. M. Schmidt, "The synthesis of magnetic core-shell nanoparticles by surface-initiatied ring-opening polymerization of epsilon-Caprolactone," *Macromol. Rapid Commun.*, 2005, vol. 26, pp. 93−97.
[57] A. V. Korobko, W. Jesse, and J. R. C. van der Maarel, "Encapsulation of DNA by cationic diblock copolymer vesicles," Langmuir, 2005, vol. 21, pp. 34−42.
[58] R. K. Shah, J.-W. Kim, J. J. Agresti, D. A. Weitz, and L.-Y. Chu, "Fabrication of monodisperse thermosensitive microgels and gel capsules in microfluidic devices," *Soft Matter*, 2008, vol. 4, pp. 2303−2309.
[59] H. Zhao, J. F. Chen, Y. Zhao, L. Jiang, J. W. Sun, and J. Yun, "Hierarchical assembly of multilayered hollow microspheres from an amphiphilic pharmaceutical molecule of azithromycin," *Adv. Mater.*, 2008, vol. 20, pp. 3682−3686.
[60] D. Lensen, D. M. Vriezema, and J. C. M. van Hest, "Polymeric microcapsules for synthetic applications," *Macromol. Biosci.*, 2008, vol. 8, pp. 991−1005.
[61] S. F. M. van Dongen, H.-P. M. de Hoog, R. J. R. W. Peters, M. Nallani, R. J. M. Nolte, and J. C. M. van Hest, "Biohybrid Polymer Capsules," *Chem. Rev.*, 2009, vol. 109, pp. 6212−6274.
[62] D. G. Shchukin, D. A. Gorin, and H. Mohwald, "Ultrasonically induced opening of polyelectrolyte microcontainers," *Langmuir.*, 2006, vol. 22, pp. 7400−7404.
[63] A. Radt, T. A. Smith, and F. Caruso, "Optically addressable nanostructured capsules," *Adv. Mater.*, 2004, 16, pp. 2184−2189.
[64] H. R. Bhagat, R. W. Mendes, E. Mathiowitz, and H. N. Bhargava, "Kinetics and mechanism of drug release from calcium alginate membrane coated *tablets," Drug Dev. Ind. Pharm.*, 1994, vol. 20, pp. 387−394.
[65] B. P. Timko, T. Dvir, and D. S. Kohane, "D. S. Remotely triggerable drug delivery systems," *Adv. Mater.*, 2010, vol. 22, pp. 4925−4943.
[66] A. Shaviv, S. Raban, and E. Zaidel, "Modeling controlled nutrient release from polymer coated fertilizers: Diffusion release from single granules," *Environ. Sci. Technol.*, 2003, vol. 37, pp. 2251−2256.
[67] B. J. Gan and L. A. Lyon, Tunable swelling kinetics in core-shell hydrogel nanoparticles," *J. Am. Chem. Soc.*, 2001, vol. 123, pp. 7511−7517.
[68] K. N. Plunkett and J. S. Moore, "Patterned dual pH-responsive core-shell hydrogels with controllable swelling kinetics and volumes," *Langmuir*, 2004, vol. 20, pp. 6535−6537.
[69] I. Tokarev and S.Minko, "Stimuli-responsive porous hydrogels at interfaces for molecular filtration, separation, controlled release, and gating in capsules and membranes," *Adv. Mater.*, 2010, vol. 22, pp. 3446−3462.
[70] S. Murdan, "Electro-responsive drug delivery from hydrogels," *J. Control. Release*, 2003, vol. 92, pp. 1−17.

www.manaraa.com

[71] B. Li and Y. Xia, "Electrospinning of nanofibers: Reinventing the wheel?" *Adv. Mater.*, 2004, vol. 16, pp. 1151−1170.
[72] Z. Y. Liu, D. D. Sun, and J. O. Leckie, "An efficient bicomponent TiO2/SnO2 nanofiber fabricated by electrospinning with a side-by-side dual spinneret method," *Nano Lett.*, 2007, vol. 7, pp. 1081−1085.
[73] Z. C. Sun, E.Zussman, A. L. Yarin, J. H. Wendorff, and A. Greiner, "Compound core-shell polymer nanofibers by co-electrospinning," *Adv. Mater.*, 2003, vol. 15, pp. 1929−1932.
[74] Y. Zhao, X. Y. Cao, and L. Jiang, "Bio-mimic multichannel microtubes by a facile method," *J. Am. Chem. Soc.*, 2007, vol. 129, pp. 764−765.
[75] H. Y. Chen, Y. Zhao, Y. L. Song, and L. Jiang, "One-step multicomponent encapsulation by compound-fluidic electrospray," *J. Am. Chem. Soc.*, 2008, vol. 130, pp. 7800−7801.
[76] M. J. Bassetti, A. N. Chatterjee, N. R. Aluru, and D. J. Beebe, "Development and modeling of electrically triggered hydrogels for microfluidic applications," *J. Microelectromech S.*, 2005, vol. 14, pp. 1198−1207.
[77] L. Dong, A. K. Agarwal, D. J. Beebe, and H. Jiang, "Adaptive liquid microlenses activated by stimuli-responsive hydrogels," *Nature*, 2006, vol. 442, pp. 551−554.
[78] N. C. Tsai and C.-Y. Sue, "Review of MEMS-based drug delivery and dosing systems," *Sensor Actuat. A-Phys.*, 2007, vol. 134, pp. 555−564.
[79] H. Yang, C. R. Lightner, and L. Dong, "Light-emitting coaxial nanofibers" *ACS Nano*,2012, vol. 6, pp. 622−628.
[80] R. Steendam, M. J. van Steenbergen, W. E. Hennink, H. W. Frijlink, and C. F. Lerk, "Effect of molecular weight and glass transition on relaxation and release behaviour of poly(DL-lactic acid) tablets," *J. Control. Release*, 2001, vol. 70, pp. 71−82.
[81] Y. S. Jo, D. K. Kim, Y. K. Jeong, K. J. Kim, and M. Muhammed, "Encapsulation of bovine serum albumin in temperature-programmed "shell-in-shell" structures," *Macromol. Rapid Commun.*, 2003, vol. 24, pp. 957−962.
[82] H. Yang, W. Hong, and L. Dong, "A controlled biochemical release device with embedded nanofluidic channels," *Appl. Phys. Lett.*, 2012, vol. 100, 153510
[83] X. Zeng and H. Jiang, "Tunable liquid microlens actuated by infrared light-responsive hydrogel," *Appl. Phys. Lett.*, 2008, vol. 93, 151101.
[84] A. Suzuki and T. Tanaka, "Phase transition in polymer gels induced by visible light," *Nature*, 1990, vol. 346, pp. 345−347.
[85] D. Troiani, J. R. Dion, and D. H. Burns, "Ultrasonic quantification using smart hydrogel sensors," *Talanta*, 2011, vol. 83, pp. 1371−1375.
[86] M. Namdeo, S. K. Bajpai, and S. Kakkar, "Preparation of a Magnetic-Field-Sensitive Hydrogel and Preliminary Study of Its Drug Release Behavior," *J. Biomater. Sci. Polym.*, Ed. 2009, vol. 20, pp. 1747−1761.
[87] I. F. Edd, D. Di Carlo, K. J. Humphry, S. Koster, D. Irimia, D. A. Weitz, and M. Toner, "Controlled encapsulation of single-cells into *monodisperse picolitre drops," Lab Chip*, 2008, vol. 8, pp. 1262−1264.
[88] H. Yang, X. Qiao, M. K. Bhattacharyya, and L. Dong, "Microfluidic droplet encapsulation of highly motile single zoospores for phenotypic screening of an antioomycete chemical," *Biomicrofluidics*, 2011, vol. 5, 044103.

www.manaraa.com

[89] T. Higuchi, "Mechanism of sustained-action medication: theoretical analysis of rate of release of solid drugs dispersed in solid matrices," *J. Pharm. Sci.* 1963, vol. 52, pp. 1145−1148.
[90] P. J. Flory and J. Rehner, "Statistical Mechanics of Cross Linked Polymer Networks II. Swelling," *J. Chem. Phys.*, 1943, vol. 11, 521−526.
[91] W. Hong, X. Zhao, J. Zhou, and Z. Suo, "A theory of coupled diffusion and large deformation in polymeric gels," *J. Mech. Phys. Solids*, 2008, vol. 56, pp. 1779−1793.
[92] T. G. Park, "Degradation of poly(d,l-lactic acid) microspheres: effect of molecular weight," *J. Control. Release*, 1994, vol. 30, pp. 161−173.
[93] S. H. Im, U. Y. Jeong, and Y. N. Xia, "Polymer hollow particles with controllable holes in their surfaces," *Nature Mater.*, 2005, vol. 4, pp. 671-675.
[94] F. Torney, B. G. Trewyn, V. S. Y. Lin, and K. Wang, "Mesoporous silica nanoparticles deliver DNA and chemicals into plants," *Nat. Nanotechnol.*, 2007, vol. 2, pp. 295-300.
[95] V. Menezes, K. Takayama, T. Ohki, and J. Gopalan, "Laser-ablation-assisted microparticle acceleration for drug delivery," *Appl. Phys. Lett.*, 2005, vol. 87, pp. 163504-163506.
[96] S. Freiberg and X. X. Zhu, "Polymer microspheres for controlled drug release," *Int. J. Pharm.*, 2004, vol. 282, pp. 1-18.
[97] M. R. Abidian, D. H. Kim, and D. C. Martin, "Conducting-Polymer Nanotubes for Controlled Drug Release," *Adv. Mater.*, 2006, vol. 18, pp. 405-409.
[98] J. K. Oh, R. Drumright, D. J. Siegwart, and K. Matyjaszewski, *Adv. Polym. Technol.*, 2004, vol. 33, pp. 448-452.
[99] D. A. LaVan, T. McGuire, and R. Langer, "Small-scale systems for in vivo drug delivery," *Nat. Biotechnol.*, 2003, vol. 21, pp. 1184-1191.
[100] D. W. Pack, A. S. Hoffman, S. Pun, and P. S. Stayton, "Design and development of polymers for gene delivery," *Nat. Rev. Drug Discovery*, 2005, vol. 4, pp. 581-593.
[101] Y. Li, R. S. Shawgo, B. Tyler, P. T. Henderson, J. S. Vogel, A. Rosenberg, P. B. Storm, R. Langer, H. Brem, and M. J. Cima, "In vivo release from a drug delivery MEMS device," *J. Controlled Release*, 2004, vol. 100, pp. 211–219.
[102] L. Dong and H. Jiang, "Autonomous microfluidics with stimuli-responsive hydrogels," *Soft Matter*, 2007, vol.3, pp. 1223-1230.
[103] Y. Qiu and K. Park, "Environment-sensitive hydrogels for drug delivery," *Adv. Drug Delivery Rev.* 2001, vol. 53, pp. 321-339.
[104] T. R. Hoare and D. S. Kohane, "Hydrogels in drug delivery: Progress and challenges," *Polymer*, 2008, vol. 49, pp. 1993-2007.
[105] M. Hamidi, A. Azadi, and P. Rafiei, "Hydrogel nanoparticles in drug delivery," Adv. Drug Delivery, 2008, vol. 60, pp. 1638-1649.
[106] P. Gupta, K. Vermani, and S. Garg, "Hydrogels: from controlled release to pH-responsive drug delivery," *Drug Discovery Today*, 2002, vol. 7, pp. 569-579.
[107] C. C. Lin and A. T. Metters, "Hydrogels in controlled release formulations: Network design and mathematical modeling," *Adv. Drug Delivery*, vol. 58, pp. 1379-1408.
[108] F. Brandl, F. Kastner, R. M. Gschwind, T. Blunk, J. Tessmar, and A. Gopferich, "Hydrogel-based drug delivery systems: Comparison of drug diffusivity and release kinetics," *J. Controlled Release*, 2010, vol. 142, pp. 221-228.

www.manaraa.com

[109] N. A. Peppasa, P. Buresa, W. Leobandunga, and H. Ichikawa, "Hydrogels in pharmaceutical formulations," *Eur. J. Pharm. Biopharm*., 2000, vol. 50, pp. 27-46.
[110] D. Li and Y. Xia, "Electrospinning of Nanofibers: Reinventing the Wheel?," *Adv. Mater*., 2004, vol.16, pp. 1151-1170.
[111] Z. Sun, E. Zussman, A. L. Yarin, J. H. Wendorff, and A. Greiner, "Compound Core–Shell Polymer Nanofibers by Co-Electrospinning,", *Adv. Mater*., 2003, vol. 15, pp. 1929-1932.
[112] H. Yang, C. R. Lightner, and L. Dong, "Light-Emitting Coaxial Nanofibers," *ACS Nano*, 2012, vol. 61, pp. 622–628.
[113] L. Dong, A. K. Agarwal, D. J. Beebe, and H. Jiang, "Adaptive liquid microlenses activated by stimuli-responsive hydrogels," *Nature*, 2006, vol. 442, pp. 551–554.
[114] P. J. Flory and J. Rehner, "Statistical Mechanics of Cross-Linked Polymer Networks II. Swelling," *J. Chem. Phys*., 1943, vol. 11, pp. 521–526.
[115] W. Hong, Z. Liu, and Z. Suo, "Inhomogeneous swelling of a gel in equilibrium with a solvent and mechanical load," *Int. J. Solids Struct*., 2009, vol. 46, pp. 3282–3289.
[116] M. L. Huggins, "A Revised Theory of High Polymer Solutions," *J. Am. Chem. Soc*., 1964, vol. 86, pp. 3535–3540.
[117] S. Cai and Z. Suo, "Mechanics and chemical thermodynamics of phase transition in temperature-sensitive hydrogels," *J. Mech. Phys. Solids*, 2011, vol. 59, pp. 2259–2278.
[118] Z. Y. Huang, W. Hong, and Z. Suo, "Nonlinear analyses of wrinkles in a film bonded to a compliant substrate," *J. Mech. Phys. Solids*, 2005, vol. 53, pp.2101–2118.
[119] H. Yang and L. Dong, "Selective Nanofiber Deposition Using a Microfluidic Confinement Approach," *Langmuir*, 2010, vol. 26, pp. 1539–1543.

www.manaraa.com

ACKNOWLEDGEMENTS

I would like to take this opportunity to express my thanks to those who helped me with various aspects of conducting research and the writing of this thesis. First and foremost, Dr. Liang Dong for his guidance, patience and support throughout this research and the writing of this thesis. His insights and words of encouragement have often inspired me and renewed my hopes for completing my graduate education. I would also like to thank my committee members for their efforts and contributions to this work: Dr. Jiming Song, Dr. Santosh Pandey, Dr. Timothy Bigelow and Dr. Wei Hong. I would additionally like to thank all the lab members in Dr. Dong's lab for their help through my doctoral study and research.

www.manaraa.com